Piezoresistance in Polymer Nanocomposites

by

Reza Rizvi

A thesis submitted in conformity with the requirements
for the degree of Doctor of Philosophy

Department of Mechanical and Industrial Engineering
University of Toronto

Piezoresistance in Polymer Nanocomposites

Reza Rizvi

Doctor of Philosophy

Mechanical and Industrial Engineering

University of Toronto

2014

Abstract

Piezoresistivity in conductive polymer nanocomposites occurs because of the disturbance of particle networks in the polymer matrix. The piezoresistance effect becomes more prominent if the matrix material is compliant making these materials attractive for applications that require flexible force and displacement sensors such as e-textiles and biomechanical measurement devices. However, the exact mechanisms of piezoresistivity including the relationship between the matrix polymer, conductive particle, internal structure and the composite's piezoresistance need to be better understood before it can be applied for such applications. The objective of this thesis is to report on the development of conductive polymer nanocomposites for use as flexible sensors and electrodes. Electrically conductive and piezoresistive nanocomposites were fabricated by a scalable melt compounding process. Particular attention was given to elucidating the role of matrix and filler materials, plastic deformation and porosity on the electrical conduction and piezoresistance. These effects were parametrically investigated through characterizing the morphology, electrical properties, rheological properties, and

piezoresistivity of the polymer nanocomposites. The electrical and rheological behavior of the

nanocomposites was modeled by the percolation-power law. Furthermore, a model was developed to

describe the piezoresistance behavior during plastic deformation in relation to the stress and filler

concentration.

Acknowledgements

"A journey of a thousand miles begins with a single step"

Table of Contents

1 Introduction

1.1 Preamble

This thesis examines the nature of electrically conductive particulate networks in polymeric nanocomposites and how those networks can give rise to electrical resistance change when mechanically deformed – a phenomenon known as piezoresistance. Electrically conductive and piezoresistive nanocomposites were fabricated by melt mixing the polymer and filler phases together. Various polymers, with different mechanical properties were used as the matrix phase. Also, carbonaceous filler particles with varying sizes and geometries were used as the filler phase. The diversity in polymer and filler phases selected was beneficial towards creating a general framework for understanding the phenomenon of filler-particle networks, electrical conduction and piezoresistance in conductive polymer nanocomposites. Furthermore the effect of plastic deformation and porosity on the electrical conductivity and piezoresistance was investigated in detail. Finally, semi-empirical methods were applied to model the electrical conduction and piezoresistance in conductive polymer nanocomposites.

1.2 Pressure Sensing

Sensors are ubiquitous in everyday life thanks to the technological revolution witnessed in the past half-century. The basis of all sensing devices is to interpret an input signal (e.g. concentration, luminance, pressure) and communicate it as an output signal, usually as voltage or current, which can easily be calibrated and measured. Fundamental to the design of physical sensors is the study of the sensing material itself. Pressure sensing materials can be classified as being passive or as active [1]. Upon stimulation passive sensor materials modify an externally sourced signal flowing through them, while active sensors will generate a signal. Piezoresistive materials are a type of passive sensor materials that

undergo a change in electrical resistance when subjected to deformations. There are several types of piezoresistive sensing materials, among which metallic and semi-conductor materials are very well known; many commercial products such as strain gauges are based on these material types. Despite their widespread use, metallic and semi-conducting materials cannot be deformed to very large strains, therefore their operating ranges are severely limited [2]. This drawback makes them unsuitable for applications such as biomechanical measurements and e-textiles, which involve large deformations.

1.3 Conductive Polymer Nanocomposites

Conductive polymer nanocomposites, are a lesser known type of piezoresistive material. A polymeric material can be made electrically conductive by randomly dispersing an electrically conductive filler phase. The filler size, shape and amount of filler material influence the observed electrical properties of the macroscopic composite. Generally, it is advantageous to have a filler particle with a small size, a high aspect ratio shape and in sufficient quantity; such a combination provides the maximum electrical conductivity [3]. Nanomaterials such as multi- and single-wall carbon nanotubes and graphene are ideally suited for imparting electrical conductivity in composite materials. The electron transport phenomenon is primarily sustained by the filler phase which, at sufficient quantities can form an interconnected network throughout as depicted in Figure 1.1. The mechanism of piezoresistance in these materials arises from the disruption of the filler network as a result of mechanical deformation. The disruption of the network influences the electrical properties of the entire composite and manifests itself as either a rise or decrease in the bulk resistance of the material. The flexible nature of polymeric materials allows for operations over large deformation ranges [1] (strain values as high as 200%). Such a high compliance also allows for them to be integrated on various substrates. In addition, polymer nanocomposites for pressure sensing are simple to manufacture and can be scaled to any size making

them one of the primary type of materials being investigated for artificial skins, gait and respiration measurements and other biomechanical measurements.
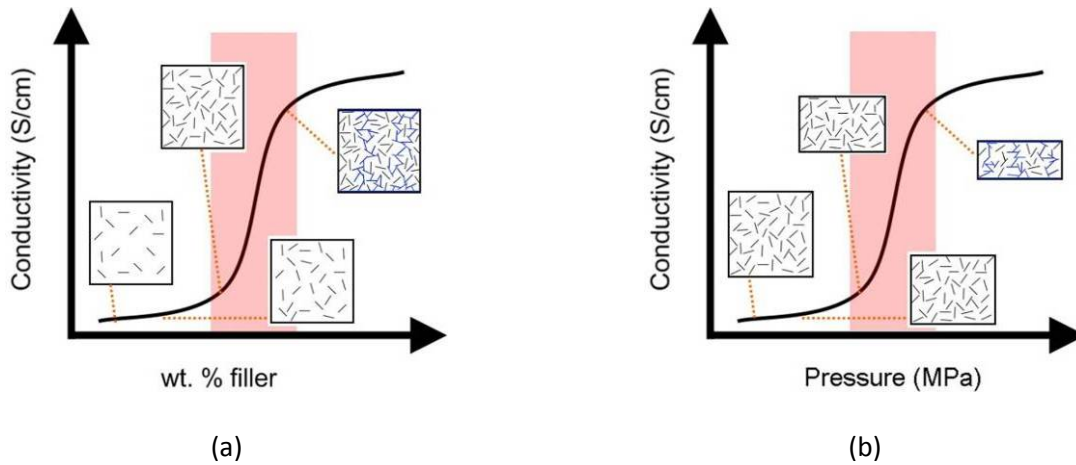
Figure 1.1. Schematics showing how the conductivity of a composite material varies with filler concentration (a) and the expected variance with applied pressure (b).

1.4 Problem Statement and Objectives

1.4.1 Problem Statement

Despite the widespread interest in conductive polymer nanocomposites for biomechanical measurements, they have several disadvantages that have restricted their use in practical applications. These include factors related to the characteristics of both the polymeric materials, such as non-linear stress-strain response, visco-elastic response, and hysteresis behavior, and the filler materials, such as low electrical conductivity and deterioration of mechanical properties. Finally, when the polymer and filler materials are combined, an electrically conductive filler particle network forms; the deformation of which results in the phenomenon of piezoresistivity. Unfortunately, we still lack a thorough understanding on the evolution of this filler particle network, its contribution to the electrical conductivity and its change with applied pressure resulting in piezoresistivity.

1.4.2 Objectives

The goal of this research dissertation is to advance the knowledge on electrical conduction in polymer nanocomposites and the phenomenon of piezoresisitivity. Particular attention is given to elucidating the role of matrix and filler materials, plastic deformation and porosity on the electrical conduction and piezoresistance. These effects can be parametrically investigated through characterizing the morphology, electrical properties, rheological properties, and piezoresistivity of the polymer nanocomposites. Furthermore, the evolution of the filler network and piezoresistance requires analytical, numerical or empirical modeling efforts to describe them. With these goals in mind, the objectives of this dissertation can be stated as follows:

1. Design and development of conductive polymer nanocomposites using compliant polymers and electrically conductive nanoparticles.

2. Determine the static piezoresistance of the conductive polymer nanocomposites and relate the macroscopic resistance and stress change to the filler network deformation.

3. Investigate the effect of filler particle structure and polymer material on the electrical conduction and piezoresistance of polymer nanocomposites.

4. Detail the effect of plastic deformation and porosity, when present in polymer nanocomposites and how they relate to the electrical conductivity and piezoresistivity.

5. Investigate and model the filler network during deformation and its contribution to electrical conduction through morphology, electrical, rheological and piezoresistance data.

1.5 Thesis Organization

This thesis is organized into 8 chapters, beginning with chapter 1, which introduces the problem statement and the objectives of the dissertation. Chapter 2 provides a brief but relevant literature review on the current state of research on multifunctional conductive polymer nanocomposites, filler

networks and piezoresistance. Chapter 3 describes the approach employed in achieving the stated objectives of the research, including the materials and experimental techniques employed. The first study, described in chapter 4, investigates the influence of filler particle types on the electrical conductivity and the piezoresistivity of polymer nanocomposites. The piezoresistance during plastic deformation of nanocomposites is characterized and detailed in chapter 5. In chapter 6, a porous morphology is introduced in polymer nanocomposites and its effects on the electrical conductivity and piezoresistance are described. Chapter 7 delves into modeling the percolation behavior describing the filler network evolution and the piezoresistance behavior of conductive nanocomposites. Finally, a summary and the key contributions of this research are provided in chapter 8, along with recommendations for further advancing the work in nanocomposite sensing materials.

2 Background and Literature Survey

2.1 Introduction

This chapter provides the necessary background and literature survey for any investigation into the piezoresistance of conductive nanocomposites. The field of carbon nanoparticles, multifunctional materials and polymer nanocomposites, including their development, characterization and application, is relatively new (20 years) however due to technological advances in communications and research, there is an explosion of sources of information on these topics. Yet several research works in these topics do not have thorough discussions of results and do not delve into identifying and understanding the underlying mechanisms involved in the results. Here in this chapter, the literature on these material topics is scoured in detail and summarized. The background on carbon nanoparticles and multifunctional composites is provided here. This is followed by percolation networks and electrical conduction in conductive polymer composite materials. The dependence of electrical properties on the aspect ratio of nanoparticles is discussed as well as inter-particle electron transport through electron tunneling. Finally, a summary of piezoresistance in conductive composites and models describing piezoresistance are provided.

2.2 Carbon Nanoparticles

Carbon has several natural and synthetic allotropes. The most common naturally occurring ones are diamond (cubic) and graphite (hexagonal) and amorphous carbon. Commonly studied synthetic allotropes of carbon are carbon nanotubes, graphene, fullerenes etc. Carbon, although abundant in our world, has several fascinating properties which make it applicable for various engineering applications. The conjugated *sp2* hybridization of the carbon-carbon double bond results in electron orbital delocalization and allows for phenomenal electrical and thermal transport properties similar to or even

better than common semiconductors and metals[4]. Furthermore, the carbon-carbon double bond has a bond enthalpy of 630 kJ/mol, one of the highest values in nature explaining the excellent mechanical properties of carbon allotropes [4]. The conjugated *sp2* hybridization exists in the hexagonal forms of carbon such as graphite, graphene, carbon nanotubes and fullerenes. Of these, graphene and carbon nanotubes have garnered significant research interest as recent advances have made possible the mass manufacture of these nanoparticles. We review these materials in more details below.

2.2.1 Carbon Nanotubes

Carbon Nanotubes (CNT) were first isolated and identified by Sumio Iijima in 1991 [5] as tubular features present in the amorphous soot on the electrodes from an arc-discharge process. They are characterized as hexagonal arrangements of carbon (graphene) rolled up into a tube (Figure 2.1). A graphene sheet can be rolled up in various lattice directions, which determine the final properties of the CNT nanomaterial, including whether its electronic transport is semi-conducting or metallic in nature. A single graphene sheet roll is termed a single-wall carbon nanotube (SWNT). Other forms of CNTs occur when two concentric sheets are rolled [Double-wall carbon nanotube (DWNT)] and when multiple sheets are rolled [Multi-wall carbon nanotube (MWNT)]. The actual production of these nanoparticles does not involve rolling, rather their growth is along the axial direction. The two most common methods of CNT production are arc-discharge and chemical vapor deposition [6]. Both methods involve some vaporization and atomic deposition of carbon. Preferential growth of CNT, as opposed to other carbon allotropes, is promoted through a precise control of processing parameters and through the use of nanometric transition metal catalysts. Carbon nanotubes can be synthesized in a variety of aspect ratios (length/diameter), usually ranging between $10^2 - 10^4$. The outstanding properties of CNTs are derived from the axial homogeneity of the crystalline graphitic structure along several length scales. It's been reported that carbon nanotubes have, along their axis, an electrical conductivity of $10^2 - 10^6$ S/m [7], a thermal conductivity of $200 - 3000$ W/m-K [6], and an elastic stiffness of 0.5-1.8 TPa [8].
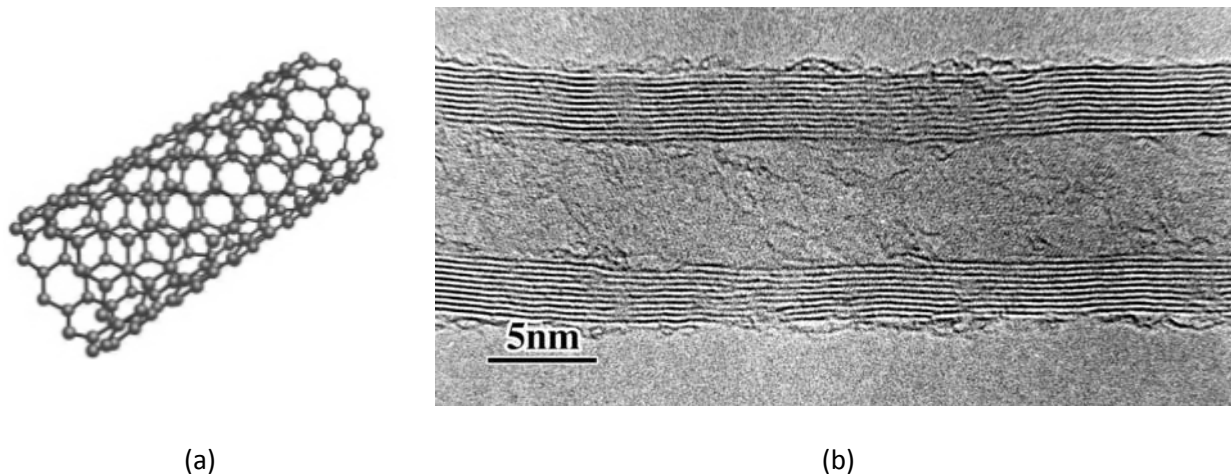
Figure 2.1. The schematic structure of a single-wall CNT (a) and the transmission electron micrograph of

a multiwall-CNT [9].

2.2.2 Graphene and Graphite

Graphene is a single atom thick layer of periodically (hexagonal) arranged *sp2* hybridized carbon atoms

(Figure 2.2). Due to its enormous surface area per particle, several graphene layers can combine and

form weak Van der Waals bonds. When extended to several thousands of layers, this stacked

arrangement of graphene gives rise to the c-axis in the hexagonal unit cell of the graphite crystal

structure. Although the structure of graphene was theorized from crystallographic analysis of graphite

early in the last century, it was only in 2004, that single layer graphene was mechanically isolated from

graphite and its properties were extensively studied by Andre Geim and Kostya Novoselov [10]. Since

then, extensive research has taken place on the fabrication, characterization and application

development of graphene. Graphene has in-plane mechanical, electrical and thermal properties similar

to axial properties of CNT, however it can have a much larger aspect ratio than CNT as single sheet

graphene can extend in-plane for several hundred micrometers. This unique attribute provides

graphene with a larger aspect ratio, surface area and more applicability than CNT and has propelled

graphene research in recent years.

(a)   (b)
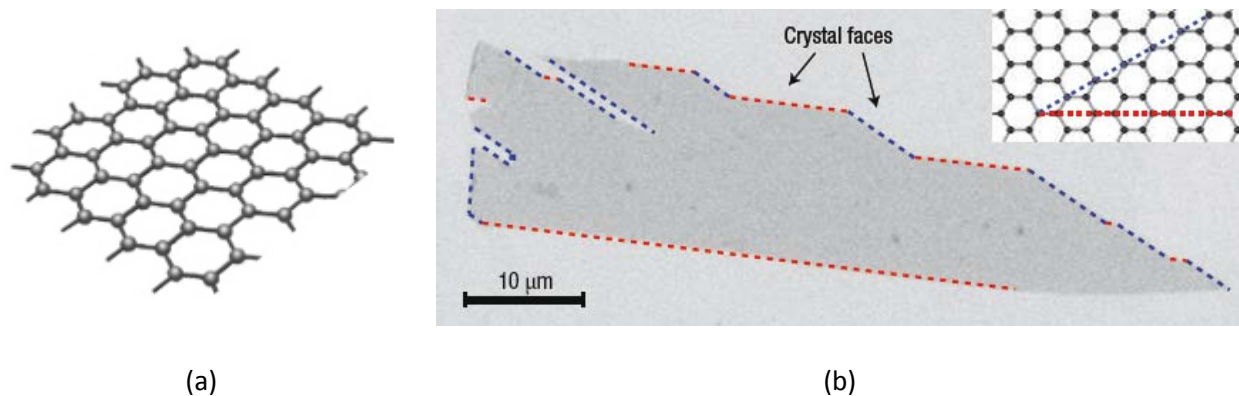
Figure 2.2. The schematic structure of graphene (a) and the transmission electron micrograph of a single

layer of graphene with its edges cleaved according to the lattice directions shown (inset) [10].

2.3 Multifunctional Materials and Polymer Nanocomposites

The superior electrical, thermal and mechanical properties of carbon nanoparticles has motivated

efforts to impart bulk materials with these attributes by forming composites between the nanoparticles

and polymers. Owing to their small dimensions and weak inter-particle adhesion, carbon nanoparticles

have very little applications as bulk materials by themselves. Polymers are usually the matrix material of

choice since they are lightweight and easy to manufacture and mold, when compared with metals and

ceramics. To this end, significant research and development have been directed towards polymer

nanocomposites containing CNT and graphene. Example applications of polymer nanocomposites

containing carbon nanoparticle includes materials for electrical conductivity [3], electrodes [11, 12],

thermal management [13], structural composites[14, 15], sensors [16-18] and actuators [19-21].

In many of the above-mentioned applications of polymer nanocomposites the benefits imparted

to the composite material arise due to the arrangement of the carbon nanoparticles (Figure 2.3). For

example, maximum stress-transfer across the polymer-nanoparticle interface will occur when the

nanoparticles are aligned axially (CNT)/in-plane (graphene) to the loading direction. Whereas, benefits in

electrical and thermal conductivity are observed when nanoparticles are homogenously and randomly

dispersed in the polymer matrix [22]. Several applications, including piezoresistive sensing, electrodes, electrostatic and electromagnetic shielding, require materials to have sufficient electrical conductivity. Unfortunately the mechanisms of electrical conductivity and piezoresistivity in conductive polymer nanocomposites are far from being identified and understood and this thesis aims to contribute to this end. However, the following two sections review the research on electrical conductivity, in terms of percolation and filler networks, and piezoresistance in polymer nanocomposites.

(a)   (b)   (c)
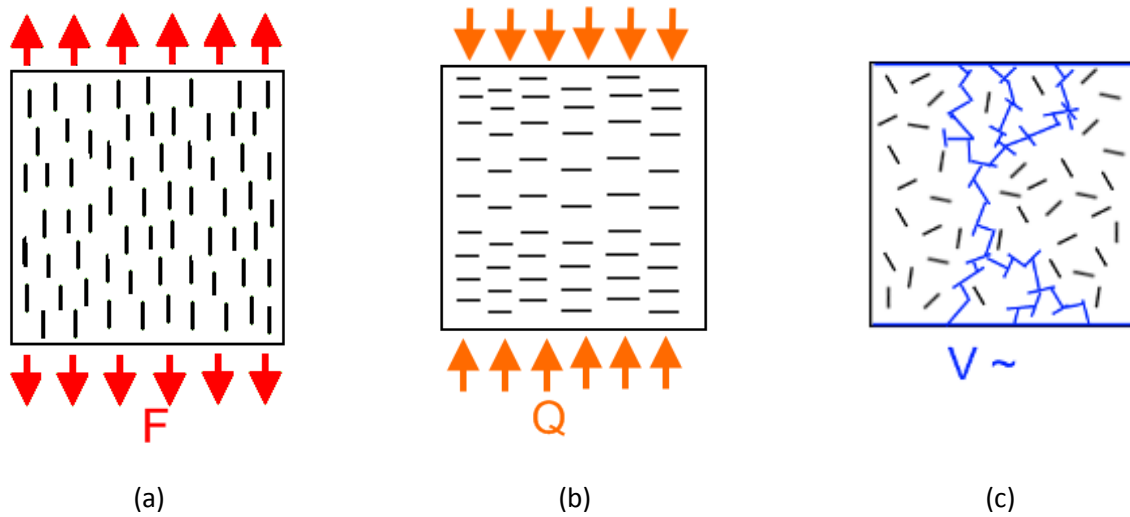
Figure 2.3. Arrangement of nanoparticles in a composite material influences its functionality. Nanoparticles aligned to the stress direction (a) allow for maximum stress transfer for structural applications. Nanoparticles aligned transverse to the heat or concentration flux (b) can impeded mass or heat transfer via barrier effects. A random dispersion of nanoparticles (c) can result in a continuous network that can conduct electricity.

2.4 Percolation and Filler Networks in Polymer Nanocomposites

Electrical conduction in polymer nanocomposites occurs because of electrical charge transport driven by a voltage difference. The polymer matrix is generally considered non-conducting and acts only as a dielectric, therefore the entire charge transport is supported only by the electrically conductive filler

phase [23]. In order to satisfy this condition and be electrically conductive, the filler phase in these composites has to be interconnected in a continuous network extending from one electrode to the next. The nature of the conductive network is significantly dependent on the conductive particle type, shape, dispersion and its concentration in the polymer phase. A sharp change in a quantifiable property is observed when a conductive particle network is established in the composite system. Usually this quantifiable property is electrical conductivity and viscoelasticity, with the former changing in value several orders of magnitude after the network is established [3]. Other properties such as thermal conductivity[24] and dielectric permittivity [25] have limited evidence of network influence, however this is out of the scope of this discussion and further work is required in this regards.

2.4.1 Percolation Power Law

The sharp change in properties observed in polymer nanocomposites with the establishment of a conductive filler network can be studied using percolation theory and network behavior [26]. Percolation theory can be applied to a variety of applications such as porous materials, epidemiology, energy transmission, information networks and in this case, composite materials [27]. Put simply, percolation theory states that a continuous network or giant cluster will be established (Figure 2.4) at a critical concentration of a randomly placed particles, pores or sites [28]. In the context of composite materials, the concentration of filler phase particles is the contributor to percolation. If the filler particles are conductive and a continuous network is established, then the conductivity of the bulk composite material, σ, should scale with filler content, ɸ, according to the statistical percolation power law [29] (Equation 2.1):

$$\sigma \propto \left(\phi - \phi_c\right)^t \qquad \text{(Eq. 2.1)}$$

where φ_c is the critical concentration of filler particles needed to establish a continuous network, t is a parameter, which has a theoretical basis in defining the dimensionality of the system. It has been shown

11

[30] that a network of randomly assembled conductive circles in a sea of non-conductive circles will form a 2D continuous conductive network at an area fraction of 0.44 and a t value of 1.3, regardless of the chosen lattice describing the system. Similarly, for spheres in a 3D system, the volume fraction will be 0.16 and a t value of 2.0. Unfortunately, this apparent universality is only applicable for the specific case of mono-disperse spherical particle composites on lattice points. These results breakdown when any deviation from the ideal scenario occurs. In such a situation the critical concentration, φ_c, and t value can be determined empirically from the fit of Equation 2.1 to the experimental data.

(a)   (b)
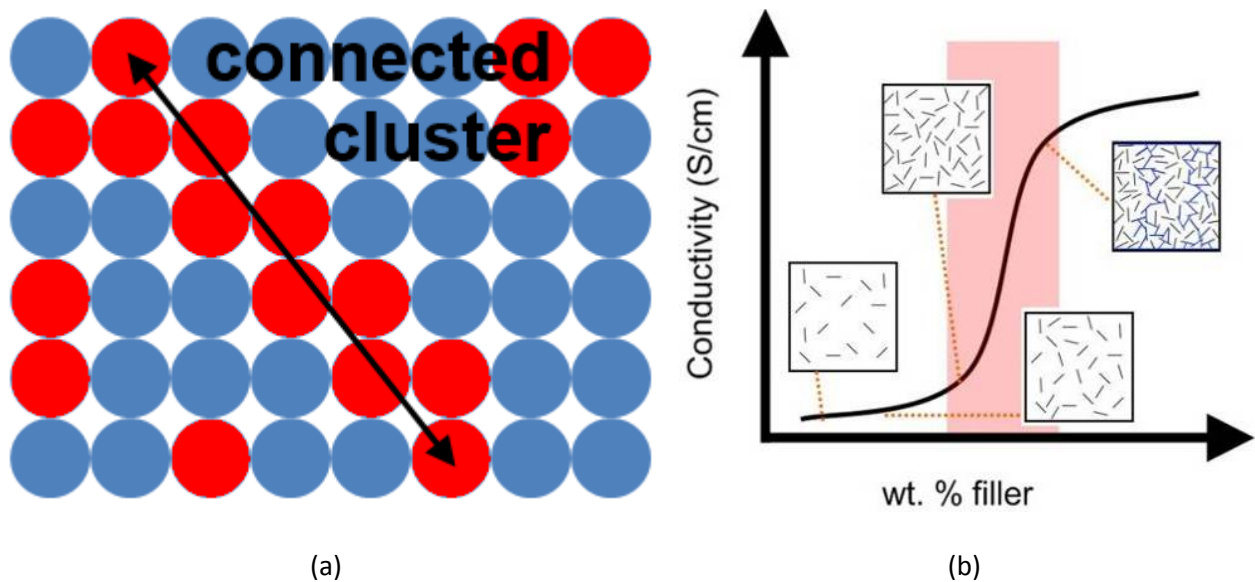
Figure 2.4. Random arrangement of spheres on a lattice (a) depicting a networked (percolated) state of the red spheres. For points on a lattice, this network of red spheres will be established at an area fraction of 0.44 which is universal regardless of the lattice system and size chosen. Composite systems exhibit a sharp rise in conductivity (b) as the concentration of the electrically conductive filler is increased. The critical concentration (pink area) is dependent on the aspect ratio, size and dispersion of the nanoparticles.

2.4.2 Continuum Percolation and Excluded Volume

The power law formulation for describing percolation and random networks (Equation 2.1) was devised using probability of occupation of sites or bonds on a point lattice. The point lattice argument does not apply to conductive polymer composites, which is a continuum of two discreet phases; the polymer matrix and the conductive particles, each with their own respective volumes [31]. Experimentally, conductive polymer composites display a sharp rise in electrical conductivity, which is indicative of a percolated structure [3], at volume fractions much less than the theorized critical values for point percolation (Figure 2.5). Values as low as 0.1 vol% have been reported for high aspect ratio SWNT based nanocomposites [32]. Moreover, the critical concentration and t exponent are not invariant, instead they are observed to be dependent on the conductive particle size and shape, and dispersion of the composite system. Percolation in continuum deviates significantly from that in lattice points, since the arrangement of particles (previously spherical, now oblong) and the size of particles can vary.

A simple concept used to account for these variations in continuum is the concept of excluded volume [33]. Put simply, this concept states that particles can interact with other particles over a larger volume of influence than the volume that physically defines them. This interaction region is termed excluded volume and it is dependent on the particle shape, orientation and dispersion. The concept of excluded volume is frequently applied to macromolecules (polymers) in order to describe their unusual properties observed when dissolved in solution. If such a condition of excluded volume does apply to percolated networks, like those in polymer composites, then it is apparent that a much lower concentration of the filler phase will be required to establish a continuous network.
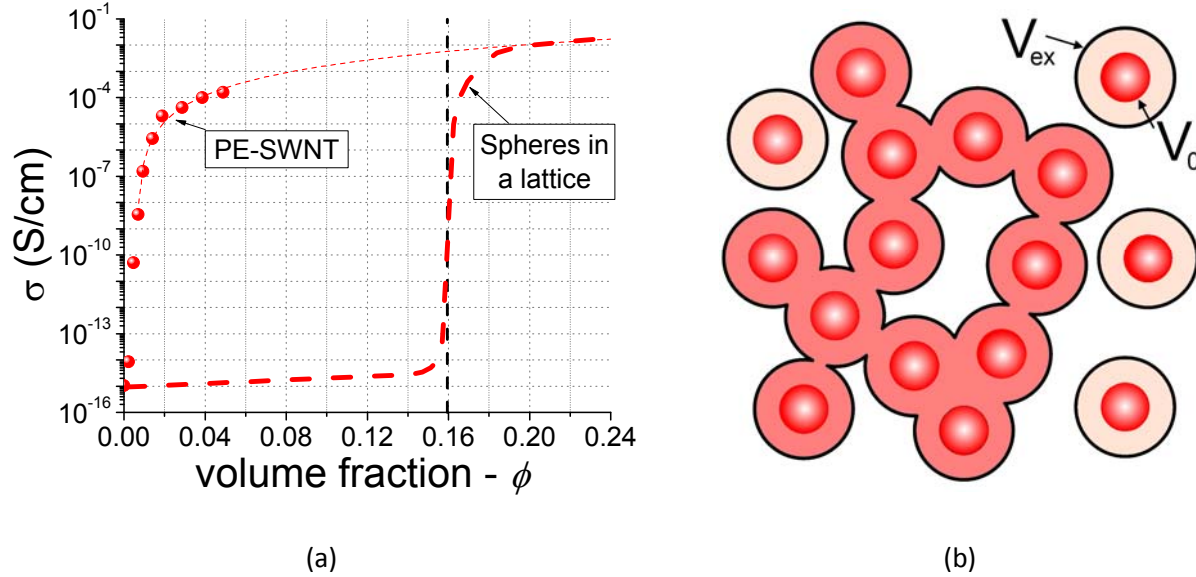
Figure 2.5. The conductivity data for a polyethylene (PE)-SWNT composite (a) shows a sharp increase in conductivity at 0.01 volume fraction. This experimentally observed value is much lower than the 0.16 volume fraction required for lattice percolation. The discrepancy arises from excluded volume considerations in a continuum (b), where the amount of filler required for interconnectivity is much less.

The excluded volume for a sphere can be defined as the volume into which a second sphere, of the same radius *r*, can come into contact. This volume would then have a radius, *2r*, and a volume 8 times greater than the initial sphere's volume. For oblong particles, e.g. sticks and disks, the excluded volume argument has to incorporate all possible particulate orientations, which are generally assumed to be random for conductive nanocomposites. For example in 2D, it has been shown [33] that the excluded region for two intersecting thin sticks of length, *L*, making angles θ_1 and θ_2 to some frame of reference, is in the form of a parallelogram (Figure 2.6) whose area is:

$$A_{ex} = L^2 \sin(\theta_1 - \theta_2)$$

(Eq. 2.2)

(a)   (b)
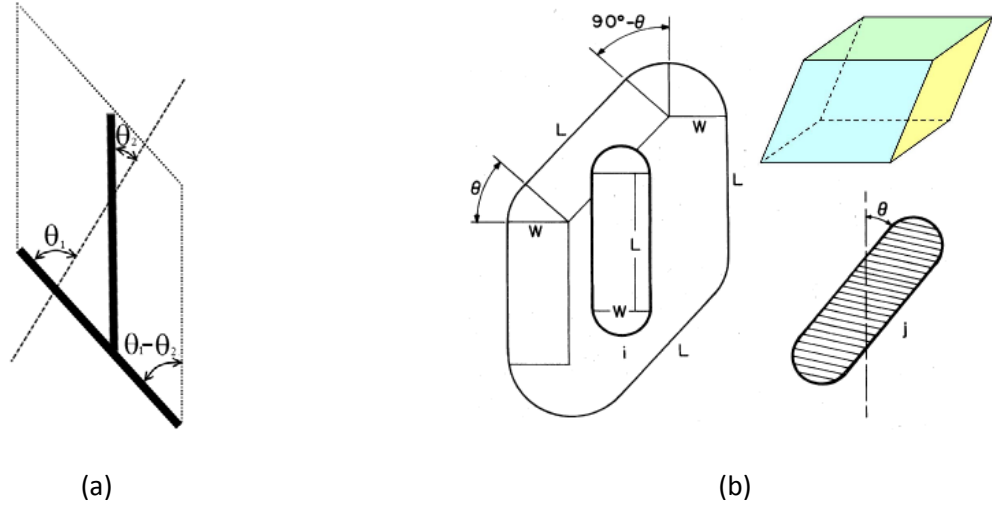
Figure 2.6. Definitions for the excluded area of two intersecting sticks (a) resulting in a parallelogram

shape and for two intersecting capped cylinders (b) resulting in a parallelepiped shape. [33]

For the isotropic case where the sticks can be randomly distributed between an angle $\pi/2$ to $-\pi/2$

relative to a frame of reference, the average excluded area, $\langle A_{ex} \rangle$, is:

$$\langle A_{ex} \rangle = L^2 / 2\pi \qquad \text{(Eq. 2.3)}$$

An excluded volume can be now be defined through a similar approached for capped cylinders with

length, L, and radius, W, in 3D. The region defined by two intersecting capped cylinders, oriented to

each other with an angle, γ can be visualized as a 3D parallelepiped (Figure 2.6) whose volume is given

by:

$$V_{ex} = (4\pi/3)W^3 + 2\pi W^2 L + 2WL^2 \sin\gamma \qquad \text{(Eq. 2.4)}$$

Similar to the 2D case, an isotropic expression for the average excluded volume where the two cylinders

are oriented randomly between possible angles $\pi/2$ to $-\pi/2$, is:

$$\langle V_{ex} \rangle = (4\pi/3)W^3 + 2\pi W^2 L + (\pi/2)WL^2 \qquad \text{(Eq. 2.5)}$$

Writing this in terms of the aspect ratio, $\eta = L/W$, one obtains:

$$\langle V_{ex} \rangle = (4\pi/3)W^3 + 2\pi W^3 \eta + (\pi/2)W^3 \eta^2 \qquad \text{(Eq. 2.6)}$$

An important consideration here is that the excluded volume is not directly proportional to the particle volume (V_p), as is the case for spherical and aligned particles [33]. The particle volumes are contained in the first two terms in Equation 2.6. The last term scales with the square of the aspect ratio of the particles. Therefore, the excluded volume for non-spherical, randomly oriented particles is more influenced by the aspect ratio of the particles as opposed to the volume of the particles themselves.

The expressions obtained for the excluded area and volume can be used to determine the area and volume fraction, respectively, at the onset of percolation. This exercise involves the consideration that at percolation there is a critical number density, N_c, of particles per unit volume in the material. The total excluded volume, $\langle V_T \rangle$, occupied by the particles at percolation is $N_c \langle V_{ex} \rangle$. Through Monte Carlo simulations this total excluded volume amount has been shown to be a constant depending on the geometry and orientation of the particles [34]. The total excluded volume in continuum for deformable spheres or parallel objects is 2.8, while the value for random, infinitely thin rods is 1.4 and for random, infinitely thin discs is 1.8. Moreover, comparisons with Monte Carlo results have shown that the total excluded volume value is a good approximation of the number of bonds per particle – i.e. random spheres have 2.8 bonds per particle and random sticks have 1.4 bonds per particle. The quantity N_c can be determined by the ratio $\langle V_T \rangle / \langle V_{ex} \rangle$, then the volume fraction at percolation is simply the product $N_c V_p$. When considering a distribution and probability of orientations, the percolation threshold (volume fraction) is related to the total excluded volume by the following relation:

$$\phi_c = 1 - \exp\left(-\frac{\langle V_T \rangle V_p}{\langle V_{ex} \rangle}\right) \qquad \text{(Eq. 2.7)}$$

Substituting the volume of a capped cylinder particle, V_p, and the excluded volume of a particle, $<V_{ex}>$ (Eq. 6), into Equation 2.7 and assuming that $\eta \gg 1$, the percolation threshold can be stated as:

$$\phi_c \approx 1 - \exp\left(-\frac{\langle V_T \rangle}{2\eta}\right) \qquad \text{(Eq. 2.8)}$$

For large values of, η, Equation 2.8 can be simplified to:

$$\phi_c \approx \frac{\langle V_T \rangle}{2\eta} \qquad \text{(Eq. 2.9)}$$
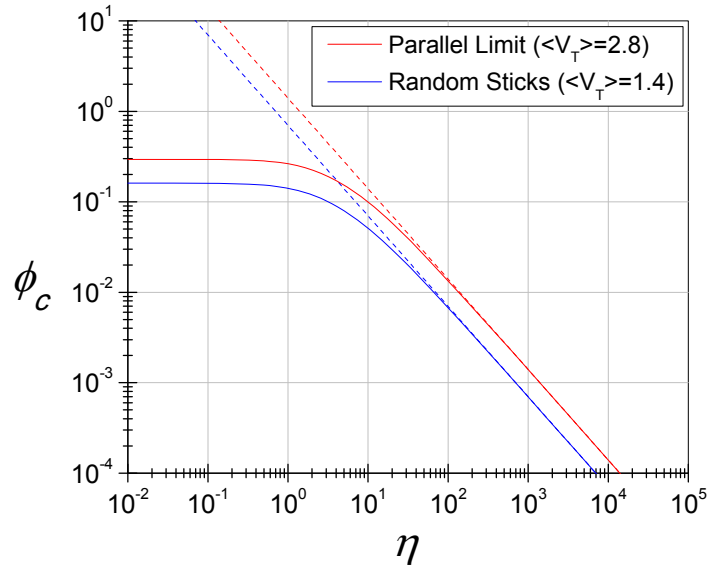
Figure 2.7. The dependence (solid) of percolation threshold (φ_c) on the particulate aspect ratio (η) as predicted by the excluded volume approach (Equation 2.7). The approximation for large aspect ratios (dash) can be made by Equation 2.9.

Despite its simplicity Equation 2.9 is a very important relationship as it suggests that larger aspect ratio particles will provide a lower percolation threshold value, as is experimentally observed [3]. Figure 2.7 depicts how the percolation threshold varies with the aspect ratio (Equations 2.8 and 2.9), at two extreme cases, when all particles are in parallel with each other and when they are all oriented randomly. The excluded volume approach explains the significantly reduced percolations thresholds observed for oblong particle composites.

2.4.3 Inter-particle Conduction

Electrical transport in conductive polymer composites involves electron flow due to a voltage bias along a network of conductive fillers. The advantage of conductive nanoparticles such as carbon nanotubes (and graphene) is the ballistic conduction in the axial (in-plane) direction due to extremely low scattering events [6]. The electron transport properties of the polymer matrix are far inferior when compared to the conductive nanoparticle. However, these properties must be considered since the polymer is a part of the filler network, existing in between the particles as a thin layer especially at low particle contents. At particle contents much higher than the percolation threshold, the number of particle-particle contacts increases [35] and the influence of the polymer layer on the composite's electrical property is reduced.

The electron transport between two conductive nanoparticles separated by a polymer dielectric layer is non-Ohmic in nature. The only means of transporting an electron past the polymer barrier is through fluctuation induced tunneling (FIT) or quantum tunneling. Fluctuation induced tunneling theory describes the electron hopping phenomena across a dielectric layer due to thermally activated voltage fluctuations [36]. The wave-functions of the electron on either side of the barrier are non-coherent. The FIT phenomena is highly temperature dependent with high tunneling probability at high temperatures while providing similar results to quantum tunneling at low temperatures (room temp). Quantum

tunneling occurs when the electron wave functions in two particles separated by a barrier interact to form one continuous wave function [37]. According to Schrodinger's equation then there exists the probability for electrons to exist in both particles. This process requires that a sufficient voltage bias be provided and that the width of the barrier is small enough (typically <2-3 nm). Simmons [38] has devised a simple relationship describing the current density, *J*, between two electrodes separated by a thin dielectric layer of thickness, *s*, due to an external bias, *V*, as:

$$J = \frac{3\sqrt{2m\varphi}}{2s}\left(\frac{e}{h}\right)^2 V \exp\left(-\frac{4\pi s}{h}\sqrt{2m\varphi}\right)$$ (Eq. 2.10)

where *e* is the elementary charge (1.602×10^{-19} C), *h* is Planck's constant (6.626×10^{-34} J-s), *m* is the electron mass (9.109×10^{-31} kg) and *φ* is the height of the potential barrier between the two electrodes. The barrier height can be obtained by subtracting the electronic work functions of the electrode and barrier materials. Simmons relationship has been found to be effective in describing the electron transport at the junctions between carbon nanoparticles in a polymer composite. The exponential form of Equation 2.10 limits the dielectric layer thickness to be only on the order of a couple nanometers; thicker layers will not sustain sufficient tunneling currents even at high voltages. If ballistic conduction in carbon nanoparticles is assumed, then electron tunneling between particles (as described in Equation 2.10), along with contact resistances, are factors limiting the electrical conductivity in conductive polymer composites.

2.5 Piezoresistance in Polymer Nanocomposites

2.5.1 History of Piezoresistive Composites

Piezoresistive composites have been researched as far back as 1966 when Massey and Kavrak [39] employed a conductive rubber for a pressure transducer capable of measuring pressure fluctuations in the wake from aerofoils. Piezoresistivity was observed in samples as thin as 0.5 mm with rubber

conductivities ranging from 1×10^{-5} S/cm to 2×10^{-3} S/cm. However, the exact mechanism for the piezoresistivity was not described. Ukrainetz and Hertz [40], also in 1966, described the piezoresistive behavior of conductive paints and employed them to make a pressure sensitive paint force transducer. These conductive paints contained rare-earth elements as the conductive filler. Despite their limitations piezoresistive conductive polymer composites have been used in special circumstances, especially for applications requiring high compliance and large strain measurements. For instance, Brown and Muratori [41] utilized the compliant nature of a piezoresistive conductive elastomer sensor for slow-dynamic contact-stress measurements requiring a high degree of flexibility. A paper by Snyder and St. Clair [42] details their efforts in implementing a commercially available conducting rubber for robotic tactile sensing in a large array configuration.

2.5.2 Piezoresistance in Polymer-Carbon Nanotube Composites

Recent materials innovations, such as the emergence of graphene and carbon nanotubes, have renewed interest in piezoresistive sensing using conductive polymer composites, particularly for tactile sensing and other applications requiring high compliance. One such application is in the field of electronic-textiles (e-textiles), where a high degree of compliance and manufacturing versatility is required from fabric substrate-integrated sensors. De Rossi and co-workers [43-45] have developed piezoresistive sensorized garments for posture detection using a commercially available conductive silicone. Silicone is a material that is easy to fabricate and is not as prone to hysteresis as other filled elastomeric compounds. The filler particles in the sensing silicone material were carbon black particles. Although the amount of filler concentration is not described, the resistances of the commercial conductive silicones suggest that the composites are well above the percolation threshold concentration. In their work, De Rossi et al. [43] report a gage factor (resistance change/strain change) of about 2.5, which is similar to that expected for metallic strain gages. The use of new and emerging materials such as silicones and

nano-particle fillers hold significant promise in improving the piezoresistance performance of the sensorized e-textiles.

Pan and co-workers [46] have examined in detail the dynamic piezoresistance behavior of various polymers filled with spherical metal particles. The mean particle diameters varied from 0.2 – 0.7 μm and filler volume fractions on the order of 0.2 – 0.3 were used. The composites exhibited significant piezoresistive behavior, which was well described by a constitutive model developed for the resistance of conducting fillers in an insulating matrix. The reason for such good correlation between the model and experimental results might be the use of linearly elastic polymers such as Poly(ethylene), Poly(styrene) and Epoxies, as well as the nearly spherical filler particles and their homogenous dispersion. Such good correlations might not be expected if highly non-linear materials, like elastomers, or high aspect ratio fillers, like graphite or carbon nanotubes, were used. Luheng and co-workers [47, 48] attempted to model the piezoresistance of carbon black (CB) filled silicone rubber using a similar model with limited success. They had to resort to a semi-empirical model for describing the piezoresistance behavior due to the polymer's non-linear behavior, aggregation and non-homogenous shape of CB particles.

Dang and co-workers [49] have fabricated piezoresistive PDMS-MWNT composites using high and low aspect ratio MWNT. A wet-mixing technique consisting of diluting the PDMS in a solvent was used to disperse the MWNT. They studied the composite piezoresistivity under a compressive pressure and surprisingly found a positive piezoresistive behavior characterized by a proportional increase in resistance as the applied pressure is increased. This behavior was attributed by the authors to the destruction MWNT networks in PDMS due to the applied stress. However, the exact observations and mechanism of network destruction requires further work. In particular the observation that network deformation was found to occur at even low forces (< 10 N) remains unexplained.

2.5.3 Modeling Piezoresistance in Conductive Composites

Any practical use and widespread application of piezoresistive conductive composites requires that their response is appropriately modeled. These models must predict the resistance of the composite as a function of the applied pressure or strain. A few researchers have attempted to model the piezoresistive response of specific conductive polymer composites; however no general scheme or strategy exists for modeling the piezoresistance of composite material. Perhaps the first study that comprehensively examines piezoresistance and attempts to model it is by Carmona et al [50]. This study experimentally describes the phenomena of piezoresistance and attempts to predict it using a derived model. The basis for the model is in describing how the local volume fraction varies due to compressibility of the matrix and filler phase, which is dependent on external pressure. Through the application of stress, the local particle concentration will change, which according to the conductivity-concentration s-curve relation, will also result in a change in the composite's conductivity. The final model for the relative resistivity change, $\Delta\rho/\rho$, as a function of the applied pressure difference, (P-P_0) is given by:

$$\frac{\Delta\rho}{\rho} = \left(\frac{\phi}{\phi + (1-\phi)\exp(-a(P-P_0))} - \phi_c \right)^{-t} (\phi - \phi_c)^{-t} - 1$$

(Eq. 2.11)

where, φ_c and t, are the critical percolation threshold and critical exponent as determined by the empirical fit of the conductivity data at P_0 using Equation 2.1. The term a is a fit constant describing the sensitivity of the piezoresistive effect. Comparisons of the model to the experimental results showed that higher sensitivity values (a) were achieved when the concentration of the composites was closest to the percolation threshold and when the compressibility (modulus) difference between the polymer matrix and the conductive particle is the greatest.

A piezoresistance model was proposed by Zhang et al [51] to describe the piezoresistive behavior of polyurethane-Multiwall Carbon Nanotube composites. The composites were prepared by

solvent casting processes and were found to have a low percolation threshold of 0.35 wt%. The resistance-strain behavior was found to be exponential in nature, which the authors attribute primarily to the tunneling effect. The conductivity behavior of the composites is described by the fluctuation induced tunneling (FIT) model, which has a single exponential form. The FIT model comprises of constants that contain quantum mechanical terms such as the tunneling width (inter-particle distance) and the potential barrier height between the matrix and the filler. The authors consider an image force correction for a rectangular tunnel barrier considered in the composites and are able to rewrite the FIT based derivative of resistivity w.r.t. strain as a non-exponential:

$$\frac{d(\ln \rho)}{ds} = c + \frac{1.48T_1}{T + T_0} - \frac{0.02T_1T_0}{(T + T_0)^2}$$
(Eq. 2.12)

where, c, is a constant term, T, is the temperature and T_1 is a FIT parameter, which includes information about the tunneling gap. The derivative consists of a constant term and a term comprising FIT model parameters. The FIT parameters are found by fitting the zero-strain temperature dependence of conductivity.

A model employing Simmons' approximation of the tunneling current (Equation 2.10) in composite materials was derived by Zhang and Pan et al [46]. The developed analytical model was for spherical inclusions in various polymer materials and had excellent agreement with the experimental data. The authors derive their model by combining the approach of Ruschau et al [52], describing the resistivity of straight conducting paths in a network, and the tunneling current formulations derived by Simmons et al [38, 53, 54]. The derivation assumes a simple cubic lattice of spherical conducting particles homogeneously dispersed in a dielectric medium. Assuming isotropic deformation any macroscopic strain, will directly affect the inter-particle gap and result in a change of the tunneling current. The final static model describes the relative resistance change as a function of stress, σ,

composite elastic modulus, *E*, particle diameter, D, volume fraction, θ, and the tunneling potential barrier height, *φ*, between the matrix and the filler:

$$\frac{\Delta R}{R_0} = \left(1 - \frac{\sigma}{E}\right)\exp\left\{-\gamma D\left[\left(\frac{\pi}{6}\right)^{1/3}\theta^{-1/3} - 1\right]\frac{\sigma}{E}\right\}$$

(Eq. 2.13)

where:

$$\gamma = \frac{4\pi}{h}\sqrt{2m\varphi}$$

(Eq. 2.14)

The composites modeled consisted of Polyethylene (PE), Polystyrene (PS) and Epoxy matrices filled with 30 vol. % of various metallic powder particles (Sn-Pb, Cu, Al). Although the assumptions made are very simplistic (e.g. cubic filler lattice, parallel channels of series resistors) the validation between experiments and the model are quite strong. The model is limited in that it is only for spherical particles and not for high aspect ratio particles such as carbon nanotubes or graphene nano-platelets. Despite this several studies using high aspect ratio fillers have used some modified form of it to semi-empirically fit their data, in order to obtain information about system parameters such as particle size and tunneling work function.

2.6 Summary

A brief introduction to carbon nanoparticles, including graphene and carbon nanotubes, is provided in this chapter. This is followed by a description of multifunctional polymer nanocomposites and how various architectures in polymer nanocomposites can impart multiple functionalities. With a focus on electrical conduction for piezoresistive sensing, the network percolation model is introduced as a power-law form. Percolation in continuum systems is also described and the aspect ratio dependence of percolation is derived through excluded volume considerations. Although electrical conduction in

polymer nanocomposites is confined to the network of nanoparticles, inter-particle electron tunneling between nanofillers occurs because of the thin polymer dielectric barrier. The tunneling currents can be approximated by Simmons equation which is dependent on the barrier width and the work functions of the polymer and filler materials. Pressure-resistance dependence (piezoresistance) is dependent on the interparticle distance and network path dynamics. Briefly, the development of piezoresistive polymer nanocomposites is discussed along with a few models that have been developed to describe the piezoresistance phenomena.

3 Approach and Methodology for Development of Piezoresistive Composites

3.1 Introduction

The approach and methodology for fabrication and characterizing the properties of piezoresistive conductive polymer composites are outlined in this chapter. The approach described consists of investigating electrical conduction and piezoresistance in the context of matrix materials, nanoparticle fillers, plastic deformation during piezoresistance, and a porous internal structure. The rationale for selecting the polymer matrix materials and the filler nanoparticles is provided. The physical properties for the various matrix and filler materials are compared. Finally, the various fabrication and characterization techniques for the piezoresistive composites are discussed in detailed.

3.2 Approach for Developing Piezoresistive Nanocomposites

Central to the development of piezoresistive nanocomposites for pressure sensing applications is the study of percolated filler networks and their variations with stress. Characterization of the percolated filler networks can be performed using electron microscopy which provides local visualization of filler particles and their dispersion in the polymer matrix. Electrical and rheological properties can provide a macroscopic measure of filler networking, and along with electron microscopy, present information on the state of the percolated filler network across length scales. Variations of the filler network with stress can be observed by *in situ* electrical property measurements during deformation. The percolation behavior and the piezoresistance that follows is expected to vary according to the system parameters chosen. The system parameters that will be studied are filler particle type and content, polymer matrix,

plastic deformation (stress) and internal porosity. These parameters are schematically depicted in Figure 3.1 and the rationale for their selection is provided below.
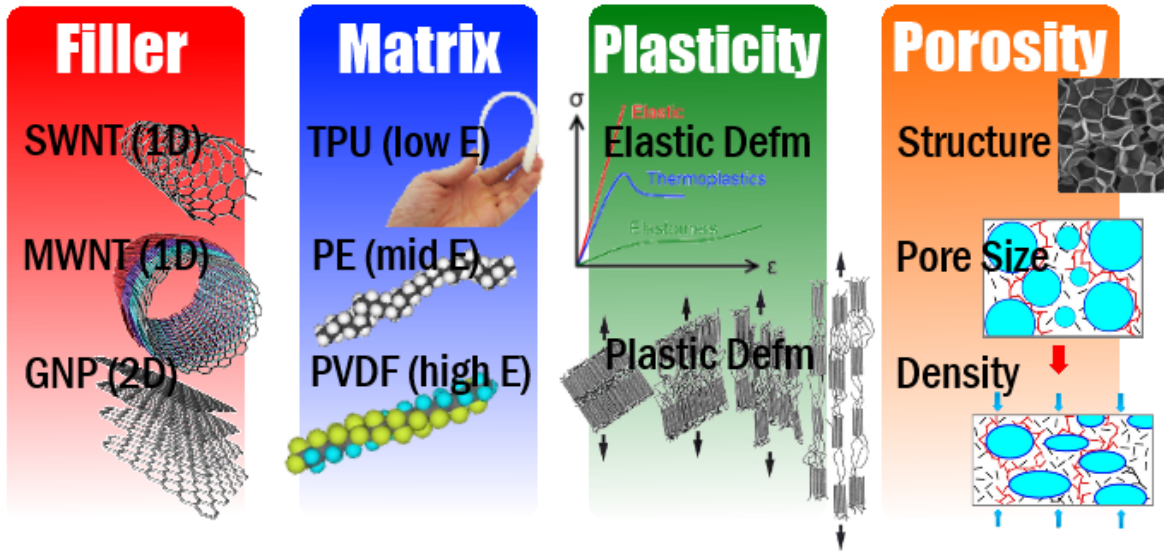
Figure 3.1. Schematic of the approach employed for development of piezoresistive nanocomposites.

3.2.1 Influence of polymer matrix on the percolation and piezoresistance of nanocomposites

The polymer matrix will have a significant influence on the filler percolation and piezoresistance in polymer nanocomposites. Several factors such as polymer viscosity and secondary interactions will influence the percolation of the nanoparticle filler network, even when processed under similar conditions. Once a percolated filler network is formed, the polymer work function will influence the electrical conduction at nanotube junctions according to Equation 2.10. The polymer's modulus and mechanical behavior will influence how the filler network gets modified during the deformation process, which in turn affects the piezoresistivity of the nanocomposites. In order to investigate the influence of

these factors on the percolation and piezoresistance behavior, three polymers with varying mechanical properties will be used as the matrix phase in the polymer nanocomposites.

3.2.2 Influence of nanoparticle structure on the percolation and piezoresistance of nanocomposites

The nanoparticle structure and amount are the primary factors influencing the filler network and nanocomposite piezoresistivity. The nanoparticle structure can be described by its size and shape (aspect ratio), which as described in Chapter 2 dictates the percolation threshold. Additionally, the electrical conductivity of the nanoparticles will determine the final nanocomposite conductivity. The nanoparticle structure will play a role in the piezoresistive response of the nanocomposites, as the deformation of the network will be different for each nanoparticle type. Finally, the percolation behavior and the piezoresistance response will vary based on the fraction of nanoparticles in the nanocomposite. Three nanoparticles with differing structures will be employed in the nanocomposites to investigate these factors and their influence on percolation and piezoresistance.

3.2.3 Piezoresistance during plastic deformation

The uniaxial compressive deformation of polymers generally consists of three deformation regimes. The first regime is where mechanical slack is removed and contact is established. This is followed by elastic deformation regime where the volume of the material being compressed is reduced. The third regime is plastic deformation which is exhibited by polymers that yield (generally semi-crystalline polymers) and undergo isochoric deformation with a 3D stress state. The nanoparticle networks will undergo a significant conformation change due to the plastic deformation of polymer nanocomposites. The piezoresistance during plastic deformation will be characterized according to the polymer being deformed and the nanoparticle amount.

3.2.4 Percolation and piezoresistance of porous nanocomposites

Electrically conductive nanocomposites can be made homogenously porous using a batch foaming process. The internal porosity is expected to have a significant influence on the percolation behavior and the piezoresistance response of the nanocomposites. The percolated filler network exists in the solid phase in porous nanocomposites, whose structure in turn depends on foam parameters such as relative density, pore size and pore density. The influence of these factors on the percolation and piezoresistance of a porous nanocomposite will be elucidated.

3.3 Polymer Matrix Material Selection

Three polymer matrix materials, covering a spectrum of mechanical properties, were selected as matrix materials. The contrast in mechanical properties should prove to be useful in elucidating the effect of matrix materials on the electrical conductivity and piezoresistance of conductive polymer nanocomposites. The materials selected were thermoplastic polyurethane (TPU), linear low density polyethylene (PE) and polyvinylidene-fluoride (PVDF). The physical properties of these three polymers are listed in Table 3.1 and are described in detail below.

Table 3.1. Physical properties of polymer matrix materials investigated.

Property	TPU [55]	PE [55]	PVDF [56]
Density, ρ (g/cm^3)	1.20	0.925	1.78
Young's Modulus, E, (MPa)	62	700	2310
Elongation (%)	500	500	50
Melt Temperature, T_m (°C)	160	125	170
Glass Temperature, T_g (°C)	-43	-125	-38
Processing Temperature (°C)	200	200	230
Dielectric Constant	5.8	2.2	14

Polyurethanes are formed by the reaction of isocyanates with polyols. Thermoplastic polyurethanes (TPU) are linear block copolymers consisting of alternating regions of short chain and long chain di-isocyanates. The short chain segments can crystallize to form phase separated 'hard' regions while the long chain segments remain flexible ('soft'). The combination of hard and soft regions has the effect of temporary cross-links in the material, allowing for high flexibility and elastomeric properties of TPU. The TPU polymer Desmopan 385E by Bayer Material Science was selected because of its high compliance and thermal process-ability.

Polyethylene (PE) is the most common and simplest polymer possible made by the addition polymerization of ethylene gas. There are many variants of PE, with the linear low density one possessing adequate melt strength for processing at high temperatures and shear, while maintaining high mechanical compliance in the solid crystalline state. The PE selected was LL8555 manufactured by ExxonMobil Chemicals.

Polyvinylidene fluoride (PVDF) is a highly non-reactive fluorinated hydrocarbon that consists of alternating vinyl and fluoride arrangement on the backbone carbon chain. It has a low melting temperature compared to other flouropolymers while having a high crystallinity, modulus and strength. Moreover, PVDF has one of the highest dielectric constant for polymers and some of its allotropes are piezoelectric, although they require further processing. The PVDF selected was Kynar 760 manufactured by Arkema Chemicals.

3.4 Nanoparticle Material Selection

Three nanoparticles were selected for evaluating the effect of nanoparticle shape and type on the electrical conduction and piezoresistance of conductive polymer composites. The nanoparticles selected were Singlewall Carbon Nanotube (SWNT), Multiwall Carbon Nanotube (MWNT) and Graphene

Nanoplatelets (GNP). The selected nanoparticles have distinct structures and as result provide a variety of physical properties listed in Table 3.2.

Table 3.2. Physical properties of the carbon nanoparticles investigated.

Property	SWNT [57]	MWNT [58]	GNP [59]
Density, ρ (g/cm^3)	2.1	2.1	2
Carbon Purity (%)	90	90	-
Diameter/Thickness, d (nm)	1-2	10-20	10
Length, L (μm)	5-30	10-30	5-25
Minimum Aspect Ratio [L/d]	2500	500	500
Surface Area (m^2/g)	400	250	100
Electrical Conductivity (S/m)	100	100	-

Single-wall carbon nanotubes (SWNT) were selected (Figure 3.2a) for their large aspect ratio and high surface area, providing a structural contrast to the Multiwall Carbon Nanotube (MWNT). The SWNT consist of a single layer of graphene roll about 1-2 nm thick and 5 to 30 μm in length, however inter-tube Van der Waal interactions mean that bundles or ropes of up to 10 SWNT can form. The processing of SWNT is usually done by arc-discharge process and involved significant purification steps, therefore SWNT costs are much higher (~ $100/g) than MWNT or GNP. The SWNT were purchased from Cheaptubes Inc (Battleboro, VT).
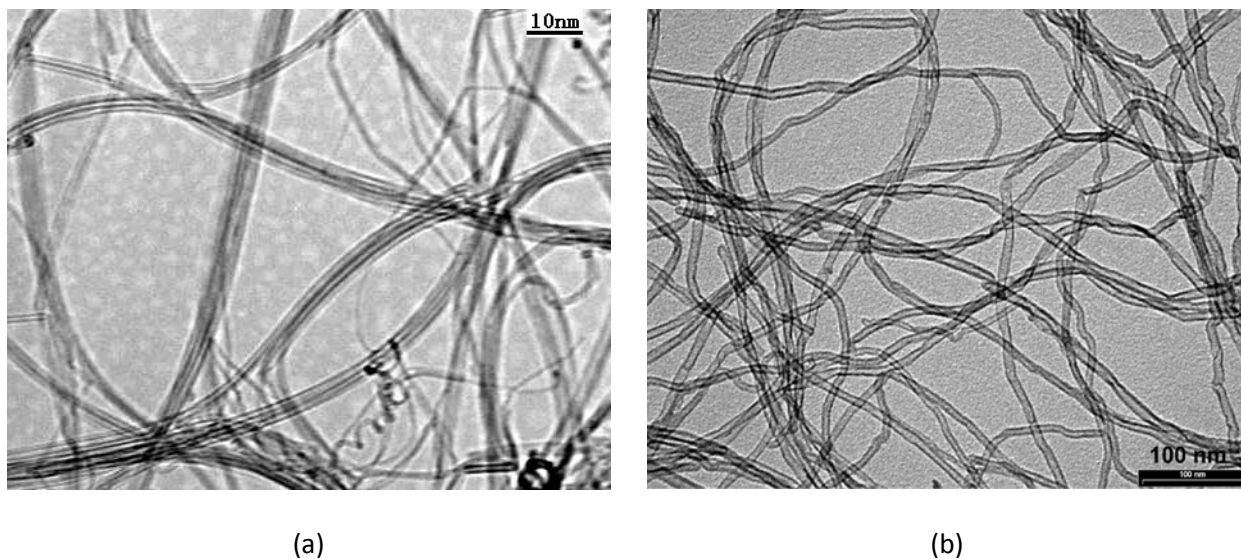
Figure 3.2. Transmission electron micrographs of SWNT (a) and MWNT (b) nanoparticles.

Thin Multiwall Carbon Nanotubes (MWNT) were selected (Figure 3.2b) with intermediate aspect ratio in order to provide a contrast to SWNT. The diameter of MWNT (10-20 nm) was much larger than the SWNT, while their lengths were about the same. The MWNT were produced from a catalytic chemical vapor deposition process and as a result had some heavy metal oxide impurities (~ 10%). The MWNT employed were NC7000 produced from Nanocyl S.A. (Belgium).

Graphene nanoplatelets (GNP) were selected in order to provide a geometrical contrast to the two carbon nanotube variants. A GNP particle (Figure 3.3) is around 10 nm thick, consisting of several layers of graphene, and can be anywhere between 5 and 25 μm in diameter. The particles have a surface area of approximately 100 m^2/g and a density of 2 g/cm^3. The GNP (grade 2) were acquired from Cheaptubes Inc. (Battleboro, VT).

<div align="center">(a)　　　　　　　　　　　　　　　　　(b)</div>
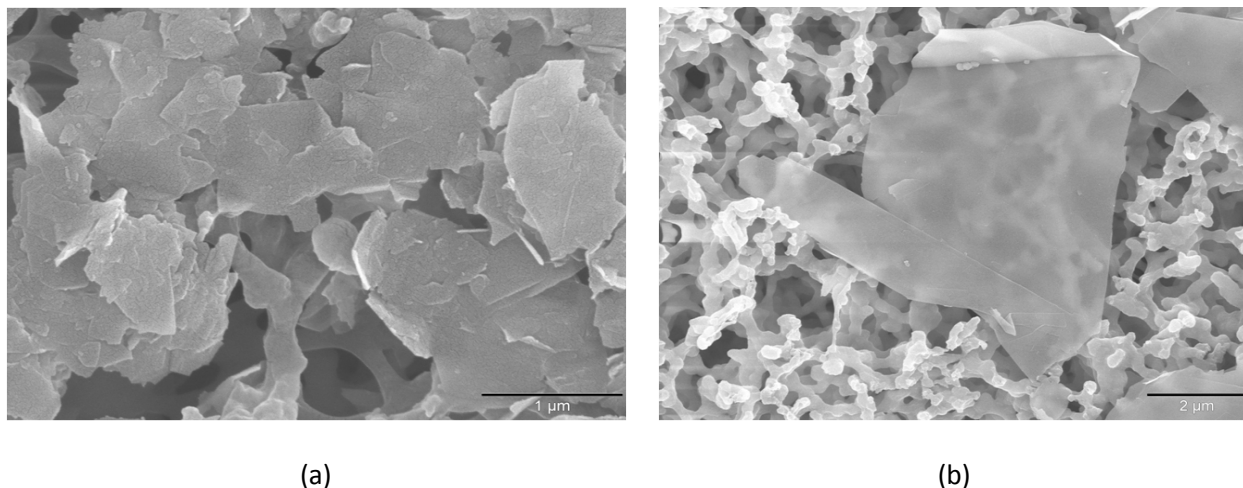
Figure 3.3. Scanning electron micrographs of multiple (a) and single (b) graphene nanoplatelet.

3.5 Nanocomposite Fabrication Process

Polymer nanocomposites containing various filler concentration were prepared using twin screw melt compounding. The amount of filler particles were measured on a weight basis and blended with the polymer amount in a DSM Xplore 15 mL twin-screw, co-rotating, bench-top micro-compounder (Dutch State Mines, The Neatherlands). The high shear mixing process was performed at 200 rpm and 200 °C (220 °C for PVDF) for total process time of 10 min. Due to thermal degradation concerns, the TPU nanocomposites were processed in an inert N_2 gas environment. For property characterization, the extruded material was pelletized and compression molded into a disc geometry (12.5 mm dia, 1.6 mm thick) on a Model 4386 hot press (Carver Inc, IN) operated at a temperature of 200 °C for a melt time of 5 min and a pressure of 1.3 MPa for 5 min.

3.6 Nanocomposite Characterization Techniques

Prior to all electrical testing, the two surfaces of the conductive polymer composite samples were cleaned with ethanol, dried and sputter-coated with Platinum. This reduces the effects of contact resistance, which can be a significant measurement artifact, especially in 2-probe techniques. Electrical properties of the nanocomposites were measured using dielectric impedance spectroscopy on a Alpha-n

spectrometer (Novocontrol Technologies, Hundsangen, Germany). This technique measures the impedance of the sample by measuring the current at 1 V_{rms} and at frequencies ranging from 10^{-1} to 10^5 Hz. The real and imaginary components of impedance data can be fit to an equivalent RC circuit in order to obtain the sample's electrical conductivity and permittivity. The real component of the electrical conductivity at 10^{-1} Hz is used as the measure of the samples. The rheological properties of the conductive polymer composites were measured using a dynamic strain controlled Ares rheometer (TA Instruments, New Castle, DE) operated at 2% strain, sweeping between a frequency of 10^{-1} Hz to 79 Hz at a temperature of 200°C (225° C for PVDF composites).

The piezoresistive behavior of the conductive polymer composites under compression was observed through the use of a high precision source meter (model 2400, Keithley Instruments Inc. – Cleveland OH) in a two-wire resistance measurement configuration coupled with a micro-testing system (model AG-I 50KN, Shimadzu – Kyoto, Japan) reading resistance and stress information to a National Instrument's LabView data acquisition system (Figure 3.4). The disc samples for compressive piezoresistance characterization were platinum sputter-coated, placed between two copper electrodes, which were electrically insulated on the opposite side and sandwiched between the compressing platens. The piezoresistance of the composites was observed under conditions of quasi-static compression with a pre-load force of 100N. For compression experiments the samples (three or more) were compressed at 0.1 mm/min (strain rate ~ 0.001 s^{-1}). Three or more samples were used for all electrical and piezoresistance testing and averaged.

The morphology of the nano-filler and nanocomposites was observed using Atomic Force Microscopy (AFM; model Multimode 8, Bruker Nanosystems – Santa Barbara, CA) and Scanning Electron Microscopy (SEM; model JSM 6060, JEOL Ltd – Tokyo, Japan). Cross section SEM images were obtained by freeze-fracturing and platinum coating the nanocomposites. X-ray diffraction (Kα-Cu XRD; model

34

D5000, Siemens AG – Munich, Germany) of the nanoparticles and the nanocomposites was measured, with the beam incident to the transverse direction of the nanocomposite.
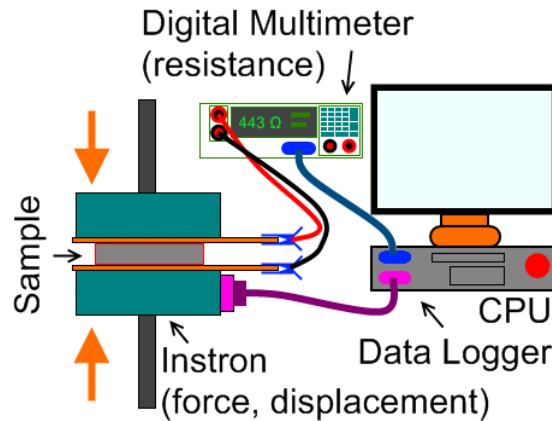
Figure 3.4. Schematic of the custom electromechanical setup used for piezoresistance characterization.

3.7 Summary

The approach and methodology for developing piezoresistive nanocomposites has been outlined. The framework for a comprehensive study investigating the effect of matrix and filler nanoparticles on the percolation and piezoresistance is provided. Furthermore, the piezoresistance response in elastic and plastic deformation will be compared along with the effect of a porous internal structure. The fabrication techniques, including details of the twin screw compounding process employed, are detailed here. Finally, the electrical, rheological, morphology and piezoresistance characterization techniques are discussed. The proceeding chapters will detail the results and the analysis of these characterization techniques.

4 Piezoresistive Polyethylene Nanocomposites: Influence of Filler

4.1 Introduction

The focus of this chapter is to characterize the influence of filler on the percolation and piezoresistance of conductive polymer composites. This is done by examining polyethylene (PE) composites containing single-wall carbon nanotube (SWNT), multi-wall carbon nanotube (MWNT) and graphene nanoplatelets (GNP), which were dispersed in PE through melt blending in concentrations ranging between 0.5-10 wt%. The dispersion and nanocomposite morphology were investigated using SEM and X-ray diffraction with strong evidence found for shear-induced orientation of GNP nanoparticles during the compression molding process. The conductivity and permittivity of the composite materials was investigated using impedance spectroscopy and the lowest percolation threshold and highest electrical conductivity was observed for SWNT composites, followed by MWNT and GNP. The compressive piezoresistance of the nanocomposites was measured and the initial, elastic and plastic deformation regions were all identifiable by the resistance measurements. The piezoresistance response for MWNT nanocomposites had a non-monotonous filler content dependence indicating an evolving filler network as more filler are added to the nanocomposite. In contrast, the piezoresistance response of the SWNT nanocomposite was monotonic suggesting a static state of filler network at varying stress and filler content.

4.2 Nanocomposite Morphology Analysis

A clear insight of GNP and MWNT nanoparticle morphology was obtained using AFM imaging (Figure 4.1a and 4.1b respectively). The GNP filler consists of stacked platelet-like morphology with steps between platelets clearly evident, while entangled nanotube features are visible in the MWNT filler. Features similar to those observed for the nanoparticles by AFM are evident in the nanocomposites

observed by SEM. Freeze-fractured cross sections of 6 wt% MWNT- and 6 wt% SWNT- PE nanocomposites are shown in Figures 4.2a and 4.2b respectively, after the melt blending and compression molding process. The fibrous features in both MWNT and SWNT nanocomposites appear randomly dispersed, with no large scale aggregates apparent for either material. Figure 4.3 depicts the SEM micrographs of 6 wt% GNP nanocomposites, which have distinct morphologies before (Figure 4.3a-c) and after (Figure 4.3d-f) compression molding. The platelet like GNP features in the nanocomposites are well dispersed in both situations however the GNP particles become oriented orthogonal to the direction of compression during the compression molding process. This indicates significant shear induced alignment of the nanoparticles during compression molding of the GNP nanocomposites.

(a)   (b)
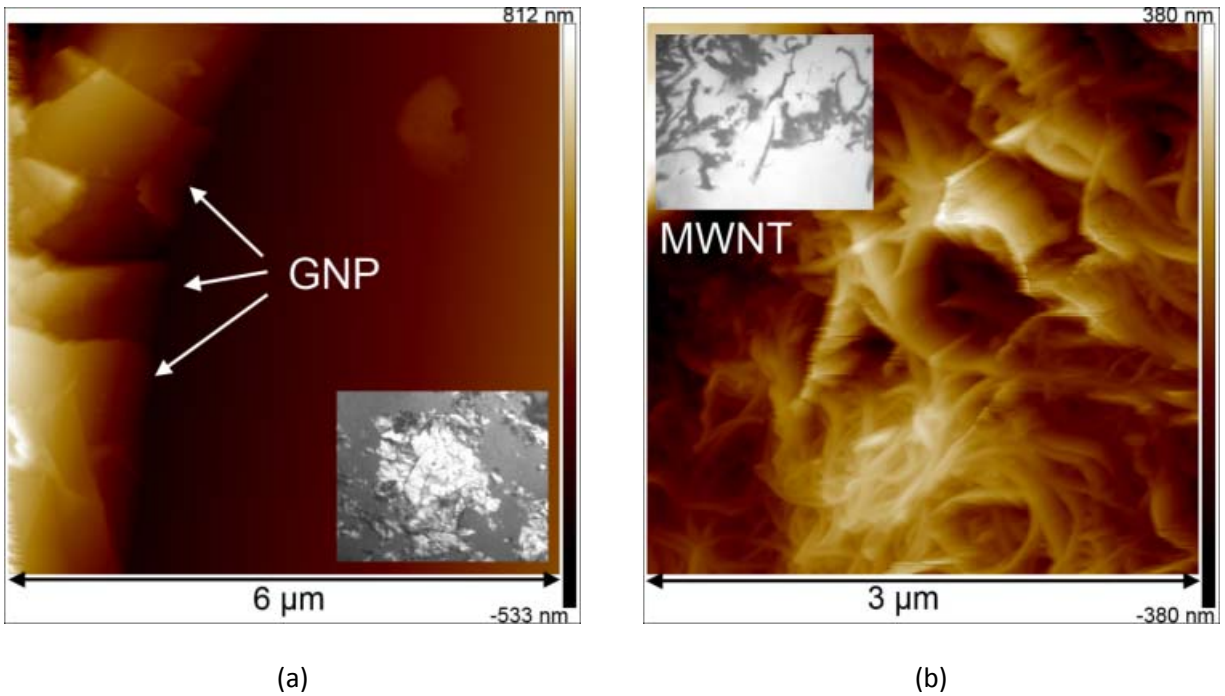
Figure 4.1. Structure of GNP (a) and MWNT (b) as revealed by height image in Atomic Force Microscopy. Inset is the optical image of the filler particles. The layered and tubular structure for the GNP and MWNT, respectively, is clearly distinguishable.
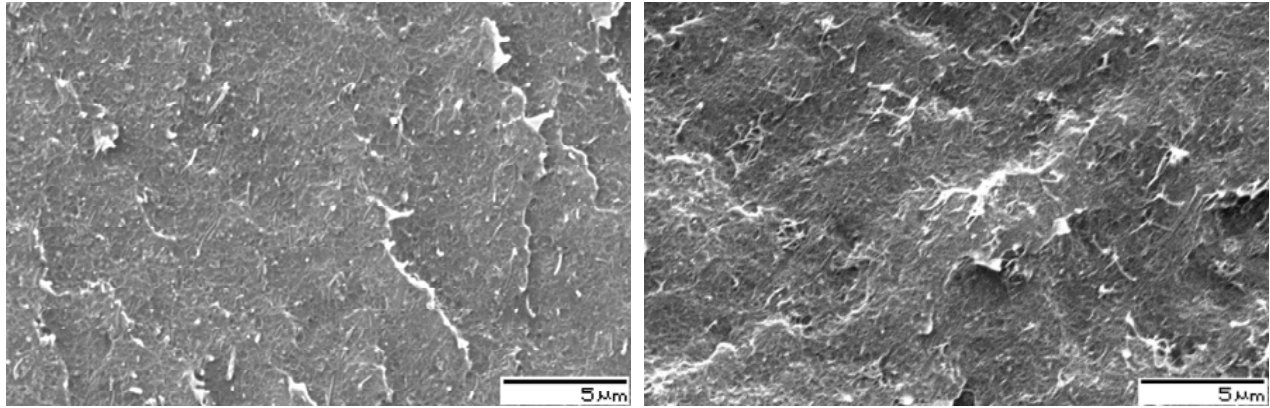
<div align="center">(a)   (b)</div>

Figure 4.2. Scanning electron micrographs of 6 wt% (a) PE-MWNT and (b) PE-SWNT nanocomposites.

The morphology of the nanoparticle powders and nanocomposites was elucidated further using XRD analysis. Figure 4.4a-c show the X-ray diffraction spectrum, measured in the direction of processing, of PE-MWNT, -SWNT and -GNP, respectively. It can be seen from these spectra, that the graphitic (002) peak for the three nanoparticles analyzed in this study occurs at approximately 26° and is the most intense for GNP followed by MWNT and then SWNT. This indicates a greater degree of order of the graphitic structure [60] in the GNP particles followed by that in MWNT and then SWNT particles. Graphene Nanoplatelets consist of 10-15 nm thick stacks of graphene sheets, which extend across in-plane for a few micrometers. In contrast MWNT are concentric arrangements of graphene sheets rolled into a tube, while SWNT are rolls of single graphene sheets with significant amounts of amorphous carbons present as well from the manufacturing process [61].
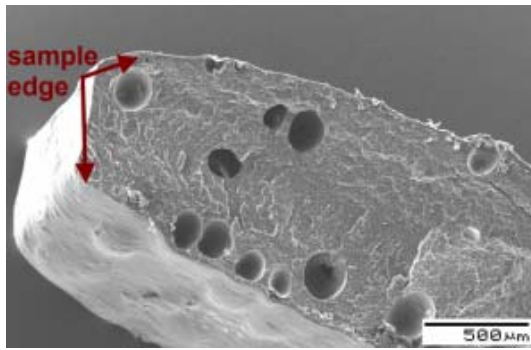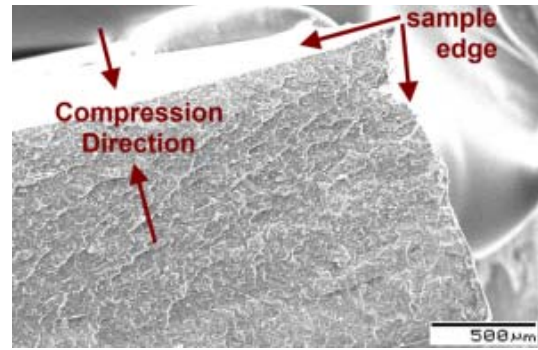
(a)   (d)
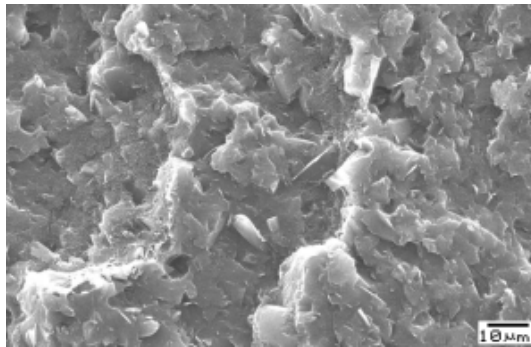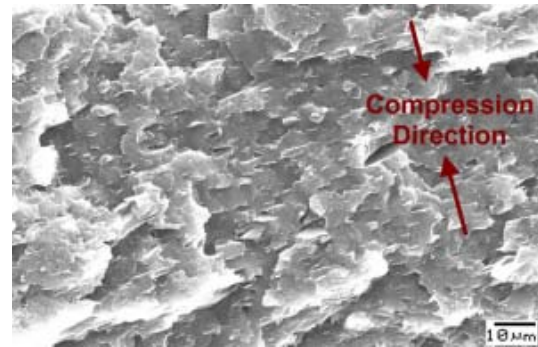
(b)   (e)
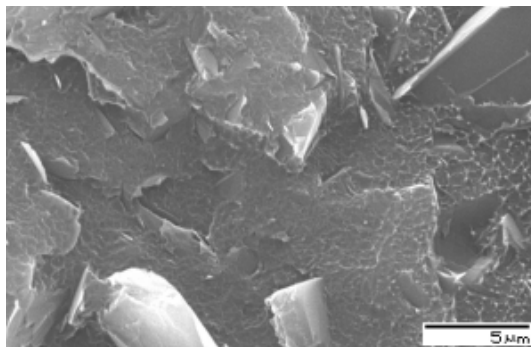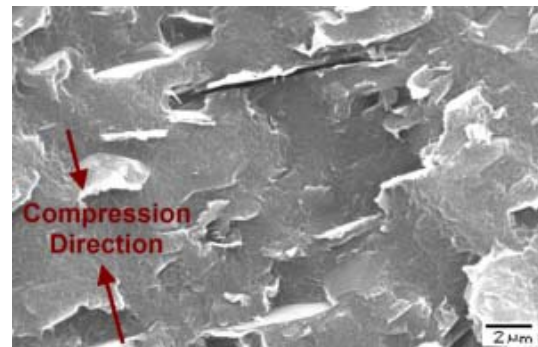
(c)   (f)

Figure 4.3. The SEM morphologies of 6 wt% GNP nanocomposites at various magnifications after

extrusion (a, b, c) and after extrusion proceeded with compression molding (d, e, f). The orientation of

GNP nanoparticles after compression molding is evident.

| (a) | (b) | (c) |
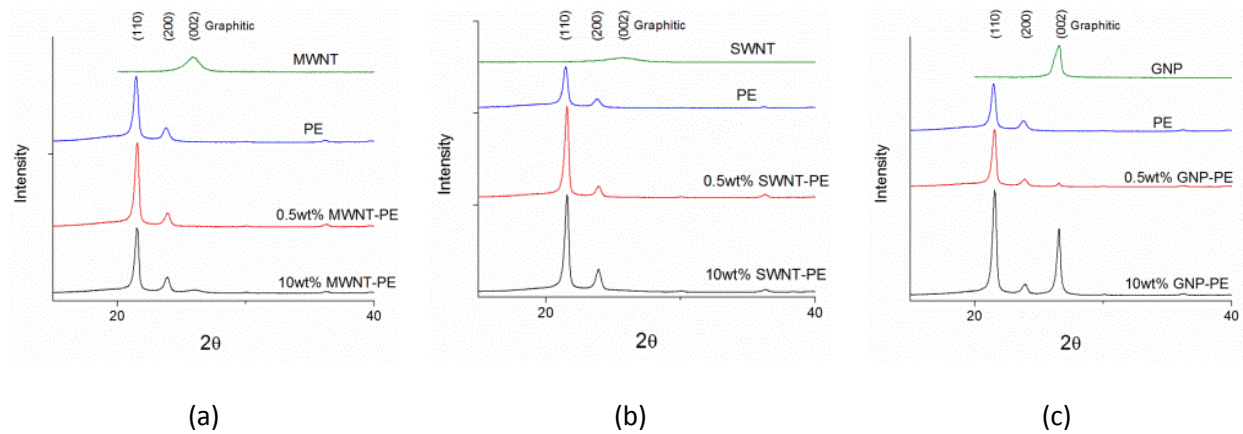
Figure 4.4. XRD spectrographs for (a) SWNT, (b) MWNT, (c) GNP fillers and nanocomposites containing

0.5 and 10 wt% filler. The (110) and (200) peaks for PE, along with the (002) peak for graphitic

nanomaterials are identified.

The X-ray diffraction spectrum of neat PE consists of strong (110) and (200) diffraction peaks indicating the orthorhombic unit cell [62]. Addition of just 0.5 wt% of nanoparticles (MWNT, SWNT, GNP) is sufficient to increase the PE peak intensity. The greater intensities and peak areas in the nanocomposites indicate preferred crystal orientations as well as increased crystallinity in the presence of nanomaterials. The high surface area and aspect ratio of the all three nanomaterials (MWNT, SWNT and GNP) provide a large number of surfaces for PE crystals to heterogeneously nucleate. This was confirmed by faster crystallization kinetics and lower crystallization temperatures by differential scanning calorimeter (DSC) measurements.

A significant observation from the X-ray diffraction spectrums is the evolution of the (002) graphitic peak in the MWNT and GNP nanocomposites at 26°, indicating the diffraction of the filler particles inside the nanocomposite. This peak is absent from SWNT nanocomposites as the graphitic order of SWNT is weak in comparison to MWNT and GNP. In addition, the (002) graphite peak intensity of 10 wt% GNP nanocomposites is greater than that for GNP powder. Such a nanocomposite diffraction

signal would be obtained if platelet orientations were orthogonal to the beam direction, which is also the compression direction during processing. This provides further credence to the SEM observation (Figure 4.3) of platelet orientation orthogonal to the compression molding direction.

4.3 Electrical Properties of Polyethylene Nanocomposites

Dielectric impedance spectroscopy (DIS) was used to characterize the electrical conductivity as well as the dielectric permittivity of the Polyethylene nanocomposites filled with various carbon nanoparticles. DIS is used to measure the impedance of the composites at various frequencies and then estimate the conductivity and permittivity of the material through modeling the data to an R-C circuit in parallel [63]. Figure 4.5a, shows the real component of electrical conductivity data for PE-MWNT nanocomposites. The conductivity-frequency response of other nanocomposite systems (PE-GNP and PE-SWNT) had a response similar to that of PE-MWNT (Figure 4.5a). The electrical conductivity of neat PE is dependent on the applied frequency which at 0.1 Hz is 10^{-15} S/cm, indicative of an insulating behavior. By incorporating 0.5 wt% MWNT filler content, the electrical conductivity is improved but is still insulating. At 3.0 wt% MWNT filler content, the electrical conductivity is 10^{-6} S/cm, independent of frequency and is now electronically conducting indicating the establishment of interparticle contacts between MWNT embedded in the matrix. At 10 wt% MWNT, a maximum conductivity of 1.1×10^{-4} S/cm is achieved which is within the minimum value of 10^{-5} S/cm required for electrostatic discharge (ESD) material applications [64, 65].
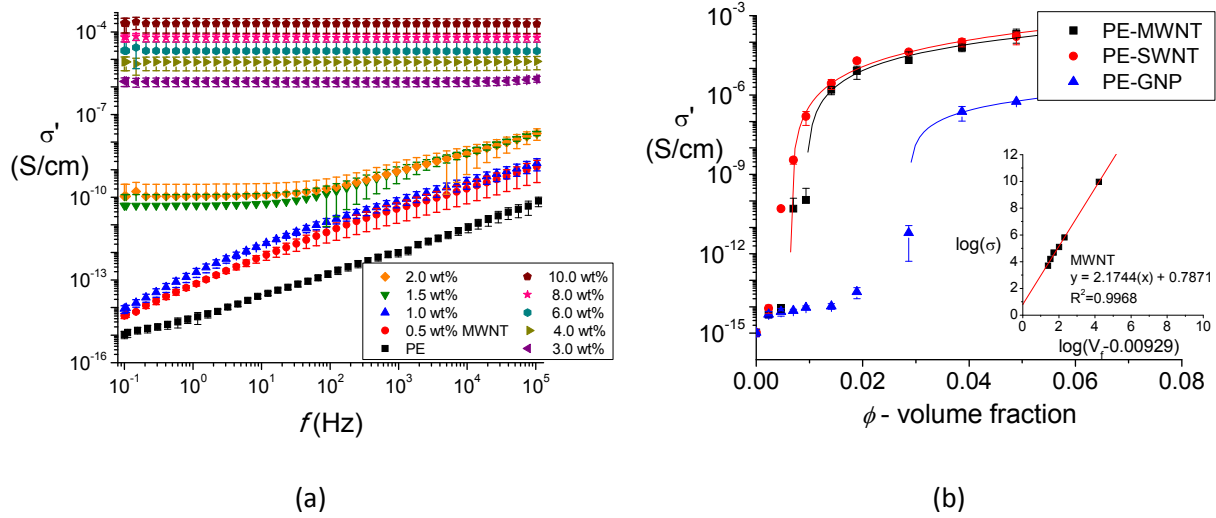
Figure 4.5. Real electrical conductivity vs applied frequency plot (a) of PE-MWNT nanocomposites at varying contents, and electrical conductivity vs. volume fraction plot (b) of PE-MWNT, -SWNT and -GNP nanocomposites at 0.1 Hz. The solid lines in (b) are the fit to the statistical percolation model (Equation 2.1) and the inset shows a sample optimization results for MWNT.

The conductivity for all three nanoparticle fillers at 0.1 Hz is plotted with respect to the particulate volume fraction content in Figure 4.5b. The fits to the power-law form of statistical percolation (Equation 2.1 - $\sigma \propto (\phi - \phi_c)^t$) are shown as the solid lines in Figure 4.5b and the results are summarized in Table 4.1. The percolation threshold concentration for PE-MWNT nanocomposites, according to Equation 2.1, was found to be 2.0 wt% (0.9 vol.%). The SWNT nanocomposites had a threshold concentration of 1.4 wt% (0.6 vol.%) and a maximum conductivity of 1.6×10^{-4} S/cm at 10 wt%. Nanocomposites containing SWNT, owing to their smaller diameters and superior electrical transport properties [66], have a slightly lower percolation point (0.6 vs. 0.9 vol%) and a higher maximum conductivity (1.6×10^{-4} vs. 1.1×10^{-4} S/cm) than MWNT nanocomposites. The percolation point values for MWNT (2 wt%) and SWNT (1.4 wt%) achieved through melt blending in this study are lower than those

achieved in other studies for MWNT (7.5 wt% [60] and 8 wt% [25]) and SWNT (4 wt% [67]) based polyethylene nanocomposites. Solvent casting [68] or fiber drawing [69] of PE-nanocomposites can provide lower percolation values (<0.6 wt%) however the fabrication approach is complex preventing its manufacturing scale-up.

Table 4.1. Results from the fit to the power-law statistical percolation model.

	σ_0 (S/cm)	ϕ_0 (vol. frac)	ϕ_0 (wt%)	t	R^2
MWNT	1.63×10^{-1}	0.0093	1.99	2.17	0.997
SWNT	7.06×10^{-1}	0.0064	1.38	2.56	0.991
GNP	1.25×10^{-4}	0.0287	5.99	1.37	0.999

In contrast to the SWNT and MWNT nanocomposites, the GNP nanocomposites had a much higher threshold concentration of 6 wt% (2.9 vol.%) and a lower maximum conductivity of 5.6×10^{-7} S/cm at 10 wt%. The higher threshold concentration along with the low maximum conductivity for GNP nanocomposites is attributed to the alignment of GNP particles during processing as confirmed by SEM (Figure 4.3) and XRD (Figure 4.4c). The oriented graphene sheets lie in the compression (measurement) plane allowing for fewer interparticle contacts in the transverse direction. The alignment of GNP is caused by large rotational moments from shear flow during processing. The rotational moments are due to the high surface area per particle, as well as the high stiffness of GNP particles. In contrast, MWNT and SWNT particles are flexible tubes with less surface area per particle. As a result, they do not get influenced to that extent by shear flow and the particles remain randomly oriented explaining their lower percolation thresholds.
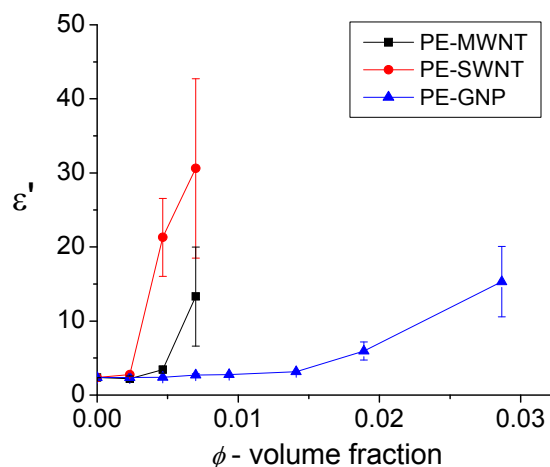
Figure 4.6. Plot of Real permittivity vs volume fraction for PE-MWNT, -SWNT and –GNP nanocomposites

at 0.1 Hz.

The effect of various carbon based nanoparticles on the permittivity of PE is shown in Figure 4.6. The permittivity of neat PE as measured by dielectric impedance spectroscopy at 0.1 Hz is 2.3. Addition of nanoparticles leads to an increase in polyethylene's permittivity which indicates a greater ability to store charge (higher capacitance). Increased permittivity in filled materials is observed because of a greater number of interfaces (surface area) allowing for greater sites for charge storage. The increased permittivity is also accompanied with greater dielectric losses due to the charging-discharging events at these interfaces. It is for this reason that materials exhibiting this effect are known as artificial dielectrics. The maximum permittivity for PE-MWNT nanocomposites is 13.3, which occurs at 1.5 wt% MWNT content; beyond this concentration, an electrically conductive filler particle network forms and the material loses its dielectric characteristic. Nanocomposites of SWNT had a much higher permittivity of 30.6 at 1.5 wt% SWNT content. The higher permittivity observed in SWNT nanocomposites is associated with the higher surface area of SWNT particles, allowing for greater quantity of charge to be stored at the particle-polymer interface. Nanocomposites of GNP did not show any appreciable

44

improvements in permittivity until 4 wt% while the maximum achieved was 15.3 at 6 wt%. This reduced dielectric performance is caused by the shear induced alignment (Figure 4.3) of the GNP particles in the nanocomposites, which decreases the effective number of particulates in contact with the sample-electrode surface resulting in a lower capacitance.

4.4 Piezoresistance of Polyethylene Nanocomposites

The compressive piezoresistance of the MWNT and SWNT filled PE nanocomposites was measured in quasi-static conditions at a strain rate of 0.1 mm/min (0.001 s^{-1}). The GNP nanocomposites did not possess sufficient DC conductivity ($\rho \approx 10$ GΩ) to be accurately measured using the custom source-meter setup. The absolute resistance, relative resistance and strain plots with respect to applied stress are depicted in Figure 4.7a-c and Figure 4.8a-c for MWNT and SWNT, respectively. These plots represent the average response of three or more samples. The resistance-stress behavior of these nanocomposites can be sub-divided into three basic regions. The first (initial) region is where a well-defined electrical contact is established through removal of mechanical slack between the compressing platens and the sample. Most of the resistance change occurs in this region for all cases of filler type and filler content. It can be observed from the strain-stress plots (Figure 4.7c and 4.8c), that this initial region terminates in the first 5 MPa of applied pressure indicating all of the slack has been overcome.

The second region of compressive deformation is where elastic compression takes place. This region occurs at stresses greater than 5 MPa and is characterized by a linear strain-stress behavior (Figure 4.7c and 4.8c). The resistance signal in this region continues to decrease, however, at a slower rate than the initial contact region. The third deformation region, which is observed in MWNT nanocomposites, is the plastic deformation zone. This occurs where the strain-stress curve begins to yield (softening), at around 30 MPa. In the plastic deformation region, the nanocomposite piezoresistance is dependent on the MWNT content, where at low MWNT content (3, 4 and 6 wt%) the

resistance is found to be increasing with respect to stress. In contrast, at high MWNT content (8 and 10 wt%), the resistance continues to undergo further decrease with respect to stress.

(a)

(b)

(c)
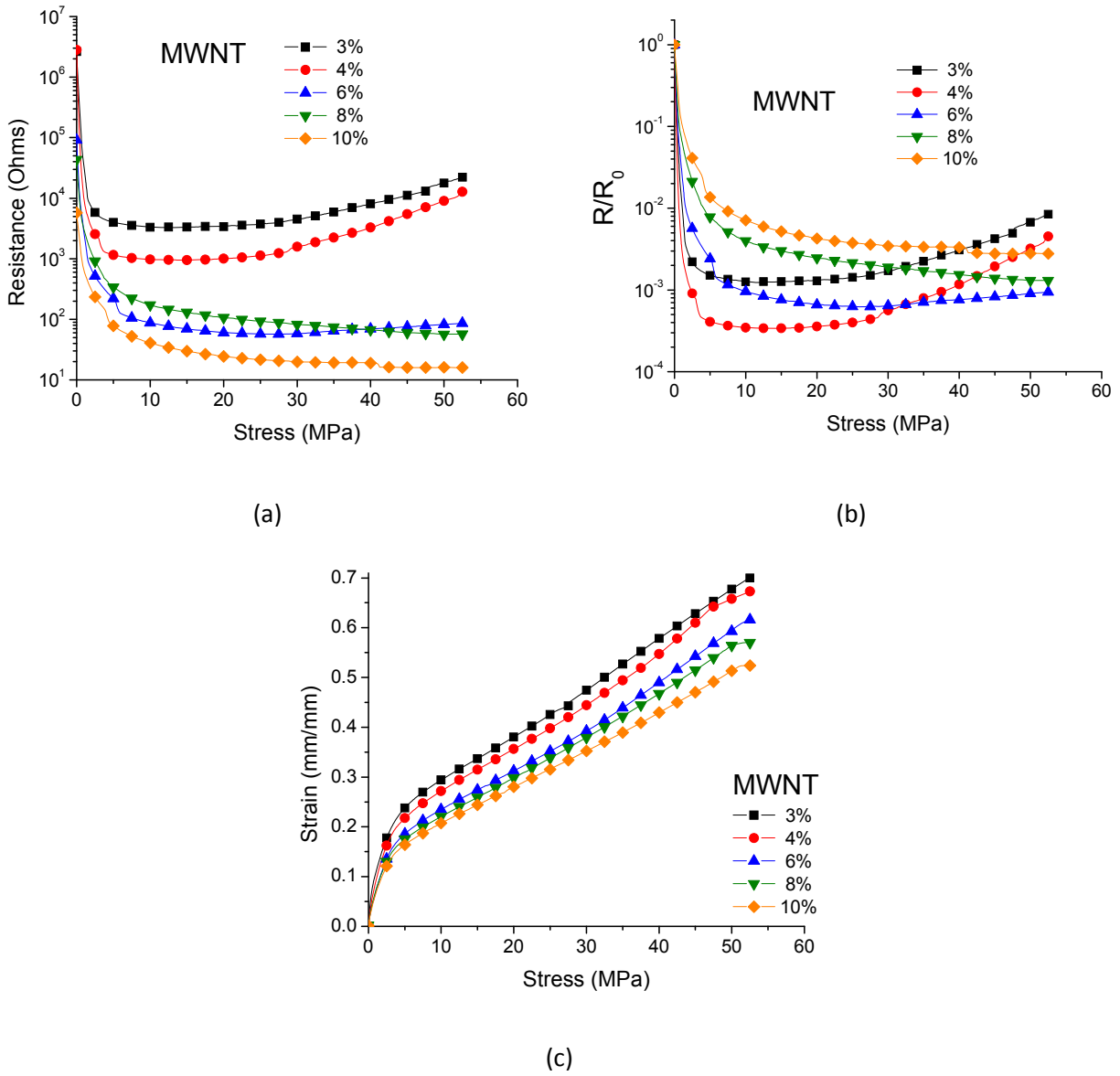
Figure 4.7. High stress piezoresistance for PE-MWNT nanocomposite depicted by the (a) absolute resistance-stress, (b) relative resistance-stress plots and (c) the corresponding strain-stress plot.
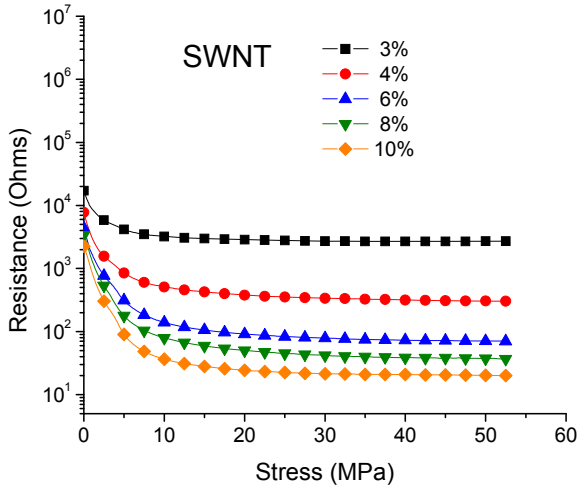
(a)
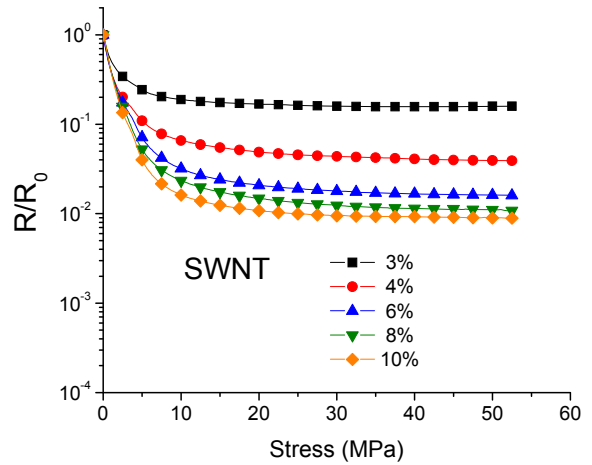
(b)
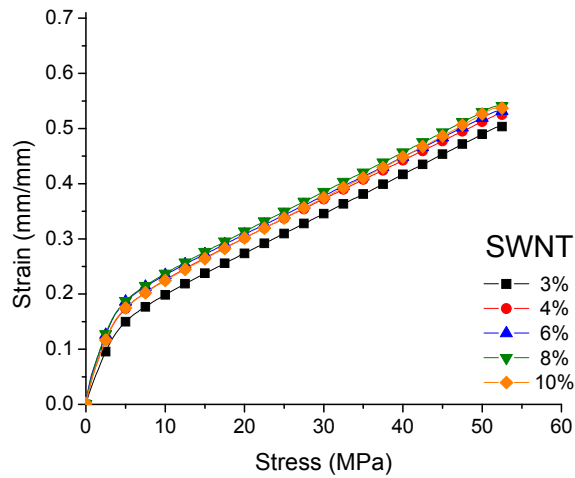
(c)

Figure 4.8. High stress piezoresistance for PE-MWNT nanocomposite depicted by the (a) absolute resistance-stress, (b) relative resistance-stress plots and (c) the corresponding strain-stress plot.

The aforementioned observations suggest that the resistance-stress dependence in PE-nanocomposites is non-linear and non-monotonous. It does however, correlate well with the different stages of deformation (initial, elastic and plastic) observed on the strain-stress curve (Figure 4.7c and 4.8c). In order to compare the responses of PE nanocomposites of different filler content and hence

different conductivities, a relative resistance response (Figure 4.7b and 4.8b) must be considered, where the resistance is plotted as a ratio of the initial resistance at the point of first contact. At low MWNT contents (3 and 4 wt%) the relative resistance displays the sharpest decrease (higher sensitivity) during the initial deformation region, after which it exhibits a gradual decrease during the elastic deformation and then finally a gradual increase during plastic deformation. The intermediate 6 wt% MWNT nanocomposite system displays a similar trend albeit with a weaker effect. The higher MWNT content (8 and 10 wt%) nanocomposites have a more gradual resistance decrease during the initial deformation which continues on into the elastic region. In contrast to MWNT, the SWNT nanocomposites display a greater resistance decrease (sensitivity) with increasing filler content (Figure 4.8b). Moreover, the bulk of the resistance decrease occurs during the initial deformation while remaining relatively unchanged during the elastic deformation process.

The effect of concentration and stress on the relative resistance change of the MWNT and SWNT nanocomposites has been depicted in surface plots in Figure 4.9a and 4.9b, respectively. Nanocomposites containing low MWNT content (3 and 4 wt%) exhibit significant resistance change (sensitivity) with relative resistances decreasing at low stresses (<5 MPa), and increasing at high stresses (30 MPa). In contrast, the higher MWNT content systems undergo a very minor resistance change at high stresses with most of the change occurring during the initial deformation region. The concentration-stress dependence of piezoresistance in SWNT nanocomposites is simpler in comparison to MWNT nanocomposites. At stresses less than 5 MPa, there is a small change in the relative resistance with respect to the filler content. At higher stresses (>30 MPa), the relative resistance signal shows negligible dependence with respect to stress, while showing a significant dependence with respect to filler content.

The different piezoresistance response between the MWNT and SWNT nanocomposites can be understood by the morphology of the materials and in particular how the filler particles are arranged in

the polymer matrix. It should be pointed out that both types of materials were processed in exactly the same manner and have a similar electrical conductivity response (Figure 4.5b). Although the shear-based mixing method is effective in promoting better dispersion for both nanocomposite systems, the smaller particle size, greater surface area and superior electrical properties of the SWNT particles contribute to a more resilient particulate network in SWNT nanocomposites. The larger surface area and aspect ratio of SWNT nanoparticles would provide more contact sites in the electrical network, manifested as a lower percolation threshold concentration (Table 4.1), and result in a more stable network during the course of deformation.

(a)

(b)

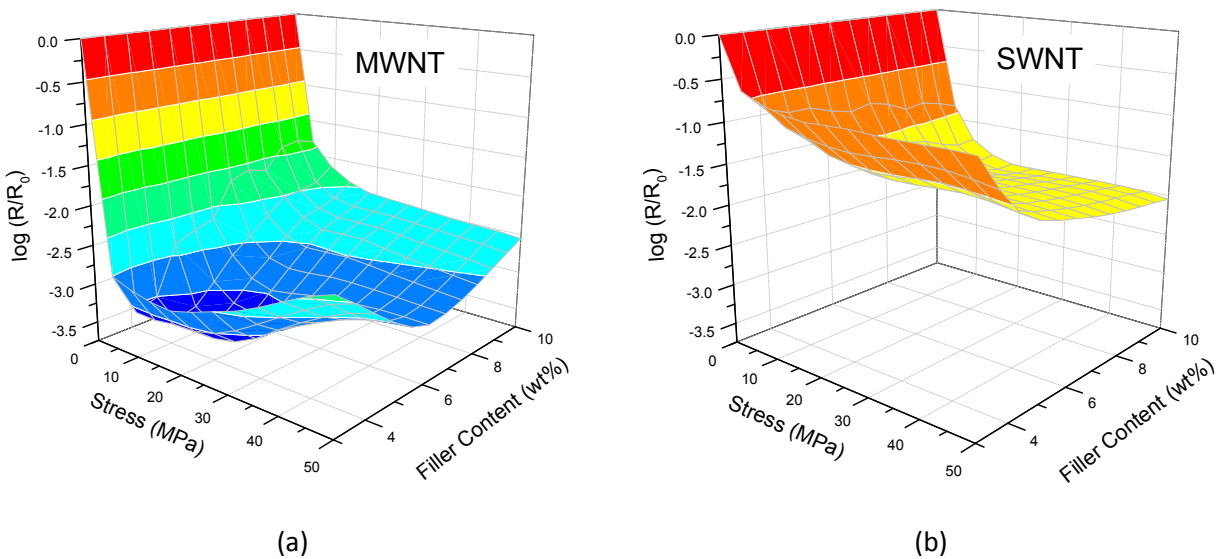**Figure 4.9.** Surface plot mapping the filler-stress-relative resistance interdependence of PE-MWNT (a) and PE-SWNT (b) nanocomposites.

The contrasting piezoresistance behavior between both filler types (SWNT and MWNT) can be suitable for several different applications. For example, there is a strong demand in flexible electronics applications for materials which exhibit little-to-no resistance change when deformed [11], therefore

preventing the circuit impedances from changing during operation. The SWNT-PE nanocomposites could be ideally suited for such an application since they have a high and stable conductivity with respect to stress. The high filler content (8 and 10 wt%) MWNT nanocomposites could be potential candidates for any load/pressure sensing. These nanocomposites have a fast initial resistance decrease followed by a gradual decrease during the elastic deformation process. This study elucidates the effect of filler type, content and stress in conductive PE nanocomposite systems and can be used for further investigations, into the piezoresistive behavior (including time response and hysteresis) of conductive composites and their applicability in pressure sensing.

4.5 Summary

The morphology, electrical properties and piezoresistive behavior of polyethylene (PE) nanocomposites containing different types of carbon nano-particle fillers has been reported here. The fillers investigated were single-wall carbon nanotube (SWNT), multi-wall carbon nanotube (MWNT) and graphene nanoplatelets (GNP), which were dispersed in PE through melt blending in concentrations ranging between 0.5-10 wt%. Morphology analysis using SEM and XRD indicated dispersion of all three filler types. It was found that GNP particles in the PE matrix were subject to significant shear-induced alignment during the molding process. The electrical conductivity of the nanocomposites was correlated to the observed morphologies, with randomly dispersed systems (MWNT, SWNT) providing low percolation threshold values. The lowest percolation threshold achieved was in SWNT nanocomposites (1.4 wt%) which was attributed to their longer aspect ratio and surface area, and therefore greater ability to form contacts in a networked arrangement. Nanocomposites containing GNP exhibited the lowest electrical conductivity and the highest percolation threshold. The low conductivity of GNP nanocomposites meant they were not suitable for further piezoresistance testing and use as sensing materials for biomechanical measurements. The compressive piezoresistance of the nanocomposites

was measured and the initial, elastic and plastic deformation regions were identifiable by resistance measurements. The piezoresistance response for MWNT based materials had a strong filler content and stress dependence indicating an evolving filler network as filler and stress amounts are varied. In contrast, the piezoresistance response of the SWNT nanocomposite was stable indicating a consistent networked state of particles.

5 Piezoresistive Fluoropolymer Composites: Plastic Deformation

5.1 Introduction

This chapter examines the fabrication of fluoro-polymer based piezoresistive nanocomposites for pressure sensing applications and their characterization, particularly when plastically deformed. The matrix material employed was Polyvinylidene Fluoride (PVDF) which was reinforced with conductive multiwall carbon nanotubes (MWNT) particles, in order to form a conductive filler network throughout the nanocomposite. The composites were prepared by melt mixing the PVDF and conductive particles in compositions ranging from 0.25 to 10 wt% conductive particle in PVDF. The dielectric permittivity and electrical conductivity of the composites was characterized and the electrical percolation behavior of PVDF nanocomposites fitted to the statistical percolation model. The morphology of the filler networks in the PVDF nanocomposites was characterized and related to the electrical properties. The quasi-static piezoresistance of the nanocomposites in the elastic and plastic deformation regimes was characterized and the relationship between MWNT content and piezoresistance in plastic deformation is elucidated.

5.2 Nanocomposite Morphology Analysis

The morphology of the fabricated nanocomposites was characterized using SEM. Figure 5.1 shows the freeze-fractured cross-section morphologies of PVDF and its nanocomposites containing 0.25, 1.5 and 6 wt% MWNT. The MWNT are apparent upon comparison of the neat PVDF morphology with that of its nanocomposites. At 0.25 wt% MWNT (Figure 5.1b) content, the MWNT are dispersed uniformly but are sparse and separated from each other on the order of several hundred nanometers. Further addition of MWNT to 1.5 wt% (Figure 5.1c) reveals a denser distribution of MWNT with shorter inter-particle

distances. A consequence of further MWNT addition is the initial evolution of aggregate particles with their locations being regions highlighted by greater intensity in the e-beam signal. At high MWNT concentrations, e.g. 6 wt% MWNT (Figure 5.1d), there is complete interconnectivity between MWNT particles. A greater degree of aggregation of MWNT particles is also present.
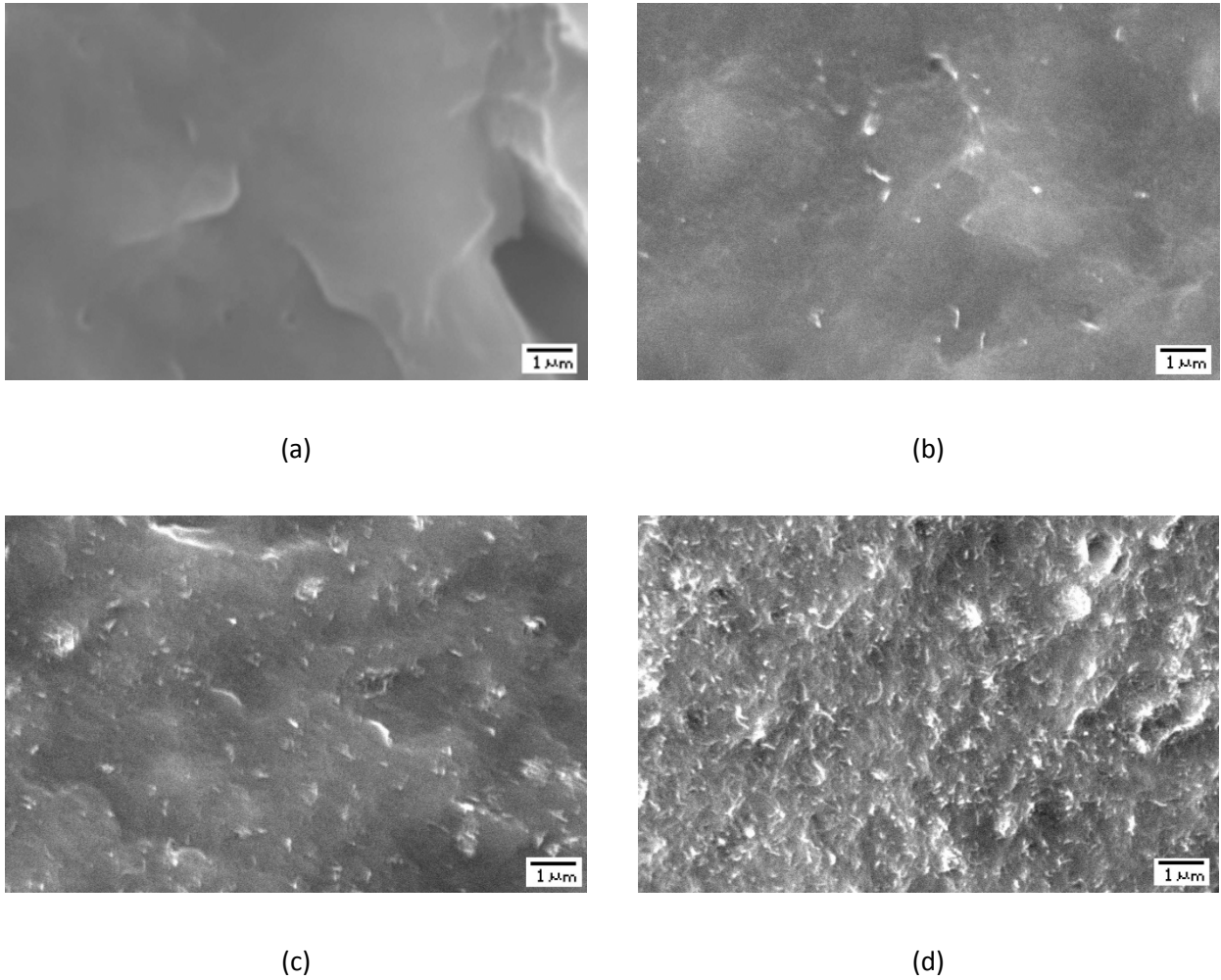

(a)

(b)

(c)

(d)

Figure 5.1. SEM Morphologies of (a) PVDF and (b) 0.25 wt%, (c) 1.5 wt%, (d) 6.0 wt% MWNT-PVDF nanocomposites.

The polymer PVDF exhibits polymorphism allowing it to exist in four different crystal structures based on the processing employed. The most commonly encountered phase during bulk processing of PVDF is the α-phase which consists of an alternating trans-gauche sequence. Due to the principle of superposition, the dipoles between the more electronegative fluorine atoms and the hydrogen atoms are cancelled out upon crystallization, resulting in the α-phase being non-polarizable. In contrast the β-phase consists of an all trans sequence resulting in a net dipole, thereby making it polarized. The piezoelectric phenomena in PVDF can be exploited if most β-phase crystals in PVDF can be polarized in a preferential direction. This can usually be done by large strain stretching of PVDF films while under the influence of an electric field. Furthermore, it has been shown in literature that presence of nanoparticles in thin PVDF cast films can result in β-phase formation and the ensuing piezoelectric effect [70]. Fourier Transform Infrared Spectroscopy was conducted on the PVDF-MWNT nanocomposites in order to determine the crystalline form of PVDF. Figure 5.2 shows the FTIR spectra of neat PVDF and PVDF-MWNT nanocomposites containing 0.25, 1, 4 and 10 wt% MWNT. The peaks on the spectra for the α-phase are prominent at 531, 613, 762 and 795 cm^{-1}, whereas in comparison the peaks indicating the β-phase (509 and 841 cm^{-1}) are significantly suppressed [71]. This indicates that based on the processing methods of melt compounding and compression molding employed to fabricate PVDF-MWNT nanocomposites, the α-phase preferentially forms. Therefore, no significant contribution of polarization and the piezoelectric phenomena is expected during the piezoresistive operation of the PVDF-MWNT nanocomposites.

5.3 Electrical Properties of PVDF-MWNT Nanocomposites

Dielectric impedance spectroscopy was used to characterize the electrical conductivity as well as the dielectric permittivity of the PVDF-MWNT nanocomposites filled with various MWNT content. Impedance spectroscopy is used to measure the impedance of the composite at various frequencies and

then estimate the conductivity and permittivity of the material through fitting the data to an Resistance-Capacitance circuit in parallel [63]. Figure 5.3a, shows the real electrical conductivity data for PVDF-MWNT nanocomposites. The electrical conductivity of neat PVDF is dependent on the applied frequency which at 0.1 Hz is 10^{-13} S/cm, indicative of an insulating behavior. By incorporating 0.25 and 0.5 wt% MWNT filler content, the electrical conductivity increases slightly but is still insulating. At 1.0 wt% MWNT filler content, the electrical conductivity is 10^{-9} S/cm, independent of frequency and is electronically conducting indicating the establishment of interparticle contacts and networking of MWNT particles within the matrix. At 10 wt% MWNT, a maximum conductivity of 10^{-2} S/cm is achieved which is well within the minimum conductivity of 10^{-5} S/cm required for electrostatic discharge (ESD) material applications [64, 65].
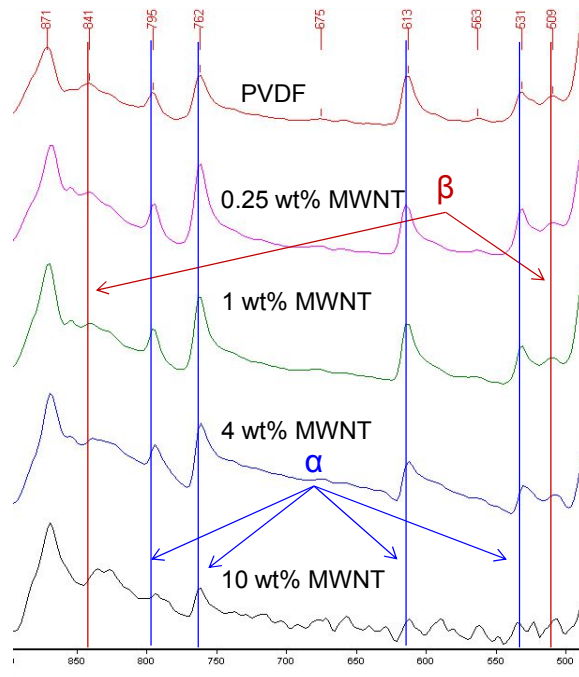
Figure 5.2. FTIR spectra of PVDF and nanocomposites containing 0.25, 1, 4 and 10 wt% MWNT. The prominence of the α-phase over the β-phase is apparent.

In order to understand the transition to an electrically conducting material from an insulating one, the conductivity can be plotted with reference to the particulate volume fraction content (Figure 5.4). The typical s-curve transition for PVDF-MWNT nanocomposites, from an insulating to conducting material is apparent in this plot. The fit to the power-law form representation of statistical percolation (Equation 2.1) is shown as the solid line in Figure 5.4b, where a percolation threshold concentration for PVDF-MWNT nanocomposites was found to be 0.95 wt% (0.85 vol%). The percolation point in PVDF-MWNT nanocomposites is associated with a 10 order of magnitude rise in the electrical conductivity. Such a sharp rise suggests a fully evolved interconnected MWNT network. Further additions of MWNT to the nanocomposites do not result in as significant an increase in conductivity.

(a)   (b)
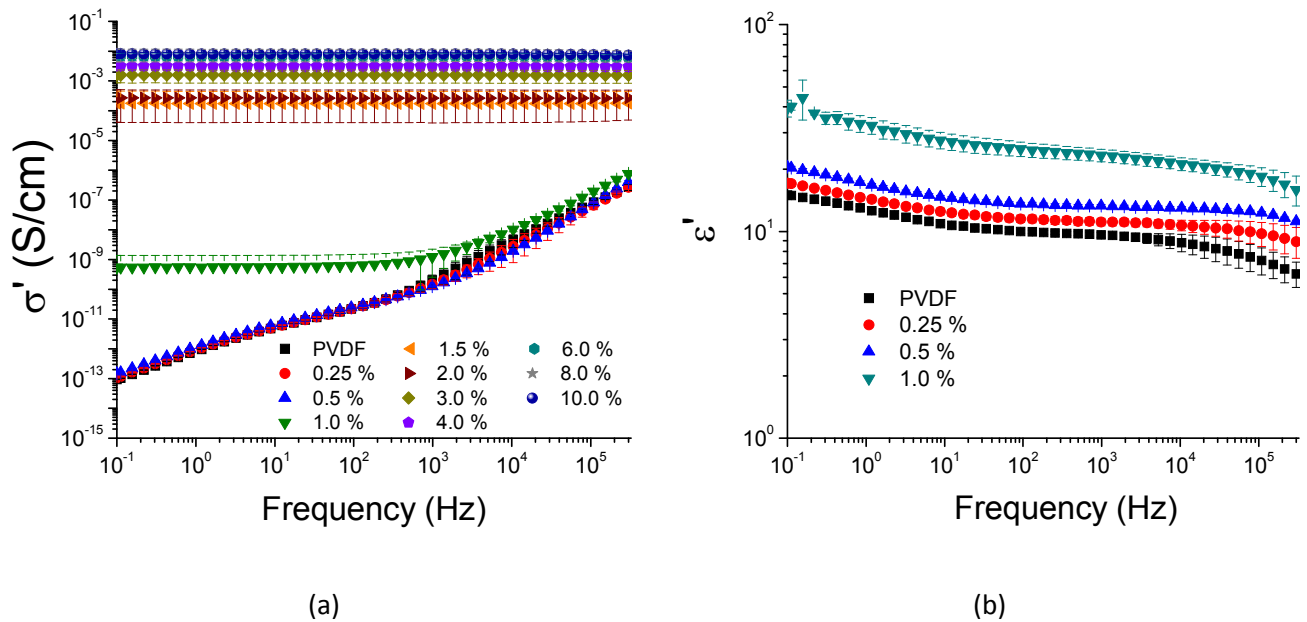
Figure 5.3. Electrical conductivity (a) and dielectric permittivity (b) of PVDF and PVDF-MWNT nanocomposites.

The permittivity (Figure 5.3b) of neat PVDF at 0.1 Hz is 15.0. Addition of 0.25 wt% MWNT increases the permittivity to 17.1, which indicates a greater ability to store charge (capacitance).

Increased permittivity in filled materials is observed because of a greater number of interfaces allowing for larger amounts of charges to be stored. This effect is most prominent at low frequencies as it allows more time for polarization to occur. The maximum permittivity of 39.4 occurs at 1.0 wt% MWNT content, beyond which a filler particle network has formed throughout and the material loses its dielectric characteristic.
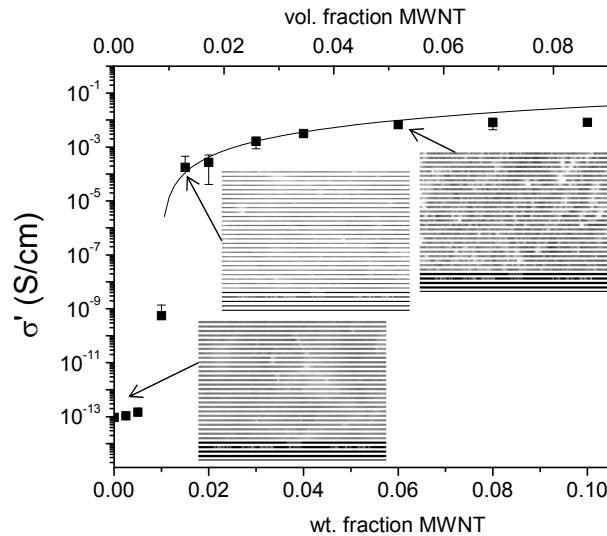
Figure 5.4. Electrical conductivity of PVDF-MWNT nanocomposites vs. MWNT content.

5.4 Piezoresistance of PVDF-MWNT Nanocomposites

The compressive piezoresistance of the MWNT filled PVDF nanocomposites were measured in quasi-static conditions at a strain rate of 0.1 mm/min ($\sim 0.001s^{-1}$). Figure 5.5 plots the stress-strain and resistance strain behavior of the MWNT nanocomposites. The curves in Figure 5.5 are average composite curves of 5 or more samples. The resistance and stress signal in Figure 5.5 can be parameterized and plotted against one another as shown in Figure 5.6a. The resistance-stress behavior of these nanocomposites can be sub-divided into three basic regions. The first/initial region is where full contact is established between the compressing platens and the sample. Most of the resistance change is observed in this region, regardless of filler content. This initial resistance change originates from

establishing a well-defined electrical contact between the compression platen and the sample surface during the initial stages of deformation; which in turn depends on establishing a well-defined mechanical contact without any slack. It can be observed from the strain-stress plots (Figure 5.5), that the 'toe'-region terminates in the first 10 MPa of applied pressure indicating all of the slack has been overcome.
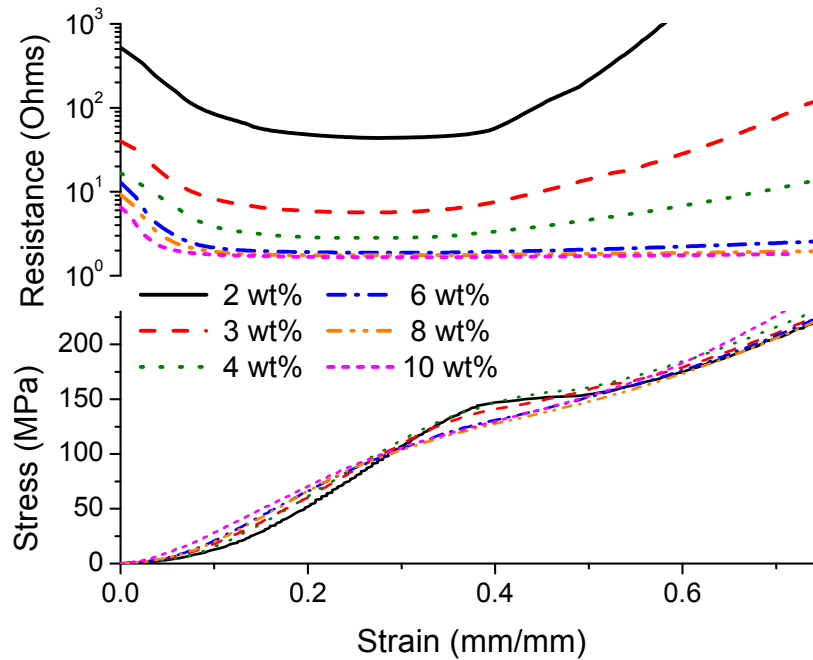
Figure 5.5. Stress-Strain and Resistance-Strain plots for PVDF-MWNT nanocomposites depicting the nanocomposites piezoresistive behavior.

The second region of compressive deformation is where elastic compression takes place. This region occurs at stresses greater than 10 MPa and is characterized by a linear strain-stress behavior. The resistance signal in this region continues to decrease, however, not as fast as the initial contact region. The third deformation region observed during the compression process is the plastic deformation zone. This occurs where the strain-stress curve begins to yield (softening).

The aforementioned observations suggest that the resistance-stress dependence in PVDF-nanocomposites is non-linear, non-monotonous and complex. It does however, correlate well with the different stages of deformation observed on the strain-stress curve. In order to compare the response of PVDF nanocomposites of different filler content and hence different conductivities, a relative resistance response must be considered, where the resistance is plotted as a ratio in reference to the initial resistance at the point of first contact. In addition, comparisons of relative resistance change between different nanocomposite compositions can be made by plotting iso-stress lines as shown in Figure 5.6b.

(a)   (b)
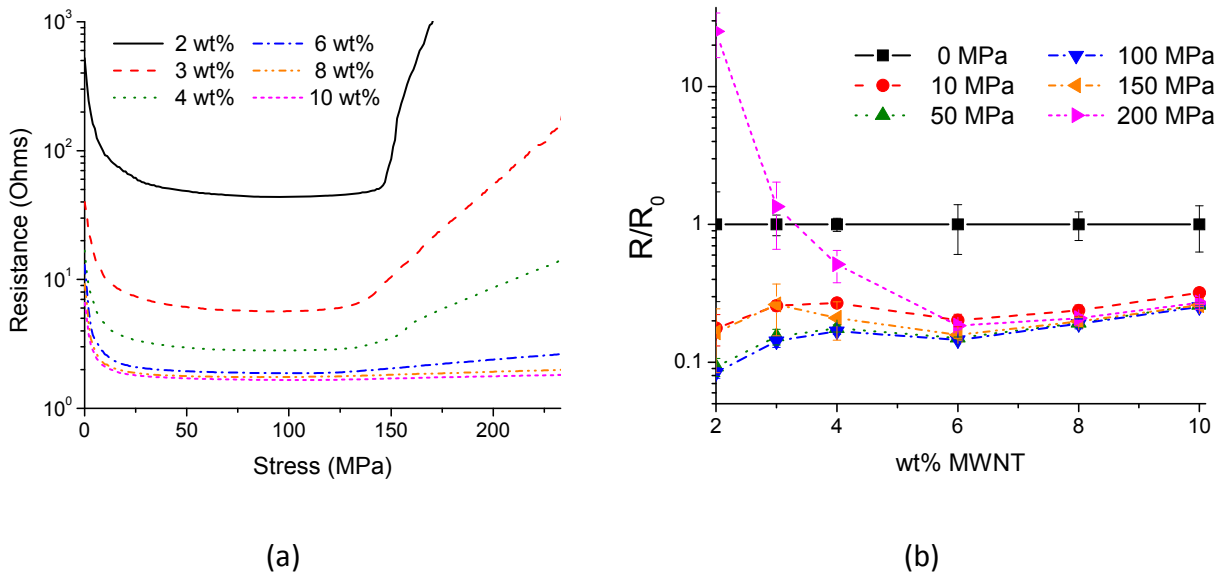
Figure 5.6. The piezoresistance response of PVDF-MWNT nanocomposites depicted by (a) plot of resistance vs. stress and (b) iso-stress plot of relative resistance vs. filler content.

A general observation from Figure 5.6b is that compositions closer to the percolation point (2, 3 and 4 wt%) display greater sensitivity in the resistance signal, than those compositions further away (6, 8 and 10 wt%), neglecting the change due to contact effects (< 10 MPa). This greater sensitivity is observed in both elastic and plastic portions of deformation. In the elastic portion (10-100 MPa) the

resistance signal at low compositions displays a greater decrease corresponding to further MWNT inter-particle distance reduction and network enhancement due to a uniaxial but largely affine deformation. In the plastic portion (>150 MPa) the resistance signal at low compositions undergoes a sharp rise, even above its initial zero-stress value. This sharp rise is associated with MWNT network destruction due to the plastic flow induced by shear-stresses that develop at high strain levels. The much smaller resistance change observed for high MWNT contents suggests that the MWNT network is much more resilient than at low MWNT contents. A higher concentration would mean more network junctions and paths throughout the composite material; therefore any path destruction would not affect the electron conduction process as other paths would be available.

5.5 Summary

This chapter detailed the fabrication of nanocomposites of PVDF and MWNT and the characterization of their electrical and piezoresistive behavior. The MWNT filler in the nanocomposites was characterized to be well dispersed at low content, with very few large size aggregates visible at high MWNT amounts. The networking of MWNTs was also clearly depicted in the electrical conductivity of the nanocomposites, which underwent a sharp rise between 0.5 and 1.5 wt% MWNT. The statistical percolation threshold for PVDF-MWNT nanocomposites was found to be 0.95 wt% (0.85 vol.%). At 0.1 Hz, the maximum conductivity achieved in the nanocomposites was 10^{-2} S/cm (10 wt%), while the maximum dielectric permittivity was 39.4 (1.0 wt%). Piezoresistance investigation of the PVDF-MWNT nanocomposites revealed a three stage deformation (contact, elastic and plastic deformation) process which has a direct influence on the MWNT networks in the nanocomposites and hence on the material's electrical resistivity. The resistance was observed to decrease during elastic deformation, while increase during plastic deformation, corresponding to reducing and increasing inter-particle distances between the MWNT, respectively.

6 Piezoresistive Polyurethane Composites: Effect of Porosity

6.1 Introduction

The development and characterization of pressure sensing porous nanocomposites is reported in this chapter. A thermoplastic polyurethane (TPU) was chosen as an elastomeric matrix, which was reinforced with multiwall carbon nanotubes (MWNT) by high shear twin screw extrusion mixing. Porosity was introduced to the composites through the phase separation of a single TPU-carbon-dioxide gas solution. Interactions between MWNT and TPU were elucidated through conductivity measurements and microstructure imaging. The piezoresistance (pressure-resistance) behavior of the nanocomposites was investigated and found to be dependent on MWNT concentration and nanocomposite microstructure. Mechanisms of piezoresistance in solid and porous nanocomposites are proposed.

6.2 Porous Nanocomposite Fabrication

Porous nanocomposites were prepared through the phase separation of a TPU nanocomposite-CO_2 solid solution in a temperature quenched batch process [72]. The single phase solid solution was prepared by saturating the nanocomposite inside a high pressure vessel filled with CO_2 gas at 4.13 MPa (600 psi) for 22 hr. The time required to form a saturated single phase polymer-solvent solution can be determined by estimating the characteristic diffusion length (cm) given in Equation 6.1:

$$L_d = \sqrt{4Dt} \qquad \text{(Eq. 6.1)}$$

where D is the solvent diffusivity (cm^2/s) in the polymer and t is the time (s) allowed for saturation. This length characterizes the distance where half of the surface (maximum) concentration is reached in a specified time during the gas sorption process. Due to the variety of thermoplastic polyurethane

chemistry available, acquiring accurate carbon-dioxide diffusivity values is very challenging. However a review of two literature sources [73, 74] suggests that the diffusivity of carbon-dioxide in various TPUs between temperatures of 25 to 40 °C is in the range of 0.9 x 10^{-7} to 38.9 x 10^{-7} cm^2/s. Based on a saturation time of 22 hr and the literature diffusivity values, the characteristic diffusion lengths are in the range of 1.7 to 11.1 mm. These values are much larger than the sample half-thickness length therefore 22hr was deemed a sufficient enough period for saturating 0.5 mm thick TPU samples with carbon-dioxide.

After saturation, the vessel was rapidly depressurized causing a thermodynamic instability and a driving force for gas-polymer phase separation. This phase separation, in the form of pore nucleation, cannot be initiated unless the polymer viscosity is lowered, which is done by exposing the material to elevated temperatures. Immersion of the saturated TPU-MWNT nanocomposites in a heated water bath at 95°C for 10s was found to be sufficient to cause the gas-polymer phase separation. During phase separation carbon-dioxide gas bubbles nucleate and grow as schematically represented in Figure 6.1. The gas bubble nucleation and growth process was ceased by lowering the material's temperature through immersion in a cold water bath. The density of the porous TPU nanocomposites was estimated based on the Archimedes principle and a modified Mettler Toledo weighing balance. The pore sizes were estimated by measuring and averaging the lengths of at least 50 porous features in a contained area. The number density of the porous features (#/cm^3) was estimated using Equation 6.2 [75]:

$$n = \left(\frac{N}{A} \right)^{\frac{3}{2}} \cdot \frac{\rho_s}{\rho_p}$$

(Eq. 6.2)

where N is the number of pores counted in a contained area A. The pore density with respect to the

initial sample volume is desired therefore a ratio of the solid (ρ_s) and porous (ρ_p) material densities,

assuming a constant mass, has to be factored.
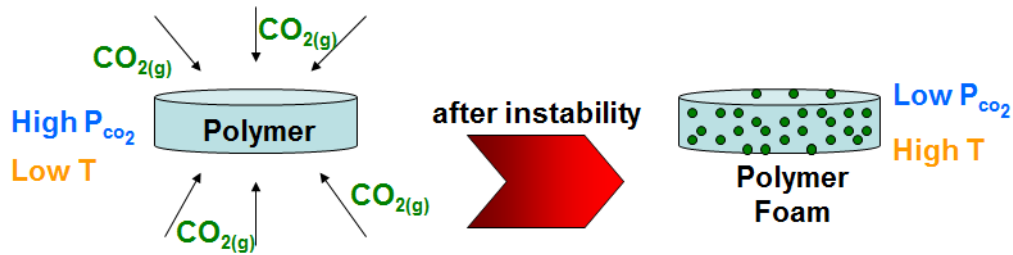
Figure 6.1. Schematic representation of the pore nucleation and growth process.

6.3 Morphology of TPU-MWNT Nanocomposites

Fundamental to any understanding of composite properties is the study of its internal structure and the

structure of its constituent phases. Particular importance must be given to the study of the smallest

feature sizes as they possess the highest interfacial area and potential for interaction between the

constituent phases. The morphology of the processed TPU-MWNT nanocomposites was analyzed using a

scanning electron microscope (SEM) and the obtained morphologies are shown in Figure 6.2.

Thermoplastic polyurethane has a flat surface free from any fine-size features which are not attributable

to the fracture process. With the addition of just 0.25 wt% MWNT (Figure 6.2b), fine-sized (< 0.1 μm)

feature are visible, which are attributed to MWNT. These features appear brighter suggesting they are

more conductive than their surroundings. Further addition of MWNT (Figure 6.2c-f) results in an

increased MWNT density in the nanocomposites. At higher concentrations of 4, 6 and 10 wt% some

aggregation of MWNT is observed but to a large extent individual MWNT dispersion is evident and their

network remains intact.

(a)　　　　　　　　　　(b)　　　　　　　　　　(c)

(d)　　　　　　　　　　(e)　　　　　　　　　　(f)
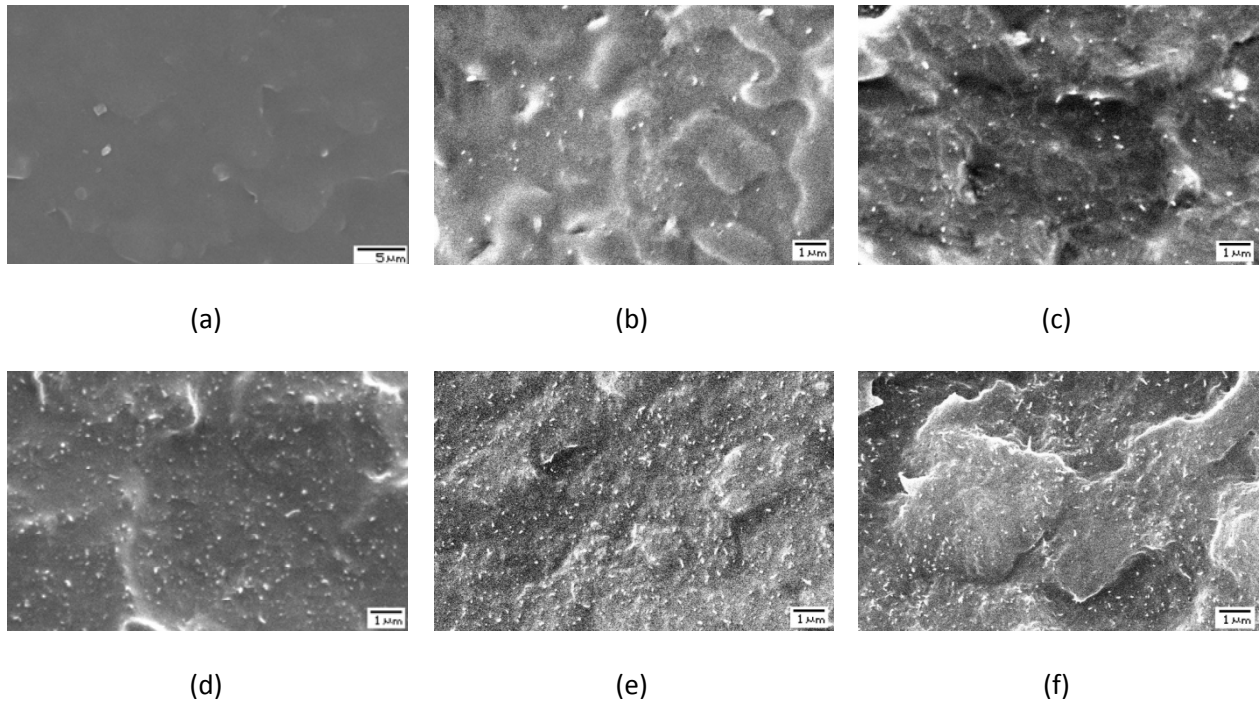
Figure 6.2. SEM cross-sections of (a) TPU (a) and TPU-MWNT nanocomposites showing the MWNT dispersion in (b) 0.25, (c) 1, (d) 4, (e) 6 and (f) 10 wt% MWNT nanocomposites.

Introducing porosity in the nanocomposite results in significantly contrasting morphologies (Figure 6.3) which depend on the amount of MWNT present. Thermoplastic polyurethane (Figure 6.3a) displays significant volume expansion (3.8x) and results in a morphology with large sized pores (6.9 µm) and a pore density of $8.7\text{x}10^9$ pores/cm^3. Introducing MWNT has the effect of decreasing pore size and increasing pore density. At a low MWNT content of 1 wt% MWNT (Figure 6.3b), the pore size is 4.1 µm and the pore density is $2.7\text{x}10^{10}$ pores/cm^3. An optimally small pore size (2.7 µm) and maximum pore density ($6.7\text{x}10^{10}$ pores/cm^3) is achieved in nanocomposites containing 4 wt% MWNT (Figure 6.3c). At the composition of 6 wt% MWNT, the porosity is no longer homogenous throughout the material which now consists of regions devoid of any pores. Despite the average pore size being 1.8 µm, the discontinuous porosity in the material results in a low pore density of $1.0\text{x}10^9$ pores/cm^3.

64

(a)   (b)   (c)

(d)   (e)   (f)
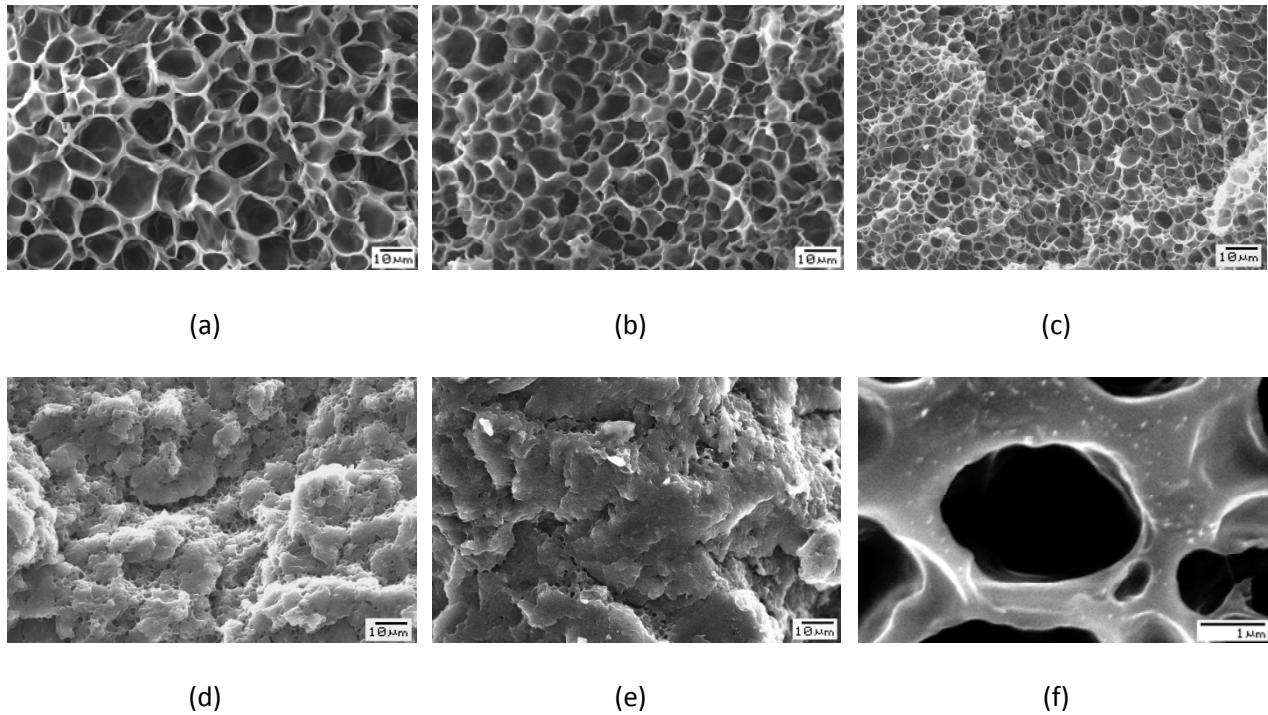
Figure 6.3. SEM morphologies of porous (a) TPU and TPU-MWNT nanocomposites containing (b) 1%, (c)

4, (d) 6 and (e) 10 wt% MWNT. High magnification (f) image of 4 wt% nanocomposite reveals

concentrated MWNT features surrounding pores.

The significant variation in pore morphology as a result of MWNT addition can be understood by

considering the competing effects of MWNT influence on (1) heterogeneous pore nucleation and (2)

nanocomposite viscosity, on the foaming process which consists of pore nucleation, growth and

coalescence. The existence of a finely dispersed MWNT phase provides interfaces which reduce the

critical pore diameter thereby increasing the probability of heterogeneous pore nucleation occurring

[76]. Therefore a fine dispersion of MWNT in polymeric composites is desired for achieving a high pore

density and the associated advantages. At the same time, addition of fine sized solid particles like

MWNT, causes a significant increase in the nanocomposite viscosity and imparts the material with an

elastic (load bearing) character [72, 77]. This increased viscosity hinders the pore growth phenomena

and limits the final pore size that is achieved. If the viscosity of the material is low enough and the pore growth phenomena is allowed to further continue, then pores impinge each other and begin to coalesce. Pore coalescence is evident by large pore sizes and broader size distributions.

(a)

(b)
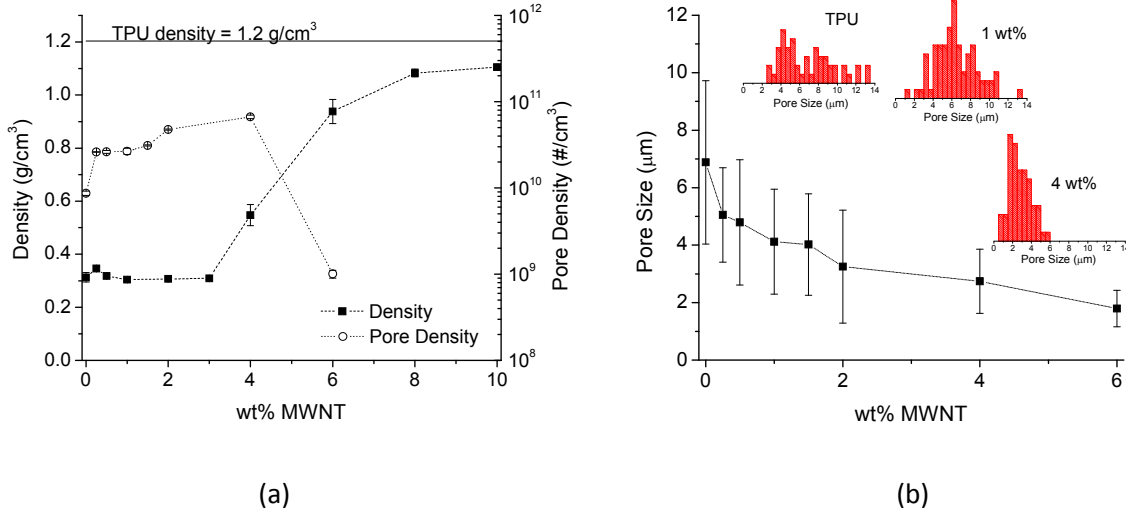
Figure 6.4. Plots of (a) bulk density, pore density and (b) pore size of porous TPU-MWNT nanocomposites and their dependence on MWNT content.

The density and pore density (# of pores/cm^3) of the TPU-MWNT nanocomposites are plotted in Figure 6.4a, while the average pore size and pore size distributions are plotted in Figure 6.4b. At low MWNT amounts, the density of the nanocomposites is quite low at 0.26 g/cm^3, which is similar to that of TPU. Although addition of low amounts of MWNT promote a slightly higher pore density (Figure 6.4a) there is a concomitant decrease in pore size (Figure 6.4b) resulting in a nanocomposite with a density similar to TPU. Such marginal gains in pore density and reduction in pore size, at low MWNT content, can be explained by the possibility of pore coalescence occurring as the viscosity of the nanocomposites is low. At higher MWNT amounts, the viscosity of the nanocomposites is significantly higher as a result of MWNT networks forming and percolation being achieved. A consequence of rheological percolation is

66

the pseudo-solid (elastic) behavior of the nanocomposites [77], which assists in restricting pore growth and pore coalescence explaining the increasing pore density and decreasing pore size beginning at 2 wt% MWNT (Figure 6.4a and b). The maximum pore density and minimum pore size for a fully homogenous porous nanocomposite is achieved at an MWNT content of 4 wt%. A narrowing pore size distribution (Figure 6.4b) as the MWNT content is increased provides further credence to MWNTs restricting pore growth and coalescence.

6.4 Electrical Properties of TPU-MWNT Nanocomposites

The electrical properties of solid and porous TPU-MWNT nanocomposites were investigated using alternating current dielectric impedance spectroscopy (DIS). The real component of electrical conductivity of solid and porous TPU-MWNT composites with respect to applied frequency is plotted in Figures 6.5a and 6.5b, respectively. The electrical conductivity of solid TPU (Figure 6.5a) is dependent on applied frequency and at a low frequency of 0.1 Hz, it is 2.8×10^{-12} S/cm, which is in the range of insulating materials. Addition of 0.25 wt% increases the conductivity to 6.6×10^{-12} S/cm, however the frequency dependence is maintained suggesting insulative behavior. This behavior is evident until an MWNT composition of 1.5 wt%, where frequency independence is exhibited at low frequencies. This behavior is also followed with a large increase in conductivity (7.4×10^{-9} S/cm at 0.1 Hz), which is caused by networking of MWNT particles. The electrical charge transport is now supported by MWNT particles in the network, which can be either by (1) electron tunneling between particles or (2) inter-particle contacts. Further MWNT addition to the nanocomposites, promotes MWNT networking and increases the conductivity of the composites. At 10 wt% MWNT, the electrical conductivity is 5.8×10^{-4} S/cm, which is within the minimum range of 10^{-5} S/cm required for electrostatic discharge (ESD) material applications [64, 65].
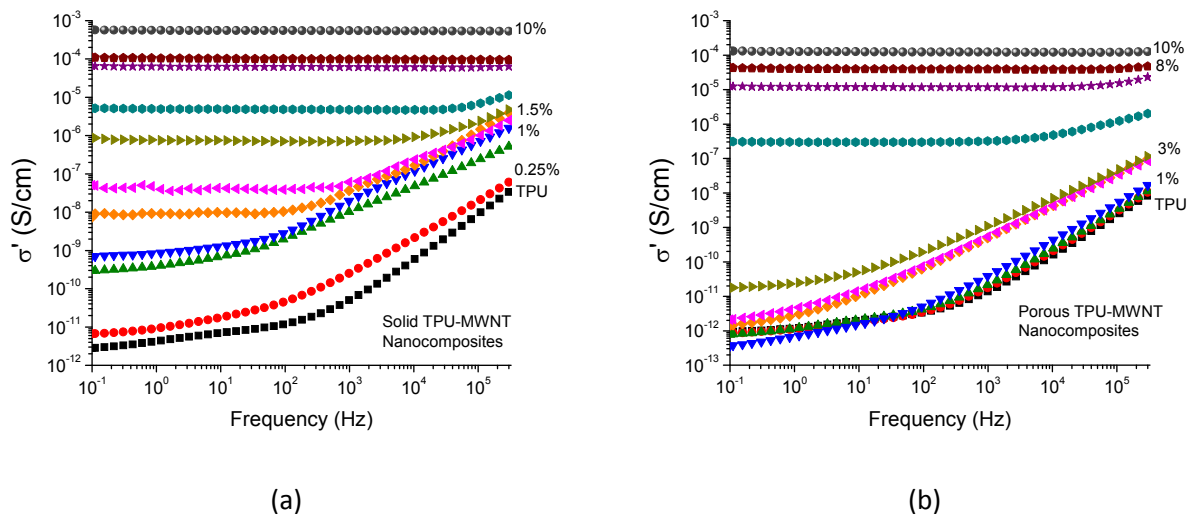
Figure 6.5. Electrical conductivity-frequency dependence for (a) solid and (b) porous nanocomposites containing various amounts of MWNT.

The electrical conductivity of porous TPU-MWNT nanocomposites is shown in Figure 6.5b. In general, imparting a porous morphology on the nanocomposite has the effect of reducing the conductivity. At low MWNT compositions (up till 3 wt%), a frequency dependent insulating behavior is observed. There is a large increase in conductivity at 4 wt% MWNT (3.1×10^{-7} S/cm) and frequency independence is observed, suggesting the establishment of an interconnected network of MWNT. Further addition of MWNT results in an increase in conductivity (1.3×10^{-4} S/cm), however the overall values of the porous nanocomposites are lower than that of their solid counterparts.
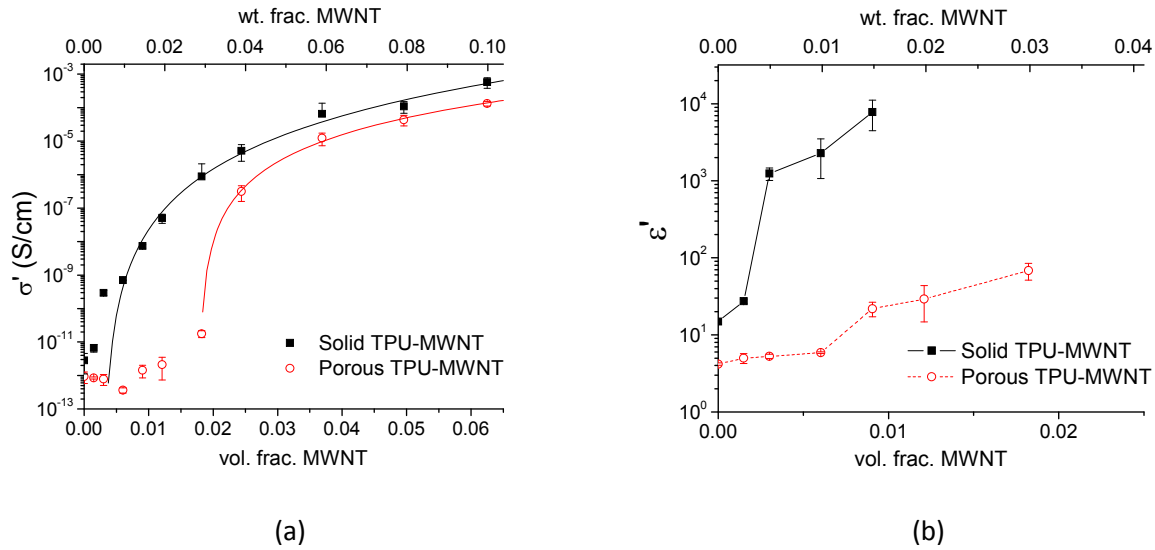
Figure 6.6. Composition dependence of (a) electrical conductivity and (b) dielectric permittivity of TPU-MWNT nanocomposites measured at 0.1 Hz.

In order to understand the transition from an insulating material to an electrically conductive one, the conductivity can be plotted with reference to the particulate volume fraction content (Figure 6.6a). An 'S-curve' transition from an insulating to conducting material for TPU-MWNT solid and porous nanocomposites is apparent in this plot. A percolation threshold of 0.301 vol% (0.501 wt%) was obtained for solid nanocomposites with an R^2 of 0.993, while a threshold of 1.795 vol% (2.965 wt%) was obtained for porous nanocomposites with an R^2 of 0.999. The lower conductivity values and higher percolation point of porous nanocomposites can be explained by two consequences of foaming: (1) larger path for electrons to travel due to the existence of pore obstacles, and (2) increase of inter-particle MWNT distance in the pore wall material during the pore growth process. Incorporating homogenously distributed pores (Figure 6.3) in the nanocomposites would provide obstacles for electron transport from one electrode to another. A larger path for electron transport increases the likelihood of electron scattering to occur and would result in a reduced conductivity. Also, the pore

69

growth process involves bi-axial expansion of pore walls which will increase the inter-particle distance between MWNT surrounding the pores. Therefore a greater amount of MWNT (3 wt%) are required to reduce the inter-particle distance and completely achieve interconnectivity (percolation) between the filler phase in the porous nanocomposites allowing for sufficient electron conduction to occur.
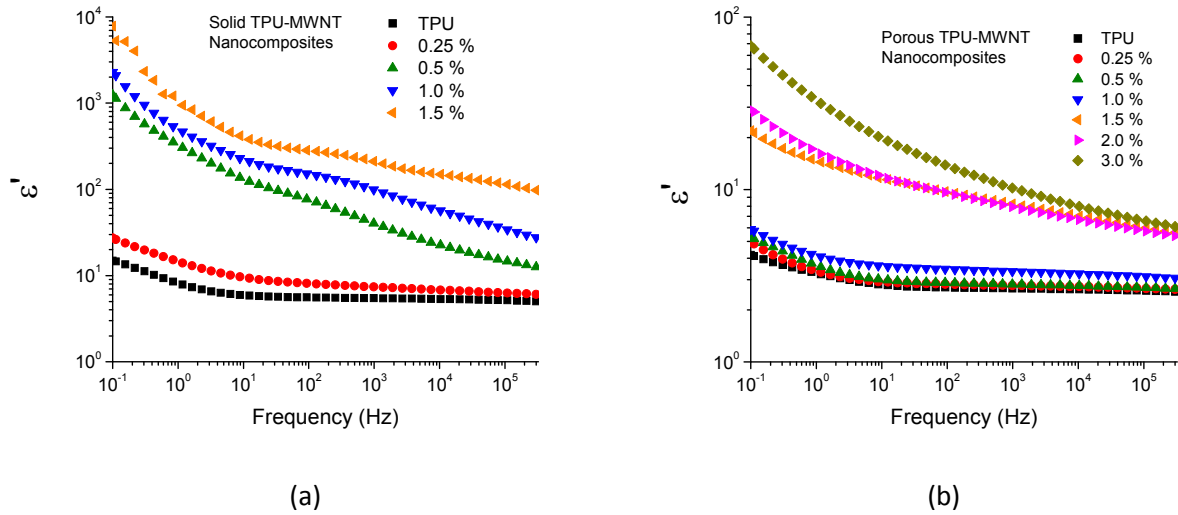
Figure 6.7. Permittivity-frequency dependence for (a) solid and (b) porous nanocomposites containing various amounts of MWNT.

The dielectric permittivity is an important material property, which is a measure of the capacity to store electrical charges. Figures 6.7a and 6.7b are plots of permittivity at various frequencies and MWNT content. The permittivity of solid TPU is frequency dependent and is 14.9 at 0.1 Hz. The increase in permittivity at low frequencies deviates from ideal dielectric behavior and corresponds with interfacial polarization (Maxwell-Wagner) effect [78], which results from charge build-up and its contribution to the electric field, at either the (1) inner-boundary layers or (2) electrode-sample interface. TPU processing requires the use of chain extenders in order to obtain a high M.W. and thus a greater number of cross-links per chain, which are the source of TPU's mechanical resiliency. The chain

70

extenders employed in TPU chemistry are usually small, mobile diols such as butanediol and hexanediol. Additionally, the hard segments in TPU are polar molecules with significant affinity for water absorption. At low frequencies, these smaller mobile species can build up on surfaces and contribute to the interfacial polarization effect resulting in higher permittivity (w.r.t. frequency). The addition of 0.25 wt% MWNT into TPU increases the permittivity to just 27.3 indicating that the majority of the interfacial polarization is still at the electrodes. A large increase in permittivity to 1240 is observed (Figure 6.7a) at 0.5 wt% MWNT, which can be attributed to the greater contribution of interfacial polarization at MWNT-polymer interfaces as opposed to just at the electrode-sample interface for TPU and 0.25 wt% MWNT nanocomposite. This effect becomes more pronounced as more MWNT (up till 1.5 wt%), hence more interfaces, are incorporated in the nanocomposites. Beyond 1.5 wt% MWNT, the nanocomposites lose their dielectric character because of the complete formation of an interconnected network of conductive MWNT particles.

The frequency and composition dependence on dielectric permittivity of porous TPU-MWNT nanocomposites is plotted in Figure 6.7b. Introducing porosity into TPU has the effect of reducing the material's apparent permittivity to 4.2 at 0.1 Hz. Interfacial polarization is still present in porous TPU indicating the presence of a build-up of charge at the electrode-sample interface despite the presence of homogenously distributed pores throughout the material. Addition of low amounts of MWNT (up till 1.0 wt%) provides only marginal improvements in permittivity suggesting minimal interfacial polarization at MWNT-polymer interfaces. A significant improvement in permittivity to 219 is observed at 1.5 wt% MWNT, which continues with further MWNT addition of 2 and 3 wt%. Figure 6.6b compares MWNT composition dependence of real component of permittivity of solid and porous TPU-MWNT nanocomposites. For both, solid and porous nanocomposites, a unique composition can be identified, 0.5 wt% for solid and 1.5 wt% for porous, where there is a significant increase in permittivity due to the

contributions of MWNT-polymer interfaces in storing charge. For the same composition, the porous nanocomposites have a reduced permittivity in comparison to their solid counterparts. Similar to the observation noted with conductivity (Figure 8a), the reduction in permittivity can be explained by the bi-axial expansion of the pore wall material during the foaming process, which would increase the inter-particle distances between MWNT. The increased inter-particle distances in the porous nanocomposites results in reduced interconnectivity and interfacial area at active sites for charge polarization therefore decreasing permittivity.

6.5 Piezoresistance of Solid and Porous TPU-MWNT Nanocomposites

The piezoresistance (resistance-stress) relationship for solid and porous TPU-MWNT nanocomposites was observed on a custom-made force-resistance setup and the averaged behavior for the two types of materials is depicted in Figure 6.8. The piezoresistance of solid TPU-MWNT nanocomposites is illustrated in Figure 6.8a. Compositions of nanocomposites less than 2 wt% MWNT did not exhibit sufficient conductivity for piezoresistance characterization. The piezoresistance behavior can be described in terms of two compression regions, (1) an initial contact region and (2) elastic compression region. During the initial contact region (stress < 3MPa), the resistance of all solid nanocomposite decreases as contact is being established between the electrodes and the sample. The least decrease is exhibited by 2 wt% MWNT, while the most decrease is observed for higher MWNT compositions of 6 and 10 wt%. At intermediate stress levels (3-25 MPa), contact is well established and the nanocomposites undergo elastic compression. During elastic compression, the resistance remains steady with respect to change in stress. At higher stresses (> 25 MPa), nanocomposites with a low MWNT content (2, 3 and 4 wt%) exhibit an increase in resistance, while those with a high MWNT content (6 and 10 wt%) continue to exhibit a steady resistance, with respect to change in stress.
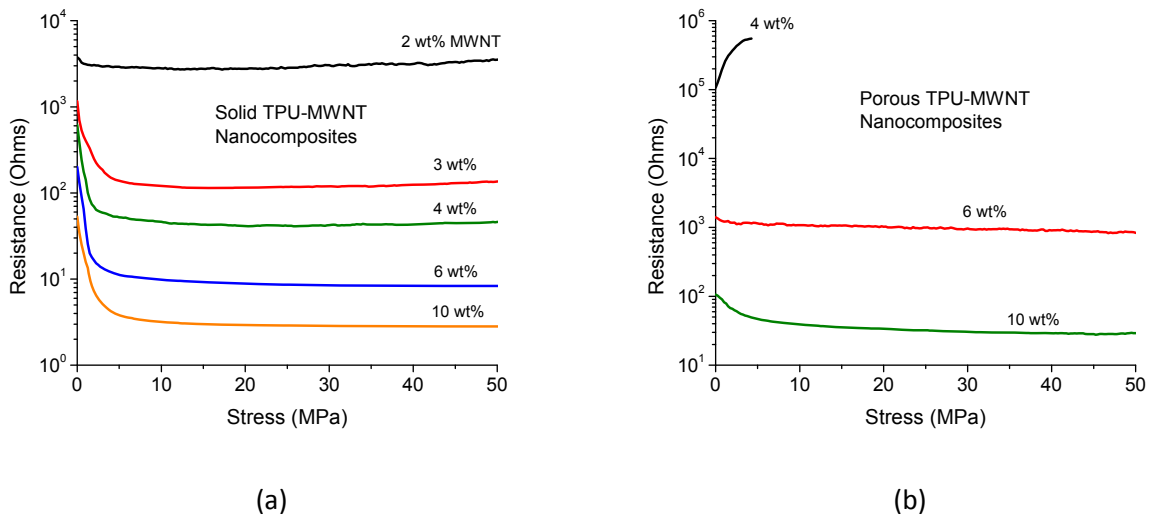
Figure 6.8. Absolute resistance-stress plots depicting the piezoresistance behavior for (a) solid and (b) porous TPU-MWNT nanocomposites.

The piezoresistance of porous TPU-MWNT nanocomposites is depicted in Figure 6.8b. Compositions less than 4 wt% MWNT were insufficiently conductive for piezoresistance characterization. The piezoresistance response of porous nanocomposites was dependent on the type of pore morphology present in the nanocomposite. Porous nanocomposites containing 4 wt% MWNT had a high initial resistance of 106 kΩ, which continued to increase with application of stress. A final value of approximately 550 kΩ was achieved beyond which the samples had compressed such that electrodes were in direct contact with each other. The nanocomposites containing 6 wt% MWNT maintained a steady resistance response with respect to change in stress. Porous nanocomposites with 10 wt% MWNT content exhibited a response similar to their solid counterpart albeit with a higher resistance and a smaller resistance decrease with respect to change in stress (Figure 6.8b).

The resistance relative to the initial resistance is a useful quantity for analyzing the degree of piezoresistance exhibited by the nanocomposites during the compression process. Figure 6.9a depicts

73

the relative resistance-stress relationship of solid and porous TPU-MWNT nanocomposites at various MWNT compositions. The shape of the piezoresistance curves in Figure 6.9a can provide useful insights into the nature of the MWNT network and the mechanisms of electrical conduction in the nanocomposites at a particular stress level. The solid nanocomposites (4, 6 and 10 wt% MWNT) exhibit most of the resistance decrease in the initial contact region. During the initial stages of elastic compression, the resistance undergoes a slight decrease due to a decreasing inter-particle distance and more interconnectivity between MWNT particles. At a low MWNT content of 4 wt%, the resistance begins to increase at higher stress levels (> 25 MPa). A similar increasing resistance trend is observed for 2 and 3 wt% MWNT nanocomposites (Figure 9a) and is attributed to MWNT network disruption. During high stress compression the MWNT can become oriented in the plane transverse to the direction of compression. This reorientation, schematized in Figure 6.10a, serves to disrupt the interconnectivity between the MWNT particles in the TPU resulting in a higher resistance at later stages of compression. A similar increase in resistance at late stages of compression isn't evident in 6 and 10 wt% MWNT nanocomposites, which could be explained by the large quantity of individual and aggregated MWNT present in these compositions. Although, the filler particulates can still reorient in the transverse plane at high stresses, the high MWNT content ensures that the interconnectivity is maintained because of a large number of contact nodes within the filler network.

(a)   (b)
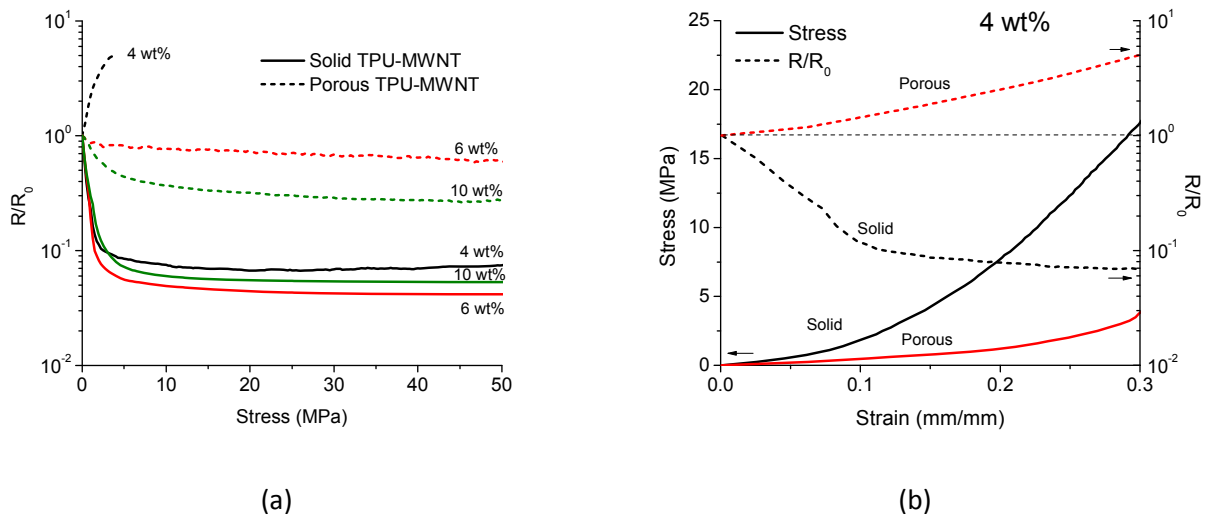
Figure 6.9. Plot of (a) relative resistance-stress plot for solid and porous TPU-MWNT nanocomposite and

(b) stress-strain and relative resistance-strain for a single MWNT composition of 4 wt%.

Porous TPU-MWNT nanocomposites containing 4 wt% MWNT exhibit an increase in resistance

(5X) with applied stress. This increase in resistance begins to occur immediately at the beginning of the

compression process suggesting a different mechanism of piezoresistance in homogenously porous TPU-

MWNT nanocomposites. In contrast to 4 wt%, the 6 and 10 wt% MWNT porous nanocomposites display

a piezoresistive behavior similar to their solid counterparts (Figure 6.9a), although with a lesser degree

of sensitivity to stress. The porous structure in these nanocomposites isn't homogeneous and consists of

sporadically distributed pores within the material, with 6 wt% nanocomposites (Figure 6.3d) having

more evidence of pores than 10 wt% (Figure 6.3e).

The stress-strain and relative resistance-strain response for solid and porous TPU-MWNT

nanocomposites containing 4 wt% MWNT content are plotted in Figure 6.9b. Porous TPU-MWNT

nanocomposites containing 4 wt% MWNT had a homogenous distribution pores (Figure 6.3c), with a

density of 0.547 g/cm^3, average pore size of 2.7 μm and a pore density of 6.7x10^{10} pores/cm^3. The

immediate increase of resistance with compression of porous nanocomposites is in stark contrast to the

initial contact and elastic compression related decrease of resistance for solid nanocomposites. The

increase can be understood from consideration of pore compression and its effect on the electron

conduction paths throughout the nanocomposites; schematized in Figure 6.10b. During pore

compression, MWNT particle networks existing along the pore walls get disrupted resulting in lesser

interconnectivity between particles and larger electron conduction paths due to compressed pore
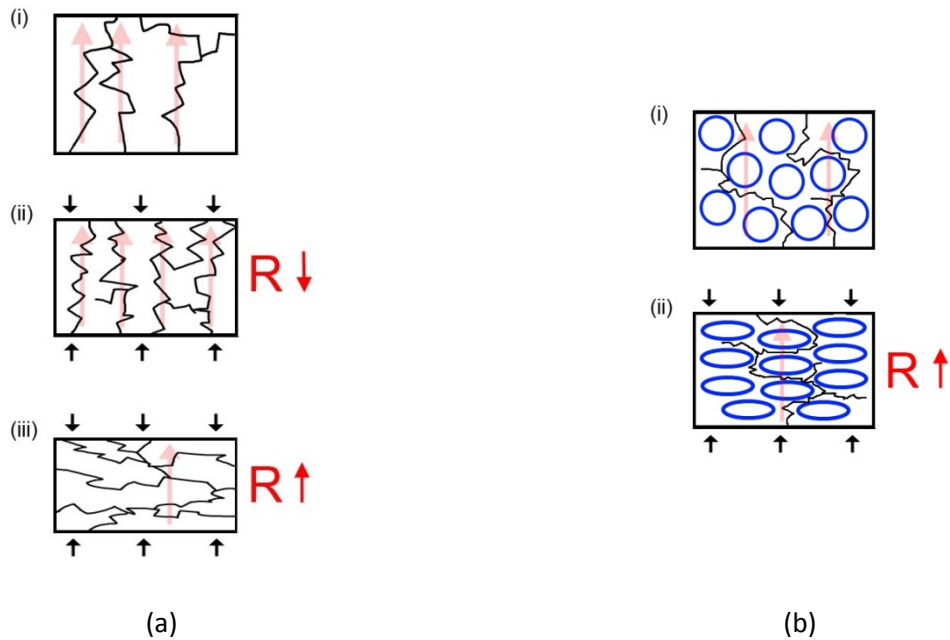
obstacles.

Figure 6.10. Illustration of piezoresistance mechanisms proposed for (a) solid and (b) porous

nanocomposites.

6.6 Summary

This chapter detailed the fabrication and characterization of pressure sensitive solid and porous TPU-

MWNT nanocomposites. Porosity was introduced to the composites through the phase separation of a

TPU-carbon-dioxide gas solution. The density of the porous nanocomposites was found to be dependent on the amount of MWNT present, with greater amounts (> 4wt%) restricting the degree of pore expansion. The smallest pore size (2.7 μm) and greatest pore density (6.7×10^{10} pores/cm^3) were obtained at an MWNT content of 4 wt%. In general, the conductivity and permittivity of the porous nanocomposites was lower than their solid counterparts while their percolation threshold was higher. The deterioration in electrical properties of the porous nanocomposites was attributed (i) to an increased inter-particle distance between MWNT during pore expansion, and (ii) to the pores acting as obstacles, thereby increasing the charge conduction paths. The piezoresistance (pressure-resistance) behavior of the solid and porous nanocomposites was investigated and found to be dependent on MWNT concentration and nanocomposite microstructure. The resistance in solid nanocomposites with low MWNT content (2, 3 and 4 wt%), increases at high stresses as a result of MWNT network disruption. The resistance remains steady in nanocomposites with high MWNT contents (6 and 10 wt%) as MWNT network disruption is mitigated because of the availability of a large number of inter-particle contacts. The resistance in porous nanocomposites containing 4 wt% MWNT underwent an increase with the application of stress, which indicated that pore compression was responsible for disrupting the filler particle network.

7 Modeling Percolation and Piezoresistance Phenomena

7.1 Introduction

This final chapter details some of the effort undertaken to model the percolation and piezoresistance phenomena. In addition to electrical properties, rheological properties can also exhibit a percolation behavior associated with the formation of the filler network. The work outlined here compares the percolation behavior of the electrical conductivity (described in earlier chapters) to the percolation behavior of the storage modulus of molten polymer nanocomposites. The results from both sets of data appear to describe a semi-empirical relationship between the threshold concentration and the critical exponent (t). The variances between electrical and rheological percolation are also examined. The next section of this chapter concerns the unique piezoresistance response of the nanocomposites during plastic deformation. The response is characterized and a model is proposed which captures the piezoresistance response of both PVDF and PE nanocomposites based on a known stress and filler concentration.

7.2 Rheological Properties of Polymer Nanocomposites

The rheological properties, in the melt state, of the polymer nanocomposites were measured using a rheometer. The addition of nanoparticles directly influences the viscosity and storage modulus of the melt, particularly if the particles are networked. The frequency dependence of the rheological storage modulus and viscosity of nanocomposites of PE, TPU and PVDF reinforced with MWNT is illustrated in Figure 7.1 and 7.2, respectively. The pure polymers show a linear increase of storage modulus as the frequency is increased. This increase of modulus is observed in polymeric materials, which are sensitive to the strain rate of deformation. Based on the time-temperature superposition principle, increasing the

frequency (strain rate) or decreasing the temperature has the effect of stiffening the polymer chain

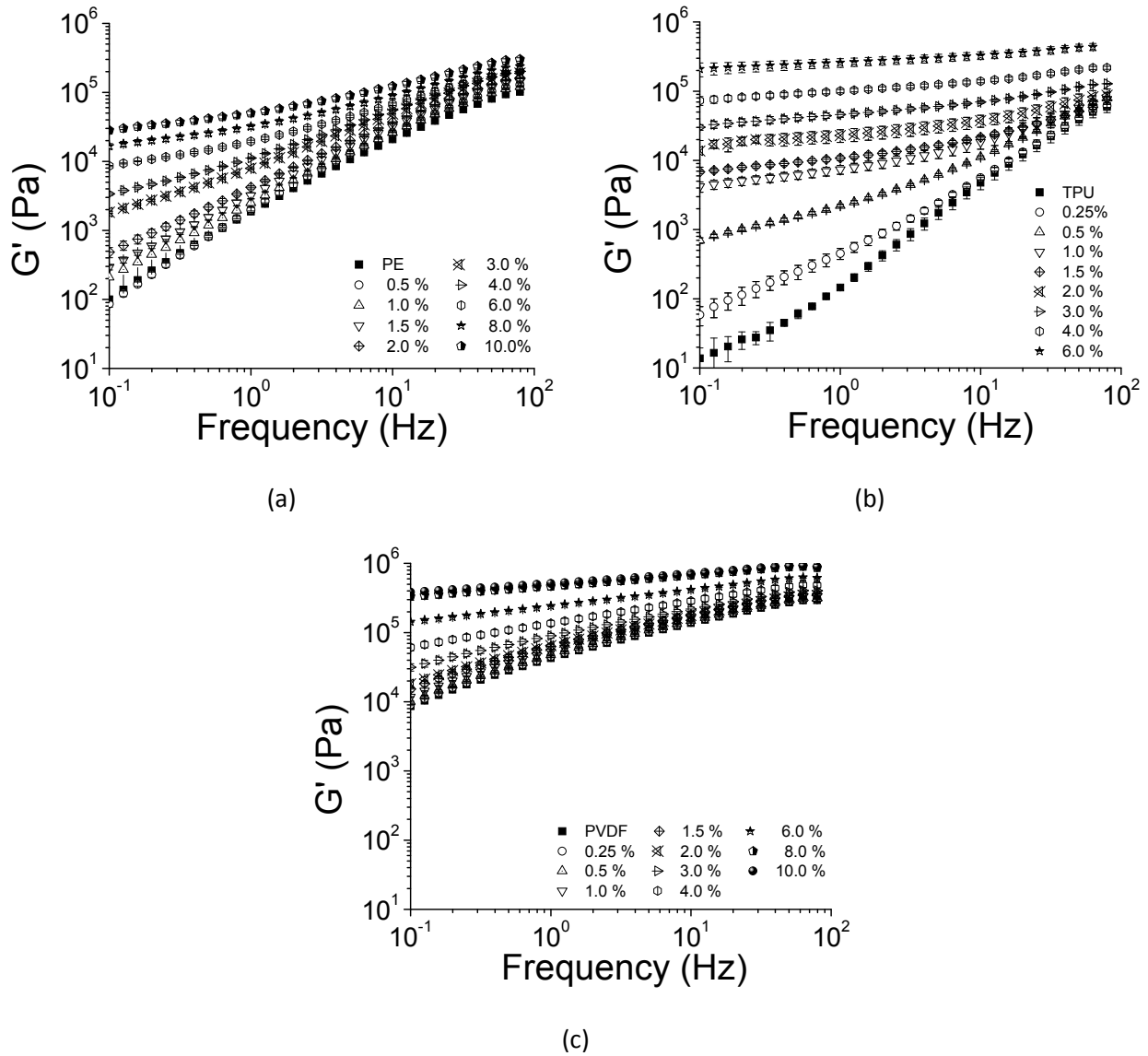motion, observed as an increased modulus of the polymers [79].

(a)

(b)

(c)

Figure 7.1. The frequency dependence of storage modulus of PE-MWNT (a), TPU-MWNT (b), PVDF-

MWNT (c) nanocomposites.

A close examination of Figure 7.1 reveals that the stiffening effect is most pronounced for TPU, followed by PE and PVDF. TPU's storage modulus and viscosity (Figure 7.1b and 7.2b) is the lowest of all the materials examined. This implies that in the melt TPU's chains are highly flexible and prone to reorientation due to an applied stress. In comparison, PE's chain flexibility is intermediary while PVDF's chains are stiff, even in the melt. Chain flexibility in the melt is influenced by several factors including molecular weight, branching, cross-linking and additives, which are the subject of our interest here.

The addition of MWNT to the polymers, results in a sharp change in the viscoelastic properties. The storage modulus increases (particularly at low frequencies) and becomes less frequency dependent, while viscosity of the sample also increases but becomes dependent on the frequency. The greatest change in viscoelastic behavior is observed for TPU nanocomposites, where the storage modulus at 0.1Hz increases from 13.8 Pa (TPU) to 2.1×10^5 Pa (for 6 wt% MWNT), while the least change is observed for PVDF nanocomposites, where the increase is from 8.6×10^4 Pa (PVDF) to 3.8×10^5 Pa (10 wt% MWNT). The addition of MWNT increases the storage modulus of the melt through stress-transfer across the polymer-MWNT interface. At higher MWNT content, the reinforcing effect of MWNT is more apparent and similar to that for solid elastic bodies. Even at low frequencies, where there is now more time for polymer chain relaxation, the MWNT particles efficiently reinforce the fluid polymer phase from relaxing. Adding MWNT to the polymers results in the melt viscosity increasing, in an effect similar to storage modulus, however the increase in viscosity is not sustained across the frequency spectrum. At higher frequencies (higher strain rates) the MWNT networks can break down resulting in a lowering of the viscosity.

(a)

(b)

(c)
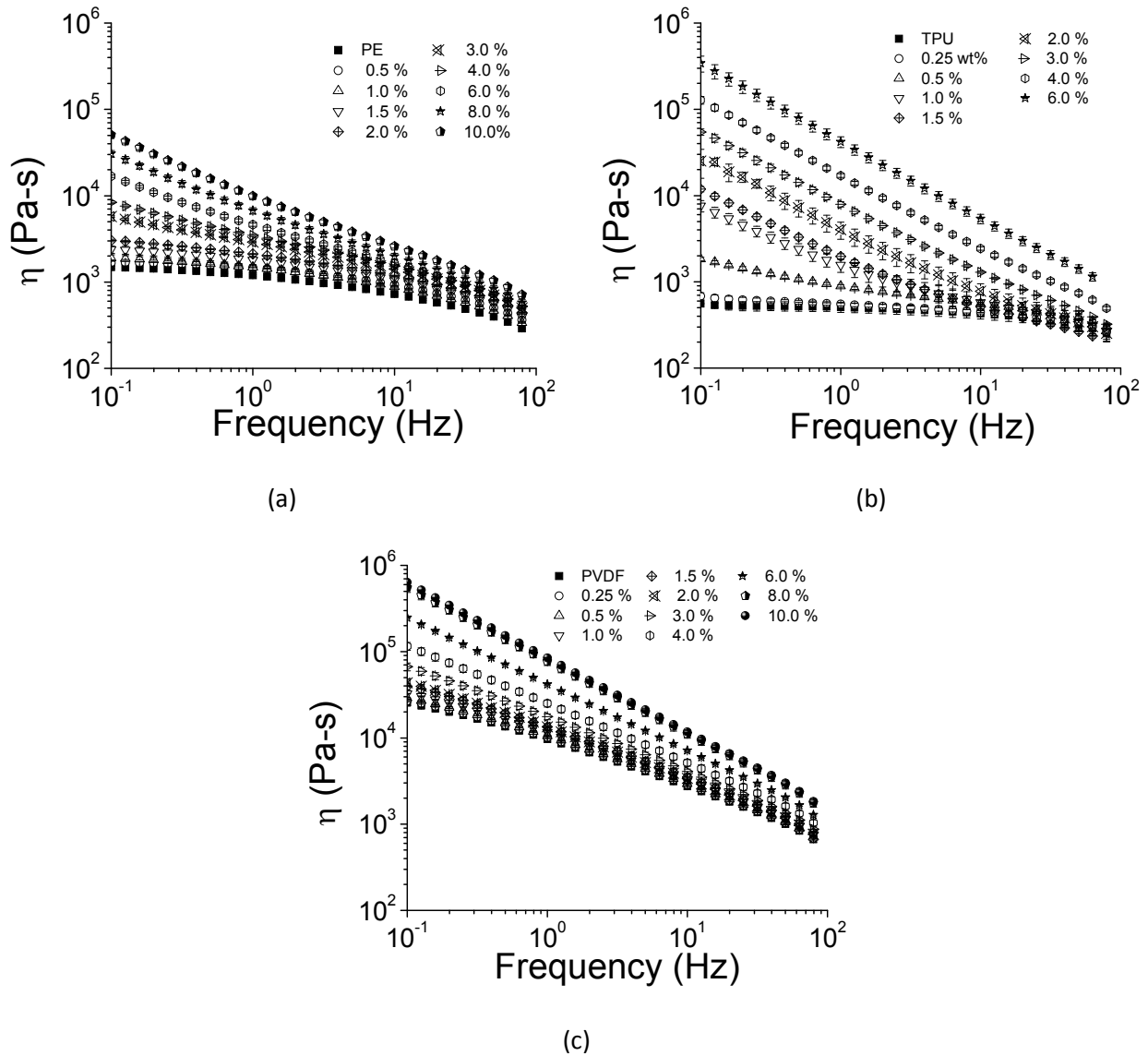
Figure 7.2. The frequency dependence of viscosity of PE-MWNT (a), TPU-MWNT (b), PVDF-MWNT (c)

nanocomposites.

7.3 Electrical and Rheological Percolation Modeling

The observed change in rheological behavior with the addition of MWNT is analogous to the change in

electrical behavior observed for each nanocomposite material examined in the preceding chapters. Just

as how impedance spectroscopy of the nanocomposites revealed a transition from a dielectric behavior

to a conductor, the rheological study of the nanocomposites reveals a transition from a viscoelastic fluid

to a pseudo-solid material. In this context, the electrical conductivity and the storage modulus are analogous to each other, while the permittivity and the viscosity are analogous. Moreover, the frequency dependence of each property is similar to its paired property. These observations imply that the underlying mechanisms, namely the filler network, for the material behavior transition in impedance and rheological behavior are essentially the same. If the filler network is responsible for both material transitions, then both the electrical conductivity and the storage modulus of the materials should be well described by the power-law form (Equation 2.1) of statistical percolation.

The electrical conductivity and storage modulus of the polymer nanocomposites are plotted against the MWNT volume fraction in Figure 7.3a and b, respectively. Both the electrical and rheological properties exhibit a sharp increase associated with percolated network formation, albeit with subtle differences. For instance, the conductivity undergoes several orders (8-11) of magnitude increase as the MWNT content surpasses the percolation threshold, regardless of the matrix material. In contrast, the storage modulus increases fewer orders of magnitude with the change depending on the matrix material chosen. Nanocomposites of PVDF, a stiffer matrix material, undergo only 1 order of magnitude increase in storage modulus with MWNT addition, whereas those of TPU undergo 4 orders of magnitude increase. Additionally the shape of the transition curves for storage modulus vary between the nanocomposite systems examined, while those for electrical conductivity have a similar uniform shape. The marked dependence of the rheological behavior on the matrix material implies that, in addition to the filler network, the rheological percolation is dependent on state of the polymer phase in the nanocomposites. In comparison the electrical percolation, apart from the initial processing where the filler network gets established, is fairly independent of the polymer phase chosen.
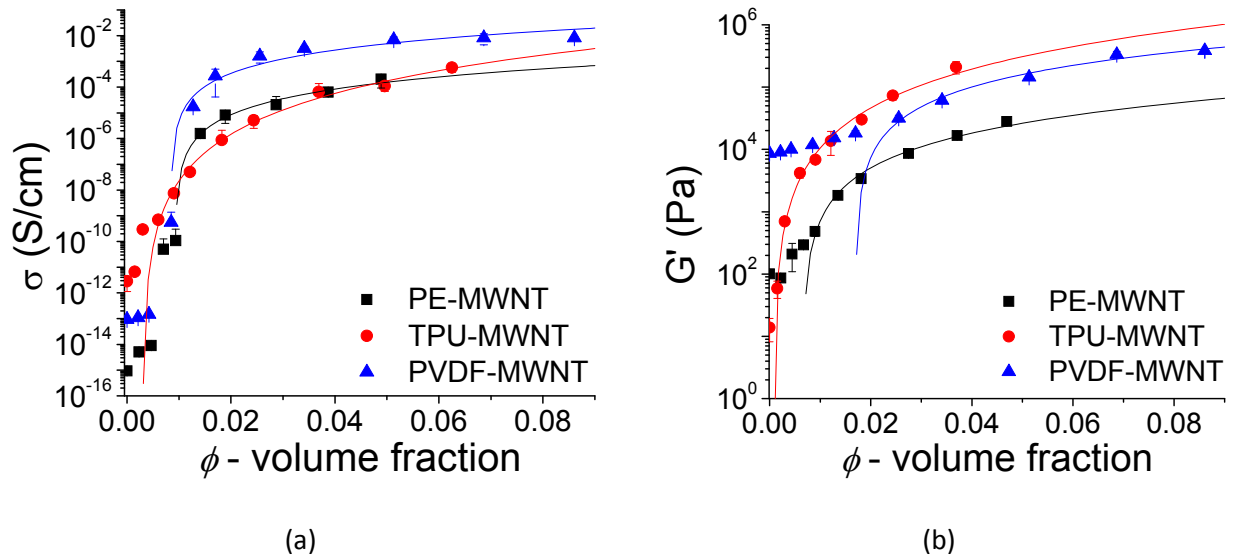
Figure 7.3. The MWNT dependence of conductivity (a) and storage modulus (b) for the various MWNT nanocomposites examined. The solid lines are the fit to the power law model (Equation 2.1) for each respective curve.

This comparison is better illustrated by examining Figure 7.4, where the possible mechanisms for electrical and rheological percolation are depicted. In electrical percolation, the charge transport is entirely supported by the MWNT network. The only means that a polymer can influence the electrical properties of the nanocomposites is through the initial network formation (during processing) and through the work function, which dictates the quantum tunneling effect dominant near the threshold concentration. Contrast this to rheological percolation, where the polymer phase actively participates in the stress-transfer to the MWNT network and the polymer-MWNT interface will be significantly influenced by the state that the polymer is in. For example, if the polymer chains are flexible (fewer entanglements, low MW, high temperature), like TPU, then the likelihood of polymer-MWNT interaction at the interface is increased and a prominent reinforcing effect due to the rigid MWNT network is observed. If the chains are rigid to begin with (more entanglements, high MWNT, low temperature), like

PVDF, then there will be reduced polymer-MWNT interaction and the reinforcing effect that the MWNT network can provide will be limited.
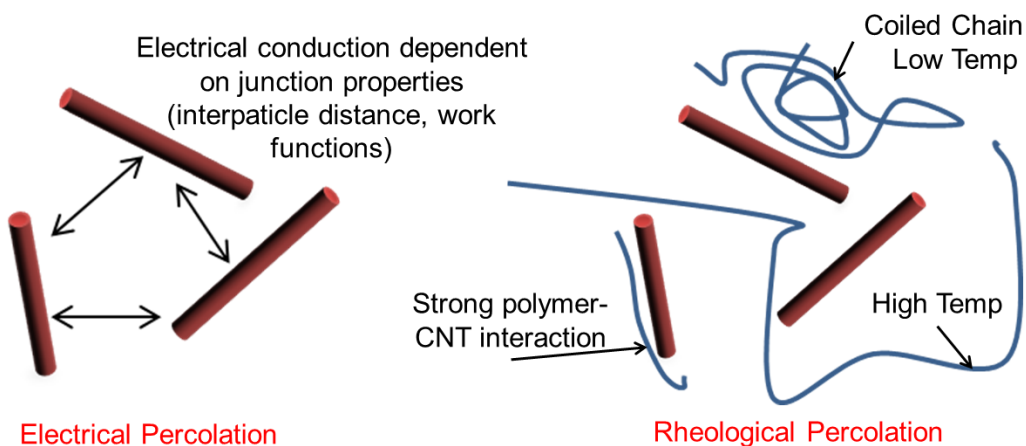
Figure 7.4. Schematic representation of the various electrical and rheological percolation mechanisms.

The power-law form was fitted against the electrical conductivity and the storage modulus of the various nanocomposites systems and is plotted as solid continuous lines on Figures 7.3a and b. The fit procedure was performed on Matlab computing software. The program iteratively scans a volume fraction range and performs linear regression to the log-reduced form of the power law model. The data set that provides the highest residuals (R^2) was selected as the optimum solution. Included in the analysis were PE nanocomposites containing Singlewall Carbon Nanotube (SWNT) and Graphene Nanoplatelets (GNP) as described in Chapter 4. The parameters of the electrical and rheological percolation power law model are outlined in Table 7.1. The power-law form provides an adequate fit for both data types with high goodness of fit (R^2) . Based on the results, the lowest electrical and rheological percolation threshold values obtained were for TPU-MWNT nanocomposites while the highest ones were for PE-GNP nanocomposites. The reason for the unusually high percolation thresholds for PE-GNP is the filler particulate reorientation (anisotropy) during processing as detailed in Chapter 4. Comparing

the electrical and rheological behavior of the nanocomposites, it is apparent that MWNT addition has more influence on the electrical conductivity. This trend is confirmed by the higher values for the critical exponent, *t*, for the case of electrical percolation.

Table 7.1. Power-law parameters for modeling the electrical and rheological percolation.

Electrical Percolation

Polymer	Filler	σ_0 (S/cm)	ϕ	t	R^2	σ_{max} (S/cm)	$\sigma_{max}/\sigma_{poly.}$	$\phi_{\sigma\text{-max}}$
PVDF	MWNT	3.5	0.0085	2.07	0.988	8.2×10^{-3}	9×10^{10}	0.086
TPU	MWNT	304.0	0.0030	4.70	0.993	5.8×10^{-4}	2×10^{8}	0.063
PE	MWNT	0.16	0.0093	2.17	0.998	2.0×10^{-4}	2×10^{11}	0.049
PE	SWNT	0.7	0.0064	2.56	0.991	1.6×10^{-4}	2×10^{11}	0.049
PE	GNP	1.3×10^{-4}	0.0290	1.37	0.999	5.6×10^{-7}	6×10^{8}	0.049

Rheological Percolation

Polymer	Filler	G'_0 (Pa)	ϕ	t	R^2	G'_{max} (Pa)	$G'_{max}/G'_{poly.}$	$\phi_{G\text{-max}}$
PVDF	MWNT	1.3×10^{7}	0.0170	1.28	0.975	3.8×10^{5}	4×10^{1}	0.086
TPU	MWNT	1.3×10^{8}	0.0008	2.02	0.995	5.0×10^{5}	2×10^{4}	0.063
PE	MWNT	2.2×10^{6}	0.0067	1.40	0.992	2.8×10^{4}	3×10^{2}	0.049
PE	SWNT	5.3×10^{5}	0.0090	1.39	0.988	6.8×10^{3}	7×10^{2}	0.049
PE	GNP	1.5×10^{5}	0.0183	1.46	0.999	8.3×10^{2}	8×10^{0}	0.049

An important trend observed from the power-law parameters (Table 7.1) is the relationship between the critical exponent, *t*, and the critical percolation threshold, ϕ_c. These parameters for both the electrical and rheological dataset are plotted against each other in Figure 7.5. The general trend

that's observed is that lower threshold concentrations result in higher t-exponents for both the electrical and rheological data. The t-exponent data points for each polymer nanocomposite system are related to the critical threshold concentration and can be well represented by the following semi-empirical relations:

$$t_{Elec} = 0.0604\phi_c^{-0.749}$$
(Eq. 7.1)

$$t_{Rheo} = 0.670\phi_c^{-0.153}$$
(Eq. 7.2)

The observed trend of lower critical concentrations resulting in higher t-values has important applications, particularly for high aspect ratio particles like MWNT and GNP. It is well known that high aspect ratio particles will have lower percolation values, and theories such as the excluded volume approach (Chapter 2) predict this result as well. The nanoparticles used in this study have high aspect ratios (500-2500), for which the excluded volume approach predicts a percolation threshold of $3x10^{-4}$ to $1.3x10^{-3}$ volume fraction. These predicted values are much lower than the obtained results, signifying that other factors such as aggregation, nanoparticle destruction (aspect ratio lowering) and interactions with polymer, play a more dominant effect than on the network formation than the geometry of the particles alone. An important example of this is the case for PE-GNP composites which exhibited filler alignment and some evidence of anisotropy, as result of which the critical exponent-threshold relationship (Equation 7.1 and 7.2) breaks down and is not applicable due to poor residual (R^2) results. Therefore Equation 7.1 and 7.2 can be said to be applicable to systems with similar nanocomposite microstructure, including similar nanoparticle isotropy and dispersion.
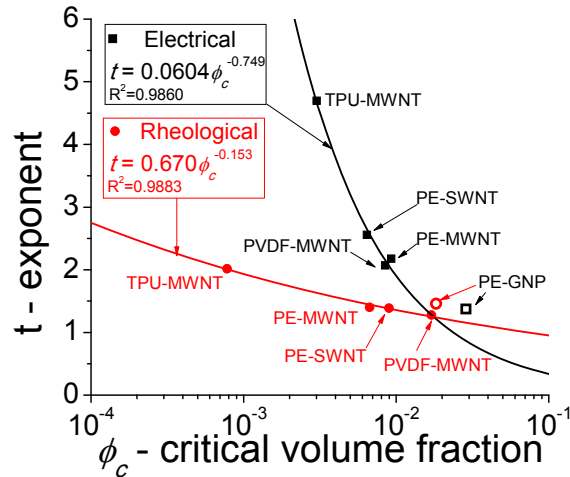
Figure 7.5. Relationship between the critical volume fraction and the t-exponent for the electrical and rheological nanocomposite data.

7.4 Modeling the Piezoresistance of Polymer Nanocomposites

The piezoresistance response of the polymer nanocomposites described in the previous chapters (Chapter 4, 5 and 6) exhibited a few interesting behaviors, which can now be examined in more detail. In particular the observation of the piezoresistance response in both the elastic and plastic deformation regimes requires further investigation. The logarithmic piezoresistance response for the various polymer-MWNT nanocomposite systems is illustrated in Figure 7.6. A logarithmic plot of relative resistance vs. stress is useful as both quantities change very fast during the test. Taking the logarithm of both quantities better distinguishes the plastic deformation, elastic deformation and initial contact resistance from each other. The plastic deformation component is associated with an upward rise in resistance at high stresses. The elastic component corresponds to the decrease in resistance at medium stresses while the contact resistance is the non-linear (on the logarithmic plot) resistance decrease at low stresses.

87
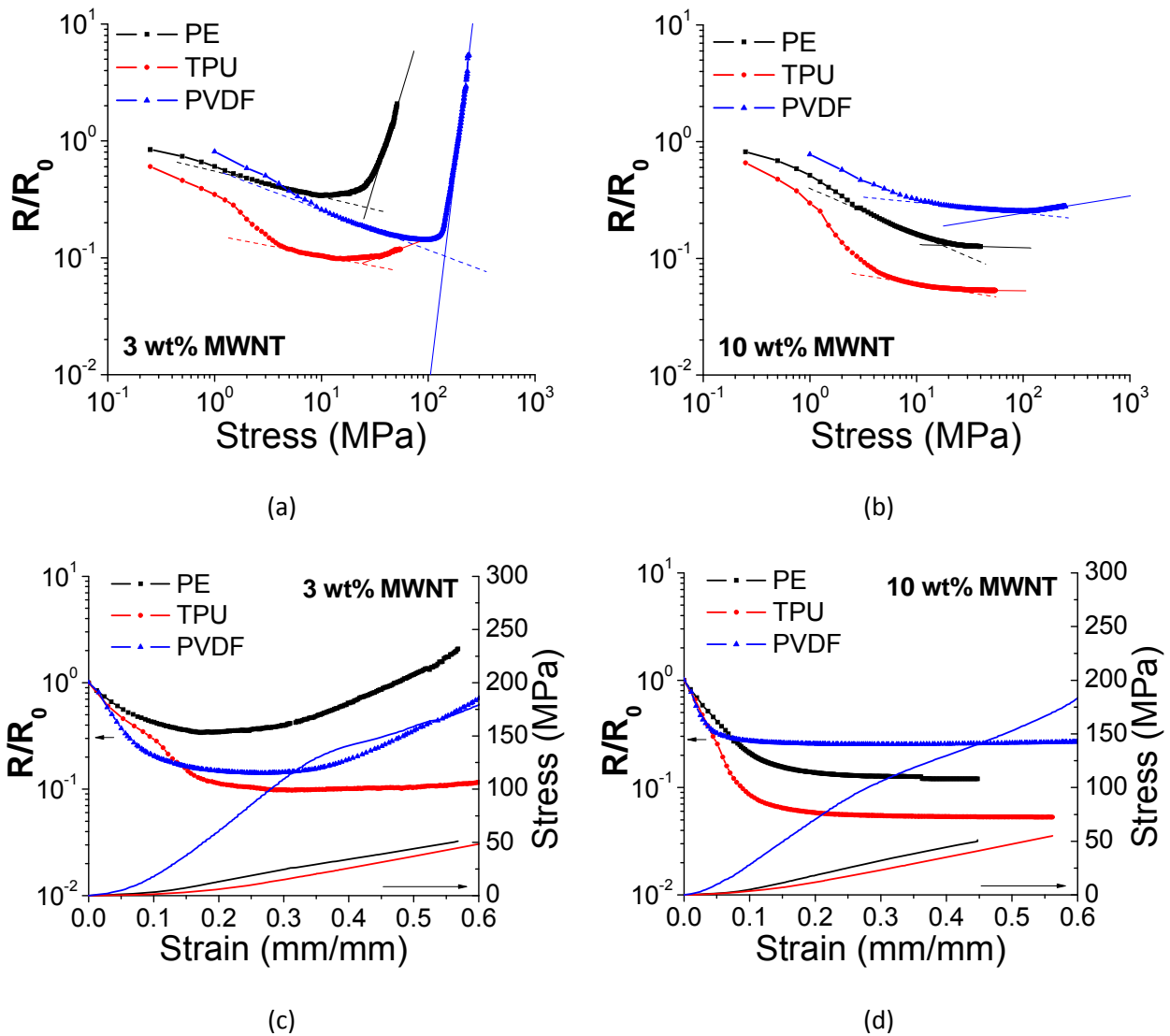
Figure 7.6. The logarithmic piezoresistance response of conductive polymer nanocomposites containing

3 wt% (a) and 10 wt% (b) MWNT amounts.

The logarithmic piezoresistance results in Figure 7.6 suggest that the piezoresistance during

plastic deformation is sensitive to the MWNT content and matrix material in the nanocomposites. At low

MWNT amounts of 3 wt% (Figure 7.6a), the resistance increases after a certain stress threshold is

crossed. As shown in Figure 7.6c, this stress threshold corresponds with the yield phenomena in the

polymer nanocomposite, which is unique for each matrix material. For example PVDF (a stiffer polymer) has an obvious yielding behavior at approximately 150 MPa (Figure 7.6c), which is also the stress at which the resistance starts to sharply increase w.r.t. stress. In comparison, TPU (a flexible elastomer), has minimal yielding, as a result of which, there is only a slight increase in resistance in comparison to PVDF and PE. At high MWNT amounts of 10 wt% (Figure 7.6b), there is no resistance increase at higher stresses, even though the yield behavior is still apparent in the stress-strain plots (Figure 7.6d). The sharp rise in resistance w.r.t. stress in the plastic deformation regime in Figure 7.6 seems to suggest an exponent relationship between relative resistance and stress:

$$\frac{R}{R_0} = A\exp(B\sigma) \tag{Eq. 7.3}$$

The parameters, *A* and *B* can be determined by taking the logarithm of relative resistance and the stress and fitting them with a straight line of the form:

$$\ln\left(\frac{R}{R_0}\right) = \ln(A) + B\sigma \tag{Eq. 7.4}$$

The parameters *A* and *B* obtained for the PVDF and PE nanocomposites are listed in Table 7.2. Nanocomposites of TPU weren't analyzed as they do not undergo sufficient plastic deformation in order to exhibit an identifiable piezoresistance response. The exponential form (Equation 7.3) describes the piezoresistance in plastic deformation reasonably well as confirmed by the high residual sum of squares (R^2). An important observation from the fit results is that the parameters *A* and *B* vary with the MWNT amount. The parameter *B* represents the exponential sensitivity of resistance to stress, and in general it decreases with stress (as shown In Figure 7.7).

Table 7.1. Fitting parameters for the exponential form (Equation 7.3).

PVDF-MWNT Nanocomposites

% MWNT	Φ (vol. frac.)	ln (A)	B	R^2
2%	0.017	-27.942	0.1748	0.999
3%	0.026	-6.0967	0.0320	0.999
4%	0.034	-3.7275	0.0153	0.999
6%	0.051	-2.2962	0.0030	0.999
8%	0.069	-1.7774	0.0011	0.999
10%	0.086	-1.4566	0.0007	0.999

PE-MWNT Nanocomposites

% MWNT	Φ (vol. frac.)	ln (A)	B	R^2
3%	0.026	-2.7261	0.0662	0.994
4%	0.034	-2.3589	0.0287	0.982
6%	0.051	-2.1605	0.0080	0.992

The dependence of B on the inverse of the MWNT amount suggests a behavior that is inverse of the power-law, which was used to describe the electrical conductivity and the storage modulus of the nanocomposites. The data for B parameter is plotted against the inverse of the power law form for PE and PVDF nanocomposites in Figure 7.7. It's apparent from this plot that the parameter B varies linearly with the inverse of the power-law form. More importantly, this linear relation is the same for both PE and PVDF nanocomposites. The proportionality constant that obtained from this method is 9×10^{-6} with

an R^2 value of 0.996. The final expression relating the relative resistance (R/R_0) of a piezoresistive material containing a certain volume fraction (ϕ) of MWNT, to the stress applied (σ) is:

$$\frac{R}{R_0} \propto \exp\left(\frac{C}{(\phi - \phi_c)^t}\sigma\right) \qquad \text{(Eq. 7.5)}$$

(a)   (b)
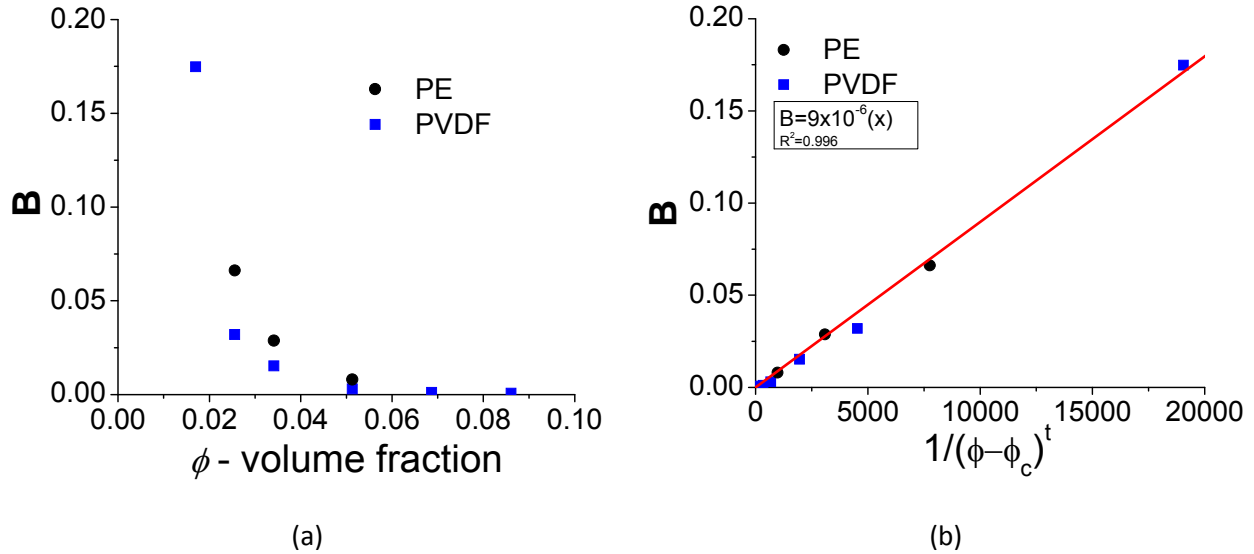
Figure 7.7. The dependence of *B* parameter on the MWNT volume fraction (a) and the inverse percolation concentration (b) for PE and PVDF nanocomposites.

where the constant *C* is 9x10^{-6} MPa^{-1} and ϕ_c and *t* are the parameters describing the power-law form of the statistical percolation for PVDF ($\phi_c = 0.008471$ and t = 2.07) and PE ($\phi_c = 0.00929$ and t = 2.17) nanocomposites. The above relationship clarifies the dependence of piezoresistance to the stress and the amount of filler present in the material. The pre-exponential, *A*, in Equation 7.3 is also dependent on the filler amount, however it's dependency is different for each nanocomposite type. Therefore information about other factors must be required in order to predict its behavior. The piezoresistance response during plastic deformation modeled by Equation 7.5 was compared against experimental
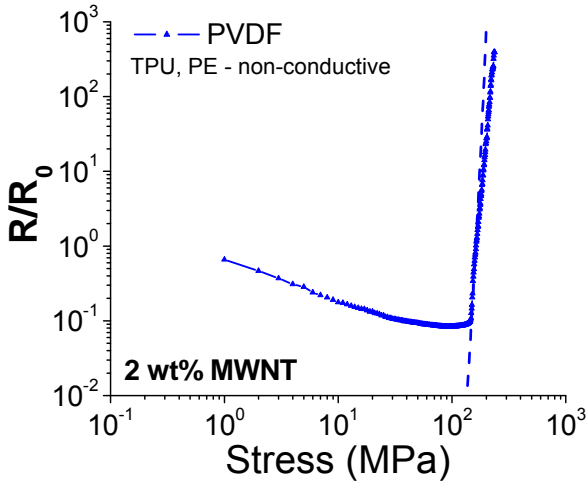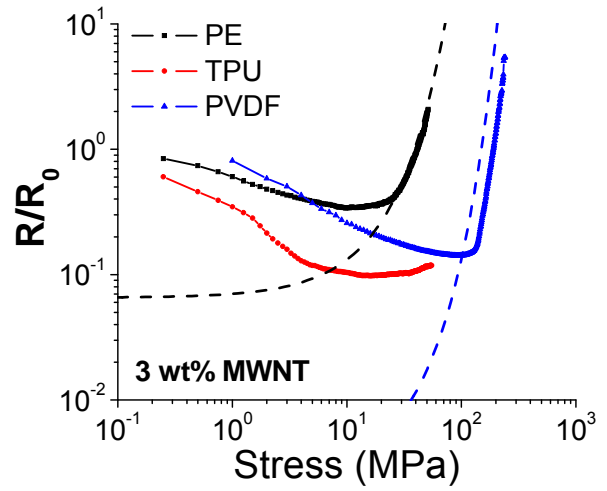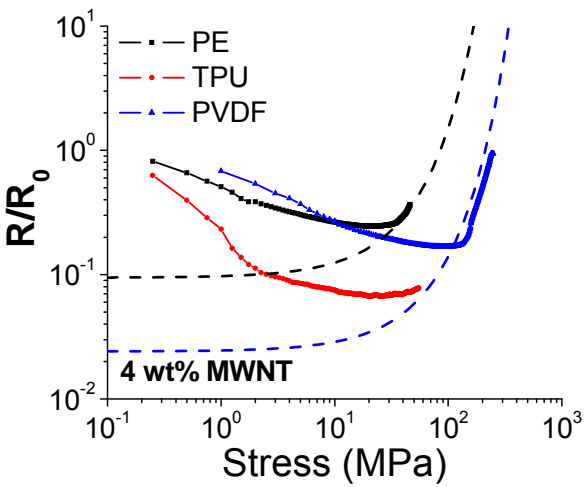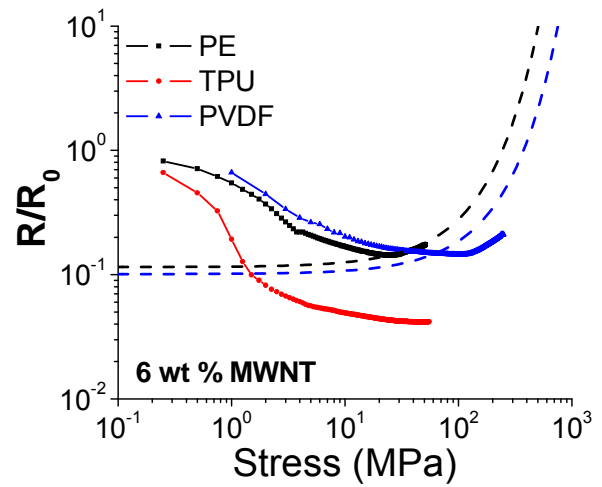
Figure 7.8. The piezoresistance response of the conductive polymer composites at 2 wt% (a), 3 wt% (b), 4 wt% (c) and 6 wt% (d). The dash lines are the piezoresistance response according to the proposed model (Equation 7.5).

results. Generally speaking, the experimental results and the model are in good agreement with each other for PE at all concentrations and for PVDF at low concentration. At higher concentrations (6 wt%

and above) the model fails to accurately capture the piezoresistance response. It's suspected that this is due to the percolation power-law form selected to represent concentration effects, as it may deviate at high filler contents.

7.5 Summary

The rheological and electrical properties of conductive polymer composites have been characterized and modeled against the power-law formulation for statistical percolation. Both rheological and electrical percolation parameters suggest that the critical exponent (t) scales inversely to the critical volume threshold for percolation. This suggests that at low critical thresholds, the exponent t can be quite high (e.g. for TPU) suggesting the breakdown of the classical percolation threshold theory in describing these systems. Also, in this chapter, a model has been proposed which represents the piezoresistance response during plastic deformation based on a known MWNT filler content and stress state. The derived model is universal for both PE and PVDF materials and can be applicable to other materials that display a unique transition in piezoresistance after the yield stress.

8 Conclusions and Recommendations

8.1 Concluding Remarks

The objective of this research was to examine the nature of electrically conductive particulate networks and how they influence piezoresistance in polymer nanocomposites. Several polymer nanocomposite systems were fabricated in a similar procedure based on the scalable process of melt compounding. The percolated network formation and piezoresistance behavior of the nanocomposites were characterized for the effects of filler, matrix, plastic deformation and porosity. A general scheme for modeling the electrical and rheological percolation response and the piezoresistance response in plastic deformation were proposed.

The effect of filler particle on the morphology, electrical properties and piezoresistive behavior of polyethylene (PE) nanocomposites containing different types of carbon nano-particle fillers was elucidated. Polyethylene nanocomposites containing single-wall carbon nanotube (SWNT), multi-wall carbon nanotube (MWNT) and graphene nanoplatelets (GNP), which were dispersed using melt blending. Morphology analysis indicated dispersion of all three filler type, however it also revealed significant shear-induced alignment of 2D GNP particles. The alignment resulted in anisotropy of the electrical properties with low through plane electrical conductivity and a high percolation threshold. The lowest percolation threshold achieved was in SWNT nanocomposites (1.4 wt%) which was attributed to their longer aspect ratio and surface area, and therefore greater ability to form contacts in a networked arrangement. Piezoresistance measurements of the nanocomposites revealed unique resistance responses during the initial, elastic and plastic deformation. The piezoresistance for MWNT based

materials had a strong filler content and stress dependence indicating an evolving filler network as filler and stress amounts are varied. In contrast, the piezoresistance response of the SWNT nanocomposite was stable indicating a consistent networked state of particles.

The piezoresistance response of PVDF nanocomposites during plastic deformation was investigated in detail. The MWNT filler in PVDF nanocomposites was characterized to be well dispersed, with a low MWNT content threshold of 0.95 wt%. At 0.1 Hz, the maximum conductivity achieved in the nanocomposites was 10^{-2} S/cm (10 wt%), while the maximum dielectric permittivity was 39.4 (1.0 wt%). Piezoresistance investigation of the PVDF-MWNT nanocomposites revealed a three stage deformation (contact, elastic and plastic deformation) process which was similar to that observed for PE nanocomposites. The resistance was observed to decrease during elastic deformation, while increase during plastic deformation, corresponding to variations in inter-particle distance between the MWNT. The resistance increase during plastic deformation, corresponding to MWNT network disruption, was inversely sensitive to the amount of MWNT phase present. At high MWNT concentrations, the nanocomposites do not undergo network disruption, despite having a yielding behavior, because of a high density of MWNT contacts which preserves current paths.

The effect of porosity on the piezoresistance of nanocomposites was investigated by introducing a cellular morphology to TPU nanocomposites by phase separating a TPU-carbon-dioxide gas solution. A porous morphology was found to be detrimental for electrical properties with the conductivity and permittivity decreasing and percolation threshold increasing compared to solid nanocomposites. This was attributed to an increased inter-particle distance between MWNT during pore expansion, and the pores acting as obstacles to electron conduction, thereby increasing the path lengths. The piezoresistance behavior of the porous nanocomposites was found to be dependent on MWNT concentration and nanocomposite microstructure. The resistance in porous nanocomposites containing

95

4 wt% MWNT underwent an increase with the application of stress, which indicated that pore compression was responsible for disrupting the filler particle network. Porous TPU nanocomposite concentrations higher than 4 wt% had a piezoresistance response similar to solid TPU nanocomposites because their microstructure lacked a homogenous porous structure throughout.

The percolation and piezoresistance of conductive polymer nanocomposites have been characterized and modeled against the power-law formulation for statistical percolation. Analysis of rheological and electrical percolation parameters suggest that the critical exponent (t) scales inversely to the critical volume threshold for percolation. Therefore systems with low critical thresholds (e.g. TPU) may not be accurately represented by the classical percolation threshold theory, which restricts the value of t to ~ 2, and other factors such as the polymer's electrical properties may need to be characterized and incorporated in the percolation behavior. A model describing the piezoresistance response during plastic deformation has been proposed. This model incorporates the MWNT filler content and stress state of the nanocomposite. The derived model is universal for both PE and PVDF materials and can be applicable to other materials that display a unique transition in piezoresistance after the yield stress.

8.2 Contributions

The key contributions of this research are:

1. Novel piezoresistive nanocomposites were developed using a simple and scalable manufacturing process with the ability to **tailor the pressure sensing response** based on the type of filler, filler amount, matrix material, deformation regime and an internal porous structure.

2. A **larger aspect ratio** of nanoparticles as well as **high nanoparticle content** will result in a greater density of network contacts and hence more paths available for electron conduction, resulting in **robust filler networks** that mitigate piezoresistance.

3. **Porosity** in nanocomposites reduces electrical conductivity and piezoresistance as expected, however it also **increases the percolation threshold** concentration, suggesting that the mean inter-particle distance between filler particles increases drastically due to pore expansion during processing.

4. Homogenously **porous nanocomposites** exhibit a piezoresistive effect opposite to their solid counterparts, with **resistance increasing due to applied pressure** because of increased conduction path lengths and inter-particle distances due to the biaxial stretching of pore walls during compression.

5. **Electrical percolation** is dependent primarily on the **filler particle arrangement** in the material, whereas **rheological percolation** is influenced by **filler particle arrangement** as well as the **polymer** and the **polymer-particle interface**.

6. A model was derived to describe the **piezoresistance during plastic deformation** observed for semi-crystalline materials. The model consists of an exponential form that takes into account **stress, filler content** and **percolation power-law** parameters.

8.3 Recommendations

Based on the results of the investigations carried out in this project, into the percolation and piezoresistance of polymer nanocomposites, the following recommendations are made for further research and development:

1. Further investigating the effect of aspect ratio on the piezoresistive behavior. This can be done by selecting an MWNT, and selectively shortening its length by ultrasound processing or acidic oxidation. Nanocomposites with higher aspect ratio particles should not undergo a piezoresistance as sharp as low aspect ratio particles during the plastic deformation process.

2. Other matrix materials should be investigated for optimum processing of porous piezoresistive polymer nancomposites. Porous processing of TPU resulted in a non-homogenous porous morphology at higher MWNT content due to high nanocomposite viscosity. The homogenous porous morphologies at low MWNT content weren't conductive enough for piezoresistive characterization. Other elastomeric material recommendations that can be processed into porous articles are Ethylene-vinyl-acetate, Fluoro-elastomers and Silicone rubber.

3. The piezoresistance behavior of the nanocomposites was affected by contact stresses which are convoluted in the resistance signal. A means of mitigating contact stresses, friction and non-uniaxial stress states is to increase the aspect ratio of the samples. This was attempted and the contact region during mechanical deformation was reduced, however, the resistance of the sample also increased significantly, resulting in low signal-to-noise. An alternative solution to the contact stress problem could be to bond two electrodes (with an area much smaller than the sample's contact area) to the center of the samples. This sandwich arrangement could then be compressed with a fairly uniaxial stress state at the electrodes, free from contact effects. However this can lead to further complexities such as, finding an appropriate electrically conductive adhesive that won't influence the results, and approximating a suitable area for normalization.

4. Further morphology characterization is required in order to accurately characterize and model the piezoresistance response. The average inter-particle distance as a function of stress and filler amount is the elusive parameter that is much sought after. Monte-Carlo simulations have been used to estimate the inter-particle distances however, the results are not very representative of the real-case scenarios and the simulations are computationally intensive. An experimental methodology for determining this parameter for particles of various shapes and sizes is required.

5. Any efforts to model the piezoresistance and network evolution must incorporate the percolation parameters (critical concentration and exponent). A comprehensive piezoresistance model should also incorporate both elastic and plastic deformation and not treat them separately. Finally, a predictive model should also account for the quantum mechanics observed in conductive nanocomposites, especially the work functions of the matrix and filler phases.

References

[1] Carpi, F., and De Rossi, D., 2005, "Electroactive Polymer-Based Devices for e-Textiles in Biomedicine," IEEE Transactions on Information Technology in Biomedicine, **9**(3) pp. 295-318.

[2] Webster, J.G., 1988, "Tactile Sensors for Robotics and Medicine," John Wiley and Sons, New York, pp. 365.

[3] Bauhofer, W., and Kovacs, J. Z., 2009, "A Review and Analysis of Electrical Percolation in Carbon Nanotube Polymer Composites," Composites Science and Technology, **69**(10) pp. 1486-1498.

[4] Yakobson, B., and Smalley, R., 1997, "Fullerene Nanotubes: C 1,000,000 and Beyond some Unusual New molecules—long, Hollow Fibers with Tantalizing Electronic and Mechanical properties—have Joined Diamonds and Graphite in the Carbon Family," Am Scientist, **85**pp. 324-337.

[5] Iijima, S. a. o., 1991, "Helical Microtubules of Graphitic Carbon," Nature, **354**(6348) pp. 56-58.

[6] Harris, P. J. F., 2004, "Carbon Nanotube Composites," International Materials Reviews, **49**(1) pp. 31-43.

[7] Ebbesen, T., Lezec, H., Hiura, H., 1996, "Electrical Conductivity of Individual Carbon Nanotubes," .

[8] Treacy, M., Ebbesen, T., and Gibson, J., 1996, "Exceptionally High Young's Modulus Observed for Individual Carbon Nanotubes," .

[9] Thostenson, E. T., Ren, Z., and Chou, T., 2001, "Advances in the Science and Technology of Carbon Nanotubes and their Composites: A Review," Composites Science and Technology, **61**(13) pp. 1899-1912.

[10] Geim, A. K., and Novoselov, K. S., 2007, "The Rise of Graphene," Nature Materials, **6**(3) pp. 183-191.

[11] Li, Y., Zhao, L., and Shimizu, H., 2011, "Electrically Conductive Polymeric Materials with High Stretchability and Excellent Elasticity by a Surface Coating Method," Macromolecular Rapid Communications, **32**(3) pp. 289-294.

[12] Zhou, Y., He, B., Zhou, W., 2004, "Electrochemical Capacitance of Well-Coated Single-Walled Carbon Nanotube with Polyaniline Composites," Electrochimica Acta, **49**(2) pp. 257-262.

[13] Biercuk, M., Llaguno, M. C., Radosavljevic, M., 2002, "Carbon Nanotube Composites for Thermal Management," Applied Physics Letters, **80**(15) pp. 2767-2769.

[14] Allaoui, A., Bai, S., Cheng, H. M., 2002, "Mechanical and Electrical Properties of a MWNT/epoxy Composite," Composites Science and Technology, **62**(15) pp. 1993-1998.

[15] Bekyarova, E., Thostenson, E. T., Yu, A., 2007, "Multiscale Carbon Nanotube-Carbon Fiber Reinforcement for Advanced Epoxy Composites," Langmuir, **23**(7) pp. 3970-3974.

[16] Li, C., Thostenson, E. T., and Chou, T., 2008, "Sensors and Actuators Based on Carbon Nanotubes and their Composites: A Review," Composites Science and Technology, **68**(6) pp. 1227-1249.

[17] Kobashi, K., Villmow, T., Andres, T., 2008, "Liquid Sensing of Melt-Processed Poly(Lactic Acid)/multi-Walled Carbon Nanotube Composite Films," Sensors and Actuators B: Chemical, **134**(2) pp. 787-795.

[18] Hu, N., Karube, Y., Arai, M., 2010, "Investigation on Sensitivity of a polymer/carbon Nanotube Composite Strain Sensor," Carbon, **48**(3) pp. 680-687.

[19] Tahhan, M., Truong, V., Spinks, G. M., 2003, "Carbon Nanotube and Polyaniline Composite Actuators," Smart Materials and Structures, **12**(4) pp. 626-632.

[20] Shi, J., Guo, Z., Zhan, B., 2005, "Actuator Based on MWNT/PVA Hydrogels," Journal of Physical Chemistry B, **109**(31) pp. 14789-14791.

[21] Bartholome, C., Derre, A., Roubeau, O., 2008, "Electromechanical Properties of Nanotube-PVA Composite Actuator Bimorphs," Nanotechnology, **19**(32) .

[22] Du, F., Fischer, J. E., and Winey, K. I., 2005, "Effect of Nanotube Alignment on Percolation Conductivity in Carbon nanotube/polymer Composites," Phys.Rev.B, **72**(12) pp. 121404.

[23] Barrau, S., Demont, P., Peigney, A., 2003, "DC and AC Conductivity of Carbon Nanotubes-Polyepoxy Composites," Macromolecules, **36**(14) pp. 5187-5194.

[24] Ishida, H., and Rimdusit, S., 1998, "Very High Thermal Conductivity obtained by Boron Nitride-Filled Polybenzoxazine," Thermochimica Acta, **320**(1) pp. 177-186.

[25] Liang, G. D., and Tjong, S. C., 2006, "Electrical Properties of Low-Density polyethylene/multiwalled Carbon Nanotube Nanocomposites," Materials Chemistry and Physics, **100**(1) pp. 132-137.

[26] Bloor, D., Donnelly, K., Hands, P. J., 2005, "A Metal-Polymer Composite with Unusual Properties," Journal of Physics D: Applied Physics, **38**(16) pp. 2851-2860.

[27] Newman, M., 2010, "Networks: An Introduction," OUP Oxford, .

[28] Broadbent, S., and Hammersley, J., 1957, "Percolation processes," Mathematical Proceedings of the Cambridge Philosophical Society, Anonymous Cambridge Univ Press, **53,** pp. 629-641.

[29] Shante, V. K., and Kirkpatrick, S., 1971, "An Introduction to Percolation Theory," Advances in Physics, **20**(85) pp. 325-357.

[30] Scher, H., and Zallen, R., 1970, "Critical Density in Percolation Processes," The Journal of Chemical Physics, **53**(9) pp. 3759-3761.

[31] Balberg, I., 1987, "Recent Developments in Continuum Percolation," Philosophical Magazine Part B, **56**(6) pp. 991-1003.

[32] Ounaies, Z., Park, C., Wise, K., 2003, "Electrical Properties of Single Wall Carbon Nanotube Reinforced Polyimide Composites," Composites Science and Technology, **63**(11) pp. 1637-1646.

[33] Balberg, I., Anderson, C., Alexander, S., 1984, "Excluded Volume and its Relation to the Onset of Percolation," Physical Review B, **30**(7) pp. 3933.

[34] Balberg, I., 1985, "Universal Percolation-Threshold Limits in the Continuum," Physical Review B, **31**(6) pp. 4053.

[35] Hu, N., Karube, Y., Yan, C., 2008, "Tunneling Effect in a polymer/carbon Nanotube Nanocomposite Strain Sensor," Acta Materialia, **56**(13) pp. 2929-2936.

[36] Sheng, P., 1980, "Fluctuation-Induced Tunneling Conduction in Disordered Materials," Physical Review B, **21**(6) pp. 2180.

[37] Kasap, S.O., 2006, "Principles of electronic materials and devices," McGraw-Hill, .

[38] Simmons, J. G., 1963, "Generalized Formula for the Electric Tunnel Effect between Similar Electrodes Separated by a Thin Insulating Film," Journal of Applied Physics, **34**(6) pp. 1793-1803.

[39] B S Massey and, I. K., 1966, "A Miniature Pressure Transducer," Journal of Scientific Instruments, **43**(8) pp. 569.

[40] Ukrainetz, P. R., and Hertz, P. B., 1966, "Pressure-Sensitive-Paint Force Transducers," Experimental Mechanics, **6**(7) pp. 19-23.

[41] Brown, T. D., and Muratori, D. R., 1979, "Miniature Piezoresistive Transducers for Transient Soft-Body Contact-Stress Problems," Experimental Mechanics, **19**(6) pp. 214-219.

[42] Snyder, W. E., and St. Clair, J., 1978, "Conductive Elastomers as Sensor for Industrial Parts Handling Equipment," IEEE Transactions on Instrumentation and Measurement, **IM-27**(1) pp. 94-99.

[43] De Rossi, D., Mazzoldi, A., Carpi, F., 2002, "Electroactive Fabrics for Distributed, Conformable and Interactive Systems," First IEEE International Conference on Sensors - IEEE Sensors 2002, June 12, 2002 - June 14, Anonymous Institute of Electrical and Electronics Engineers Inc, Orlando, FL, United states, **1,** pp. 1608-1613.

[44] Scilingo, E. P., Lorussi, F., Mazzoldi, A., 2003, "Strain-Sensing Fabrics for Wearable Kinaesthetic-Like Systems," IEEE Sensors Journal, **3**(4) pp. 460-467.

[45] Tognetti, A., Bartalesi, R., Lorussi, F., 2007, "Body Segment Position Reconstruction and Posture Classification by Smart Textiles," Transactions of the Institute of Measurement and Control, **29**(3-4) pp. 215-253.

[46] Xiang-Wu Zhang, Pan, Y., Zheng, Q., 2000, "Time Dependence of Piezoresistance for the Conductor Filled Polymer Composites," Journal of Polymer Science, Part B (Polymer Physics), **38**(21) pp. 2739-49.

[47] Wang, L., Ding, T., and Wang, P., 2009, "Research on Stress and Electrical Resistance of Skin-Sensing Silicone rubber/carbon Black Nanocomposite during Decompressive Stress Relaxation," Smart Materials and Structures, **18**(6) .

[48] Luheng, W., Tianhuai, D., and Peng, W., 2009, "Influence of Carbon Black Concentration on Piezoresistivity for Carbon-Black-Filled Silicone Rubber Composite," Carbon, **47**(14) pp. 3151-3157.

[49] Dang, Z., Jiang, M., Xie, D., 2008, "Supersensitive Linear Piezoresistive Property in Carbon Nanotubessilicone Rubber Nanocomposites," Journal of Applied Physics, **104**(2) .

[50] Carmona, F., Canet, R., and Delhaes, P., 1987, "Piezoresistivity of Heterogeneous Solids," Journal of Applied Physics, **61**(7) pp. 2550-7.

[51] Zhang, R., Baxendale, M., and Peijs, T., 2007, "Universal Resistivity-Strain Dependence of Carbon nanotube/polymer Composites," Physical Review B (Condensed Matter and Materials Physics), **76**(19) pp. 195433-1.

[52] Ruschau, G. R., Yoshikawa, S., and Newnham, R. E., 1992, "Resistivities of Conductive Composites," Journal of Applied Physics, **72**(3) pp. 953-9.

[53] Simmons, J. G., 1963, "Low-Voltage Current-Voltage Relationship of Tunnel Junctions," Journal of Applied Physics, **34**(1) pp. 238-239.

[54] Simmons, J. G., and Unterkofler, G. J., 1963, "Potential Barrier Shape Determination in Tunnel Junctions," Journal of Applied Physics, **34**(6) pp. 1828-1830.

[55] Anonymous 2004, "Texin and Desmopan - Thermoplastic Polyurethane Elastomers - A Guide to Engineering Properties," Bayer Material Science LLC, .

[56] Anonymous 2007, "Kynar and Kynar Flex - Performance Characteristics and Data," Arkema Inc., .

[57] Anonymous 2010, "Single Walled Nanotubes - SWNTs 90 wt% Specifications," Cheap Tubes Inc., .

[58] Anonymous 2009, "Nanocyl NC7000 Series - Product Datasheet - Thin Multi-wall Carbon Nanotubes," Nanocyl S.A., .

[59] Anonymous 2010, "Graphene Nanoplateles," Cheap Tubes Inc., .

[60] McNally, T., Pötschke, P., Halley, P., 2005, "Polyethylene Multiwalled Carbon Nanotube Composites," Polymer, **46**(19) pp. 8222-8232.

[61] Yu, A., Itkis, M. E., Bekyarova, E., 2006, "Effect of Single-Walled Carbon Nanotube Purity on the Thermal Conductivity of Carbon Nanotube-Based Composites," Applied Physics Letters, **89**(13) pp. 133102-133102-3.

[62] Haggenmueller, R., Fischer, J. E., and Winey, K. I., 2006, "Single Wall Carbon nanotube/polyethylene Nanocomposites: Nucleating and Templating Polyethylene Crystallites," Macromolecules, **39**(8) pp. 2964-2971.

[63] Barsoukov, E., and Macdonald, J.R., 2005, "Impedance Spectroscopy: Theory, Experiment, and Applications," Wiley, .

[64] Ikkala, O. T., Laakso, J., Vakiparta, K., 1995, "Counter-Ion Induced Processibility of Polyaniline: Conducting Melt Processible Polymer Blends," Synthetic Metals, **69**(1-3) pp. 97-100.

[65] Pud, A., Ogurtsov, N., Korzhenko, A., 2003, "Some Aspects of Preparation Methods and Properties of Polyaniline Blends and Composites with Organic Polymers," Progress in Polymer Science (Oxford), **28**(12) pp. 1701-1753.

[66] Baughman, R. H., Zakhidov, A. A., and de Heer, W. A., 2002, "Carbon Nanotubes--the Route Toward Applications," Science, **297**(5582) pp. 787-792.

[67] Zhang, Q., Rastogi, S., Chen, D., 2006, "Low Percolation Threshold in Single-Walled Carbon nanotube/high Density Polyethylene Composites Prepared by Melt Processing Technique," Carbon, **44**(4) pp. 778-785.

[68] Jeon, K., Lumata, L., Tokumoto, T., 2007, "Low Electrical Conductivity Threshold and Crystalline Morphology of Single-Walled Carbon nanotubes–high Density Polyethylene Nanocomposites Characterized by SEM, Raman Spectroscopy and AFM," Polymer, **48**(16) pp. 4751-4764.

[69] Haggenmueller, R., Guthy, C., Lukes, J. R., 2007, "Single Wall Carbon nanotube/polyethylene Nanocomposites: Thermal and Electrical Conductivity," Macromolecules, **40**(7) pp. 2417-2421.

[70] Deshmukh, S., and Ounaies, Z., 2009, "Single Walled Carbon Nanotube (SWNT)–polyimide Nanocomposites as Electrostrictive Materials," Sensors and Actuators A: Physical, **155**(2) pp. 246-252.

[71] Khodaparast, P., and Ounaies, Z., 2013, "On the Impact of Functionalization and Thermal Treatment on Dielectric Behavior of Low Content TiO_2 PVDF Nanocomposites," Dielectrics and Electrical Insulation, IEEE Transactions on, **20**(1) pp. 166-167.

[72] Rizvi, R., Kim, J., and Naguib, H., 2009, "Synthesis and Characterization of Novel Low Density Polyethylene-Multiwall Carbon Nanotube Porous Composites," Smart Materials and Structures, **18**(10) .

[73] Matsunaga, K., Sato, K., Tajima, M., 2005, "Gas Permeability of Thermoplastic Polyurethane Elastomers," Polymer Journal, **37**(6) pp. 413-417.

[74] Ito, S., Matsunaga, K., Tajima, M., 2007, "Generation of Microcellular Polyurethane with Supercritical Carbon Dioxide," Journal of Applied Polymer Science, **106**(6) pp. 3581-3586.

[75] Naguib, H. E., Park, C. B., Reichelt, N., 2002, "Strategies for Achieving Ultra Low-Density

Polypropylene Foams," Polymer Engineering and Science, **42**(7) pp. 1481-1492.

[76] Shen, J., Zeng, C., and Lee, L. J., 2005, "Synthesis of Polystyrene-Carbon Nanofibers Nanocomposite

Foams," Polymer, **46**(14) pp. 5218-5224.

[77] Rizvi, R., Khan, O., and Naguib, H. E., 2011, "Development and Characterization of Solid and Porous

Polylactide-Multiwall Carbon Nanotube Composites," Polymer Engineering and Science, **51**(1) pp. 43-53.

[78] Kremer, F., and Sch\onhals, A., 2003, "Broadband Dielectric Spectroscopy," Springer Verlag, .

[79] Sperling, L.H., 2006, "Introduction to physical polymer science," Wiley-Interscience,.